Quantifying Insect Behavior Across Scales Using Computer Vision

Thesis by

Tarun Sharma

In Partial Fulfillment of the Requirements

for the degree of

Doctor of Philosophy

CALIFORNIA INSTITUTE OF TECHNOLOGY

Pasadena, California

2026

Defended January 8th, 2026

Tarun Sharma
ORCID: 0009-0008-8945-3896

“The smallest creatures often hold the key to the grandest mysteries of our ecosystems.”

- Rachel Carson

ACKNOWLEDGEMENTS

Thank you to both my PhD advisors - Michael H. Dickinson, and Joseph Parker. To Michael, thank you for taking a chance on me having no prior experience in *Drosophila* neuroscience. Thank you for your guidance, support, friendship, and for introducing me to the beautiful world of insects and insect behavior. Thank you for the tethering lessons, writing lessons, for helping me figure out rig issues, and for giving me the freedom to pursue my ever-changing academic interests.
To Joe, thank you for taking a chance on me with no prior ecology experience. Thank you for your infectious enthusiasm and curiosity for science, and for always believing that things will work out. Thank you for your faith in me, your friendship, and also for introducing me to some top-quality Jungle and D&B.

Thank you to my committee – Elizabeth J. Hong and Thanos Siapas, for your support, guidance, and feedback. Thank you for your insight, support, and making me feel heard.

Thank you to my other mentors at Caltech. This PhD would not have been possible without you, and I am so grateful to have met you all, for your mentorship and friendship. To Jaison J. Omoto for all the *Drosophila* genetics lessons, the scientific discussions, walks on campus, listening to me rant, teaching me how to drive and about finances, and so much more. I cannot thank you enough. To Will Dickson for building and helping me modify the behavioral arena and Ethocam, teaching me so much about electronics, hardware, and programming, for always taking the time to listen, and for your positivity. To Ivo Ros for the scientific discussions and lessons, lunches from Ernie's, hearing me out, for your guidance and advice, and for always making time. To Jess Kanwal for your advice on project goals, structure, analysis, figures, and presentations, for always taking the time to listen, and for always offering solutions. To Sara Beery for introducing me to the world of computer vision for conservation, leading the way and always making space for others, the opportunity to be a part of the CV4E summer school, career advice and infectious optimism. To Roman Corfas, thank you for taking me under your wing during my first rotation.

Thank you to my lab mates from both the Dickinson and Parker labs, present and past, Johan Melis, Alysha De Souza, Francesca Ponce, Ivo Ros, Will Dickson, Jaison J Omoto, Emily Palmer, Anne Erickson, Ainul Huda, Amir H. Behbahani, Roman Corfas, Ysabel Giraldo, Kate Leitch, Kyobi Skutt-Kakaria, Gema Garcia, Lilian Porter, Albert Zhou, Yuriko Kishi, Jean Badroos, Jess Kanwal, Joani Viliunas, Hayley Smihula, Ti Eriksson, Ling Loh, Esther Okamoto, Jaeda Patton, John Truong, Tom Naragon, Caio Antunes de

Carvalho, Veronica Muller, Julian Wagner, and Yuerong Xiao, for making this such a fun and unforgettable journey. Both labs felt like large happy families and through ups and downs I could always count on you guys to be there for me and have my back. Thank you to my CNS cohort, Sarah Wandelt, Isabelle Rosenthal, Neehar Kondapaneni, and Kellan Morse. We kept the yearly dinner meetups going for a long time and that really helped me get through this PhD, especially the early years.

Thank you to all my friends, for the ones that have stuck with me for years to new friendships I have made at Caltech. Thank you for reminding me that there is more to life than work. Thank you to my closest friends Varun Menon and Yash Medipalli for always being there for me.

Thank you to Maryam (a real doctor), for loving me and supporting me through the last year and a half of this journey. You bring color into my life. I love you.

Finally, I would like to dedicate this thesis to my family. Thank you to my sister, Sukriti. You have always led the way and none of this would have been possible without your support. I could always come to you for help, advice, and guidance. Thank you for being a pillar of support through tough times. Thank you to Mom and Dad for your support and for everything you have sacrificed. This PhD is a result of your love, care, support, hardwork, and sacrifices. I never could have imagined I would one day be writing a PhD thesis at Caltech, and this would have not happened if not for you both. I love you all.

ABSTRACT

Insects exhibit extraordinary behavioral diversity from rapid sensorimotor control required for flight to coordinated behavior across large societies. While some behaviors are best studied in controlled lab settings and require precise fine-grained measurements, others demand long-term observations in more natural settings that cannot be replicated in lab. In this thesis, I demonstrate the applications of computer vision to quantify insect behavior across scales, from the level of individuals to colonies, in both lab and field conditions.

In the first part, I examine the role of mechanosensory cells, campaniform sensilla, on the stabilization response of the fruit fly, *Drosophila melanogaster.* Using tethered flies mounted on a rotating arena, I measure head and wing equilibrium responses using marker less pose estimation and edge tracking. By genetically silencing different subsets of campaniform sensilla, I show a linear relationship between the number of cells silenced and the magnitude of head and wing response, providing direct experimental evidence for their role in the equilibrium response.

In the second part, I apply computer vision techniques to study colony scale movement dynamics at the nest entrance of the ant species, *Liometopum occidentale*, in the Angeles National Forest. I introduce a custom, low-cost, field deployable multisensory camera trap, called the Ethocam, and collect an extensive dataset of hourly videos from three ant nests spanning over 100 days. Using computer vision methods for detection and multi-object tracking, I quantify circadian activity patterns, directional traffic imbalances, environmental drivers of activity and walking speed, and spatiotemporal movement dynamics across distinct trails.

Together, by integrating lab experiments, long term field data, and quantitative analysis using computer vision, this thesis presents a general framework for studying insect behavior across scales in both controlled and natural environments.

PUBLISHED CONTENT AND CONTRIBUTIONS

Román A Corfas, **Tarun Sharma**, Michael H Dickinson. "Diverse food-sensing neurons trigger idiothetic local search in Drosophila." Current Biology 29 (May 20, 2019). https://doi.org/10.1016/j.cub.2019.03.004.
T.S collected and analyzed data for experiments involving the spherical treadmill.

Tarun Sharma[*], Julian M Wagner[*], Sara Beery, William B Dickson, Michael H Dickinson, Joseph Parker. "Monitoring Social Insect Activity with Minimal Human Supervision." 2024 IEEE/CVF Conference on Computer Vision and Pattern Recognition Workshops (CVPRW) (Sept 27, 2024). https://doi.org/10.1109/CVPRW63382.2024.00131.
[*] joint first authorship.
T.S helped collecting data, performed analysis, and helped draft the manuscript.

Tarun Sharma, Anne Sustar, Jaison Omoto, Michael H. Dickinson. "The role of haltere campaniform sensilla on equilibrium reflexes of the fruit fly, *Drosophila melanogaster*." In rebuttal phase, 2026.
T.S collected behavioral data, performed analysis, generated figures, and drafted the manuscript.

Tarun Sharma, Joseph Parker. "Automated long-term monitoring of ant activity using computer vision". In preparation, 2026.
T.S collected all the data, performed all analysis, generated figures, and drafted the manuscript.

TABLE OF CONTENTS

Chapter 1

INTRODUCTION

Overview

Insects are among the most abundant, diverse, and ecologically influential animals on Earth. Of the roughly two million eukaryotic species described to date, more than half are insects. Although approximately 1 million insect species have been formally described, estimates suggest that the true number may be closer to 5.5 million. Their extraordinary diversity, abundance, and ecological reach make insects central to ecosystem function across almost all terrestrial environments. They act as pollinators, predators, decomposers, ecosystem engineers, and primary consumers, shaping nutrient cycles, soil structure, and bulk energy flow across landscapes. They are also essential components of the food pyramid for numerous birds, bats, amphibians, and fish, and act as natural pest controllers for agriculture.

Two key innovations that have catalyzed the success and terrestrial dominance of insects, are the evolution of flight and eusociality. Insects were the first to take to the skies, which endowed several evolutionary advantages, such as the ability to find food, mates, disperse to new areas, and to avoid predators. Successful flight, especially at insect scales where both inertial and viscous forces are large, requires precise stabilization and rapid sensorimotor responses. These demands have led to the evolution of specialized, highly

sensitive, mechanosensory systems that operate on the order of milliseconds. While flight enabled insects to disperse and occupy new niches, the evolution of eusociality has allowed a subset of insects to achieve extraordinary terrestrial dominance on land. Large insect societies functioning as a single organism, lead to far greater chances of finding and acquiring food, defense against predators, and reproductive success. By forming colonies, they achieve levels of ecological impact that far exceed those of solitary organisms.

Insect flight and social organization have fascinated researchers for centuries. While traditional methods of manual field observations and manipulation have yielded great insights, modern techniques such of automated analysis of video data using computer vision and AI, are fast emerging as technologies that can greatly assist in behavioral studies. This is especially the case for field studies in natural settings where manual observations or bait-based assays involve large amounts of labor and collecting data at a high temporal resolution over long periods of time is challenging.

In this thesis I focus on applying these technologies, to study insect behavior at different scales and settings, at the level of individuals in the lab, and large insect colonies in the field.

Part I: Flight stabilization in flies

While the earliest known flying insects had four wings, the order Diptera (true flies), amongst the most maneuverable of flying insects, have only one pair of wings.

The hind wings in dipterids have evolved into dumbbell shaped organs known as halteres (Figure 1), that specialize in stabilization and control during flight. The base of the halteres contain mechanosensory cells called campaniform sensilla, arranged in distinct fields, that relay information to the wings and nervous system. Halteres can be observed by the naked eye and are most prominent in crane flies (Figure 1). The pair of halteres, one on either side, oscillate in anti-phase with the wings.

Figure 1: Picture of a crane fly *Nephrotoma appendiculata* (spotted crane fly) with arrows pointing at halteres. Picture credit - Alvesgaspar - Own work, CC BY-SA 3.0, https://commons.wikimedia.org/w/index.php?curid=3970893

As early as 1714, Derham (Derham, 1714) observed that flies with halteres cut off will spiral to the ground. There have been multiple theories on the role and mechanism of

haltere function since. The current consensus is the result of pioneering work from Pringle in 1948 (Pringle, 1948), and Nalbach in 1993 (Nalbach, 1993). They demonstrated, using simplified models, that the haltere functions as a gyroscope, detecting Coriolis forces that arise during external perturbation in flight. They argued that the distinct anatomy of the haltere bulb and stalk, along with the arrangement of campaniform sensilla in disparate fields, was to allow the haltere to simultaneous detect forces arising during rotation and regular oscillation. They postulated that one specific field of campaniforms, called dF2, was positioned in a manner to be most sensitive to Coriolis forces during rotation. Although there have been many subsequent studies on haltere function, with experiments confirming the linear relationship between angular velocity (and hence Coriolis force) and behavioral responses (Dickinson, 1999), evidence for Pringle and Nalbach's theory of disparate campaniform field function and arrangement has not been proved experimentally.

Experiments involving haltere function are extremely challenging due to the extreme sensitivity of campaniform sensilla. Coriolis forces generated during external perturbation are of the order of 10^{-5} N. This makes studies involving the ablation, or artificial manipulation of haltere trajectory, difficult to interpret, as the haltere may be operating outside its natural range of motion.

Chapter 2 focuses on studying the role of campaniform sensilla for flight stabilization in *Drosophila melanogaster*. I describe experiments performed using an experimental arena which provided rotational stimulus to tethered flies, while measuring their wing and head

movements using computer vision. Marker less pose estimation and edge tracking allowed us to accurately measure head movements and wing beat amplitude from a camera mounted on the rotational arm. Using the powerful genetic toolkit available in *Drosophila*, we identified candidate driver lines targeting different subsets of campaniform sensilla. Using a rotational arena along with our identified driver lines and genetic silencing, allowed for the characterization of behavioral responses under naturalistic conditions, where the haltere is oscillating by the action of its endogenous motor drive.

Although the lack of genetic driver lines targeting cells exclusively in disparate fields prevented us from drawing conclusions on individual fields, we were able to demonstrate a direct relationship between the number of campaniform sensilla targeted and the magnitude of both the wing and head stabilization responses. We thus provide the first experimental evidence of direct involvement of campaniform sensilla in the flight stabilization. The future availability of driver lines targeting specific fields of campaniform sensilla, combined with computer vision methods and a behavioral arena like ours, will soon make it possible to test the role of the disparate fields in wing and head equilibrium responses.

Part II: Study of ant behavior at colony scale

Unlike solitary animals such as fruit flies, eusocial insects such as ants are best studied at the level of the colony. A quick observation of any ant colony in the wild reveals constant interactions between these animals via antennal contacts or by the chemical trails they lay down. Ants exhibit remarkable social behaviors such as constructing massive nests, engaging in agriculture of fungi, tending to aphids for honeydew in exchange for protection as ranchers tending to cattle, hunting down and bringing back prey often much larger than any individual ant, digging tunnels and hollowing out trees, and more. Their ecological impacts and abundance on land are unparalleled, with recent estimates suggesting the total dry biomass of ants exceeds that of all wild birds and mammals combined (Parker and Kronauer, 2021; Schultheiss et al., 2022).

One does not have to go far from Caltech to see an example of these ecosystem engineers at work. *Liometopum occidentale* (Figure 2), also known as velvety tree ant, is an ant species native to the area stretching between southern Washington and northern Mexico, and can easily found walking on trails on the forest floor or on trees in the Angeles National Forest. They form massive colonies of hundreds of thousands to millions of individuals by excavating the insides of bay, laurel, pine, and California coast live oak trees. They are a behavioral aggressive species and can be seen carrying back prey such as larger insects, seeds, bits of twigs back into their nests. They are also known to tend to aphids up on trees or on bushes. The insides of their nests consist of a carton-like structure (Figure 3 left), possibly resembling separate chambers and passageways through

the nest. On careful observation of nest entrances (either holes or crevices on nest trees), ants can be seen excavating, carrying small pieces of material to the edge, flicking it, and returning back into the nest. This usually results in a pile of sawdust at the base of the tree (Figure 3 right). The abundance of these ants, along with aggressive behavior, influencing fauna and flora through predation, pollination, excavation, aphid tending, and serving as hosts to a range of obligate myrmecophiles such as rove beetles, make them a keystone species and an ideal candidate for long term field-based observations.

Figure 2: *Liometopum occidentale* ants. Picture By (c) Jonghyun Park, some rights reserved (CC BY) - https://www.inaturalist.org/photos/334116711, CC BY 4.0, https://commons.wikimedia.org/w/index.php?curid=179004252

Figure 3: (Left) *Liometopum occidentale* construct this carton-like structure inside their nests, incorporating bits of leaves and twigs into the structure. (Right) Accumulation of sawdust at the base of an ant nest tree as a result of excavation of the insides of the tree by ants.

Past field-based studies of *Liometopum occidentale* and their sister species, using manual observations, baits, and pitfall traps (Gulmahamad, 1995; Shapley, 1920a; Wang et al., 2010) have shed great insight into the behavior and ecology of these species. However, field-based studies are limited in their temporal resolution and require a great deal of human effort. Methods such as periodically checking pitfall traps every hour, manually counting ants in a defined radius, and manually timing ants to estimate their velocity, are limited in temporal range, usually day light hours only. While there are studies involving manual observation of ants at night, these are usually limited to a few nights per season. Commercially available camera traps, usually designed to be motion-triggered for the detection of larger animal species, do not offer the ability to take high resolution footage at close ranges. Go-pros have been used in some field based ant studies (Imirzian et al., 2019a), however, the energy demands for periodically spaced imaging over long periods require frequent battery swaps, making this an infeasible solution for long-term

monitoring. Chapter 3 introduces our custom open sourced, field deployable, multisensory camera trap, called the Ethocam. The Ethocam uses a Raspberry Pi W, a WittyPi for scheduled video capture, and contains sensors such as temperature, humidity, and light sensors. The WittyPi stays in an extremely low energy state when not in use and turns the Raspberry Pi and sensors on only at fully programmable scheduled times. This enables very low energy consumption, requiring a power bank sized 3.7V LiPo battery, that is also constantly being topped up using a solar panel and LiPo charger. The entire device can be enclosed in a weatherproof box and can be mounted on a tripod making it ideal for transportation and field work. The low cost, low energy consumption, easily available components, ease of configuration, and ease of adding or swapping sensors, make the Ethocam a useful addition to the very limited arsenal of field-based monitoring technologies for insects. In Chapter 3, we discuss the Ethocam in more detail and show proof of concept demonstrating its use, in combination with computer vision, to monitor the activity of *Liometopum* ants in the field.

The nest entrance, usually a hole or crevice in a tree, serves as an ideal vantage point to study the behavior of this ant species. Chapter 4 focuses on using the Ethocam, along with computer vision techniques, to collect and analyze video data from the entrance of multiple ant nests over an extended period of time. We programmed the Ethocam to take a 30 second video every hour (day plus night) and collected an extensive dataset from three ant nests along Chaney Canyon in the Angeles National Forest, collecting data for over 100 days between August and December 2024. We created a dataset by annotating

over 1500 ant tracks, resulting in ~45,000 point annotations across day and night conditions from the three nests. We compared a range of computer vision approaches for detection and tracking, and derived novel biological insights into the behavior and ecology of this native ant species. We characterized the circadian rhythm of *Liometopum*, documenting their nocturnal activity patterns and distinct outbound efflux at sundown. Using mixed effects models, we determined the effect of environmental variables and showed that, while ant count was primarily governed by circadian rhythm (time), ant walking speed was primarily governed by temperature. We quantified hourly and daily movement patterns via flux maps, revealing persistent spatial routing patterns in data collected over periods as long as 26 days. We developed a method to automatically identify prominent trails, which enabled analysis of the spatiotemporal dynamics of ant movement. We found that while some trials were used continuously across day and night, others were active primarily at nighttime hours. Along each trail, we analyzed directional biases between outbound and inbound movement. Although all trails exhibited bidirectional movement, the distribution of traffic across trails was non-uniform, with a greater number of inbound ants concentrated along a subset of trails. We postulated that the distinct trails may correspond to ants performing different activities, such as going down the tree to forage on the forest floor versus up the tree for aphid tending. Future experiments combining computer vision with colored baits distributed across the landscape could directly test this hypothesis and inform us of ant distribution patterns beyond those visible at the nest entrance. Finally, by training a binary classifier using a small, annotated dataset of excavating ants, we demonstrated that movement trajectory

information alone (path length, path curviness etc.) were sufficient to identify nest entrance specific behaviors. This result illustrates the potential of our system to study task partitioning and to connect the behavior of individuals to that of the colony as a whole.

Computer vision for studying insects, and insect decline

A unifying theme in this thesis is the use of computational tools such as computer vision, to help advance our understanding of insect behavior. I talked about the application of computer vision and image processing methods to accurately track the wing and head movements of fruit flies in lab settings using marker less pose estimation and edge detection. I also talked about the application of computer vision to detect and track thousands of individual ants at nest entrances in the field, where high density of ants, changing light conditions, and motion blur pose substantial challenges. Together, these case studies illustrate how automated video analysis can extend behavioral measurements beyond those feasible by manual observation, both in temporal duration and measurement precision.

Despite rapid advances in computer vision, widely used benchmark datasets for training and evaluation usually underrepresent insects at best. As a result, ready to use foundational models that require no training, often fail when applied to images and videos of insects, especially those collected in naturalistic settings. These models, trained on internet scale data, are usually outperformed by smaller models trained on domain

specific data. Progress on computer vision approaches for ecological analysis therefore requires not only algorithm innovation, but also the availability of datasets, capturing insects across scales and in naturalistic environments. Field-deployable systems like the Ethocam, can help bridge this gap, providing a pathway toward long term data collection that supports both biological discovery and the advancement of computer vision methods for analyzing insect behavior in the wild.

Recent long-term studies have raised alarm bells regarding the massive rates of decline of insect populations. A study in Germany using malaise traps to measure flying insect biomass, reported a 75% decline in insect biomass between 1989 and 2016 (Hallmann et al., 2017). Since then, many other studies have confirmed these numbers, with habitat loss to agriculture being recognized as one of the leading factors for insect decline (Outhwaite et al., 2022). Other factors include global warming, climate change and increasing frequency of natural disasters (Figure 4), use of insecticides, threat of displacement by introduced invasive species and more (Wagner et al., 2021). The loss of insects and the innumerable ecosystem functions they provide, poses an immediate threat to environmental stability.

Figure 4: The recent (2025) Altadena wildfires caused massive destruction to human property and natural habitats. One of the nests used in our study, nest 1, also known as beer tree by our lab, fell due to structural damage from the fire. Beer tree was a bay tree home to a large colony of ants. No ants were found in the vicinity post fire.

Proposed actionable steps to help address these trends range from large policy changes to small, local interventions. These include limiting the use of insecticides, spreading awareness, constructing corridors which could be as simple as small patches of native flowers, or a no lawn mowing zone in your backyard (Figure 5), and outreach events to improve public perception of insects and reduce the stigma that often surrounds them.

Addressing insect decline also requires a deeper understanding of insect behavior and ecology under natural conditions. Tools for long-term monitoring combined with

automated analysis methods offer a means to study insect activity at scales and resolutions that are difficult to achieve with traditional approaches.

Figure 5: The incredible diversity and abundance of insects can be seen all around us. All these pictures were taken in my backyard in Pasadena. Insects are everywhere; one just has to stop and look to appreciate their beauty.

C h a p t e r 2

THE ROLE OF HALTERE CAMPANIFORM SENSILLA ON EQUILIBRIUM REFLEXES OF THE FRUIT FLY, *DROSOPHILA MELANOGASTER*

The contents of this chapter are reproduced from

Tarun Sharma, Anne Sustar, Jaison Omoto, Michael H. Dickinson. "The role of haltere campaniform sensilla on equilibrium reflexes of the fruit fly, *Drosophila melanogaster*." In submission, 2026.

2.1 Introduction

Flying animals use a combination of sensory modalities to maintain stable flight in the face of external and internal perturbations. Although insects rely extensively on vision for this task, members of the order Diptera possess specialized mechanosensory organs called halteres, which contain hundreds of strain-sensing campaniform sensilla that encode forces on the base of the structures as they oscillate during flight. Although the importance of halteres for flight stabilization is supported by past experiments involving surgical ablation or artificial manipulation, the requirement of the campaniform sensilla themselves has yet to be directly demonstrated. We investigated the role of haltere campaniform sensilla in the fruit fly, *Drosophila melanogaster*, by using a collection of Gal4 driver lines which are expressed in different populations of campaniform neurons while recording the equilibrium responses of tethered flies subjected to rotation about their yaw axis. We show that the magnitude of the wing and head motor responses of

flies decrease linearly with increasing number of campaniform sensilla genetically silenced or ablated, providing direct evidence for the involvement of these mechanosensory structures in the detection of angular velocity during flight.

A defining characteristic of all dipteran species is the transformation of their hindwings into dumbbell-shaped organs called halteres, which oscillate at wingbeat frequency during flight. Halteres are mechanosensory organs, equipped with strain-sensing structures called campaniform sensilla, sensory bristles, and an internal chordotonal organ (Bolles Lee, A., 1885; Cole and Palka, 1982; Gnatzy et al., 1987; Leydig, Franz, 1860; Pringle, 1948). Most of the campaniform sensilla are packed together at the base of the halteres within a set of distinct fields and linear arrays (Agrawal et al., 2017; Hicks, 1856; Pflugstaedt, 1912). Based on their morphology, the campaniform sensilla are thought to be extremely sensitive to the direction of the strains experienced as the halteres oscillate (Fox and Daniel, 2008; Fraenkel and Pringle, 1938; Pringle, 1948). In 1714, William Derham described how flies exhibited downward spiraling shortly after takeoff if he removed their halteres with fine scissors (Derham, 1714). Since then, many investigators have confirmed the catastrophic consequences of haltere ablation (Braun, A., 1939; Buddenbrock, 1919; Dickinson, 1999; Fraenkel, 1939; Mureli and Fox, 2015; Pringle, 1948; Weinland, E., 1891). Previous studies have shown that tethered flies exhibit a haltere-mediated modulation of wing kinematics that is consistent with a compensatory stabilization reflex (Dickinson, 1999; Sherman and Dickinson, 2003). In addition to regulating wing kinematics (Dickinson, 1999; Faust, R, 1952; Nalbach, 1994; Schneider, G, 1953), halteres regulate compensatory head movements that stabilize gaze

during flight (Hengstenberg, 1984; Hengstenberg et al., 1986; Land, 1973; Schilstra and van Hateren, 1998; Tracey, 1975). Despite the extensive evidence for the role of halteres in these wing and neck motor reflexes, the direct involvement of the campaniform sensilla have never been demonstrated by targeted perturbation.

The high-amplitude oscillation of the haltere during flight results from the action of one asynchronous flight muscle in the third thoracic segment (Pringle, 1948) and a mechanical linkage that transmits strains generated by the flight musculature (Deora et al., 2015). Due to the complex means by which the halteres encode rotational motion via detection of Coriolis forces (Pringle, 1948), researchers have had to employ indirect means to investigate the role of the physiological properties of the campaniform sensilla. Electrophysiological recordings and behavioral measurements can be performed in tethered flying flies with intact motor systems (Yarger and Fox, 2018) or in preparations in which the haltere is artificially oscillated using mechanical actuators (Fayyazuddin and Dickinson, 1996; Fox and Daniel, 2008; Huston and Krapp, 2009). Additionally, iron filings may be glued to the haltere bulb, making it possible to perturb haltere kinematics using a magnetic field (Rauscher and Fox, 2021). These techniques have provided critical insights into the encoding properties of the haltere (Fox and Daniel, 2008; Fox et al., 2010; Yarger and Fox, 2018), enabling exploration of the full dynamic range of stimulus-response relationships. However, performing such recordings under conditions that expose the haltere to gyroscopic forces that would arise during body rotations remains technically challenging. Moreover, external probes cannot easily replicate the time course or magnitude of the inertial and gyroscopic forces experienced during natural flight

(Nalbach, 1993; Pringle, 1948), and may impose mechanical stresses on the haltere that are not present during the natural oscillations. Further, unless each neuron is carefully filled and mapped after recording, it is not possible to determine which sensilla the recorded cells innervate. In his classic 1948 paper, Pringle attempted to circumvent these limitations by oscillating the haltere of a blowfly via electrical stimulation of its asynchronous flight muscle, while simultaneously oscillating the entire experimental apparatus to create the Coriolis forces experienced during rotation and recording compound action potentials in the haltere nerve. However, even this method did not fully replicate the natural motion of the halteres because the animals were not flying and thus the linkage system from the wing muscles was not active. Further, Pringle's electrophysiological recordings of the entire haltere nerve are difficult to interpret. In particular, it is not possible to correlate the activity of any specific group of campaniform sensilla to body rotation around a particular axis (i.e. yaw, pitch, and roll).

In *Drosophila*, the base of each haltere contains approximately 140 campaniform sensilla distributed among 5 fields (Cole and Palka, 1982). Sensilla within any given field share roughly the same anatomical orientation and are thought to respond maximally to strains within the cuticle along a specific direction (Fraenkel and Pringle, 1938). Previous researchers have postulated that the organization of campaniform sensilla into distinct fields may enable the simultaneous detection of multiple force components resulting from gravity, linear acceleration of the fly, acceleration of the haltere relative to the fly body, as well as the angular velocity and angular acceleration of the fly's body (Nalbach, 1993; Pringle, 1948). Using a simplified model of an oscillating mass subject to rotation,

Pringle showed that the Coriolis force, which is linearly proportional to the angular velocity of the fly's body, is the dominant force component acting perpendicular to the plane of oscillation, thus providing a means by which the fly might discriminate them from the much larger 'primary forces' (Pringle, 1948), which act within the plane of oscillation. Pringle also suggested that one campaniform field (dorsal field 2, dF2) and the large chordotonal organ are particularly well suited to detect deflections lateral to the stroke plane and thus might encode the Coriolis forces. This specialization of dF2 has received some experimental support, in that the campaniforms from this field make fast electrical synapses with a motor neuron of a steering muscle (the first basilar, b1) that regulates stroke amplitude (Fayyazuddin and Dickinson, 1996; Trimarchi and Murphey, 1997). However, a recent study using functional imaging methods to record activity in the dorsal campaniform fields challenged this hypothesis by showing that dF2 exhibits sustained activity during tethered flight, a condition under which Coriolis forces should be absent (Verbe et al., 2024).

Evidence suggests that by encoding both the large primary forces and small Coriolis forces, the haltere could serve two roles during flight: (1) a gyroscope to detect the angular velocity of the body, and (2) a clock for tuning the firing phase of wing steering muscles (Dickerson et al., 2019). If this new dual function hypothesis is correct, then cutting off the haltere bulb or stalk would disrupt both the gyroscopic and clock functions. Whereas the knowledge gained by many prior studies relying on ablation of one or both halteres has been extremely informative, their interpretation would benefit from alternative approaches under conditions in which the structure is mechanically

intact and oscillating via the action of its endogenous motor system. In this study, we attempt to achieve these conditions by manipulating populations of campaniform sensilla and subjecting intact flying flies to rotational stimuli with comparable speeds to previous literature (Dickinson, 1999; Hengstenberg, 1984; Sherman and Dickinson, 2003), while also recording the compensatory responses of the wing and neck motor systems simultaneously. Although hardware limitations prevented us from delivering rotational stimuli matching the peak magnitudes experienced during free flight (which can reach 1500 deg sec-1; (Tammero and Dickinson, 2002)(also see (Muijres et al., 2014; Schilstra and Van Hateren, 1999), our setup elicited robust compensatory wing and head responses sufficient to assess the effects of manipulating campaniform sensilla. We employed complimentary genetic strategies for assessing loss of function of campaniform neurons: (1) silencing using the inhibitory ion channel Kir2.1 (Baines et al., 2001) and (2) ablation using the pre-apoptotic genes, hid and reaper (Goyal et al., 2000). The value of using of multiple strategies for manipulating neurons is highly recommended in *Drosophila* due to heterogeneity in cell physiology and development (Simpson, 2009). Further, this dual approach was beneficial because as certain combination of driver and responder line did not yield viable adults. We found a negative correlation between the number of campaniform sensilla either silenced or ablated and the amplitude of the equilibrium responses of the head and wing motor systems, thus providing evidence for the direct involvement of these sensory cells in the equilibrium responses mediated by the halteres.

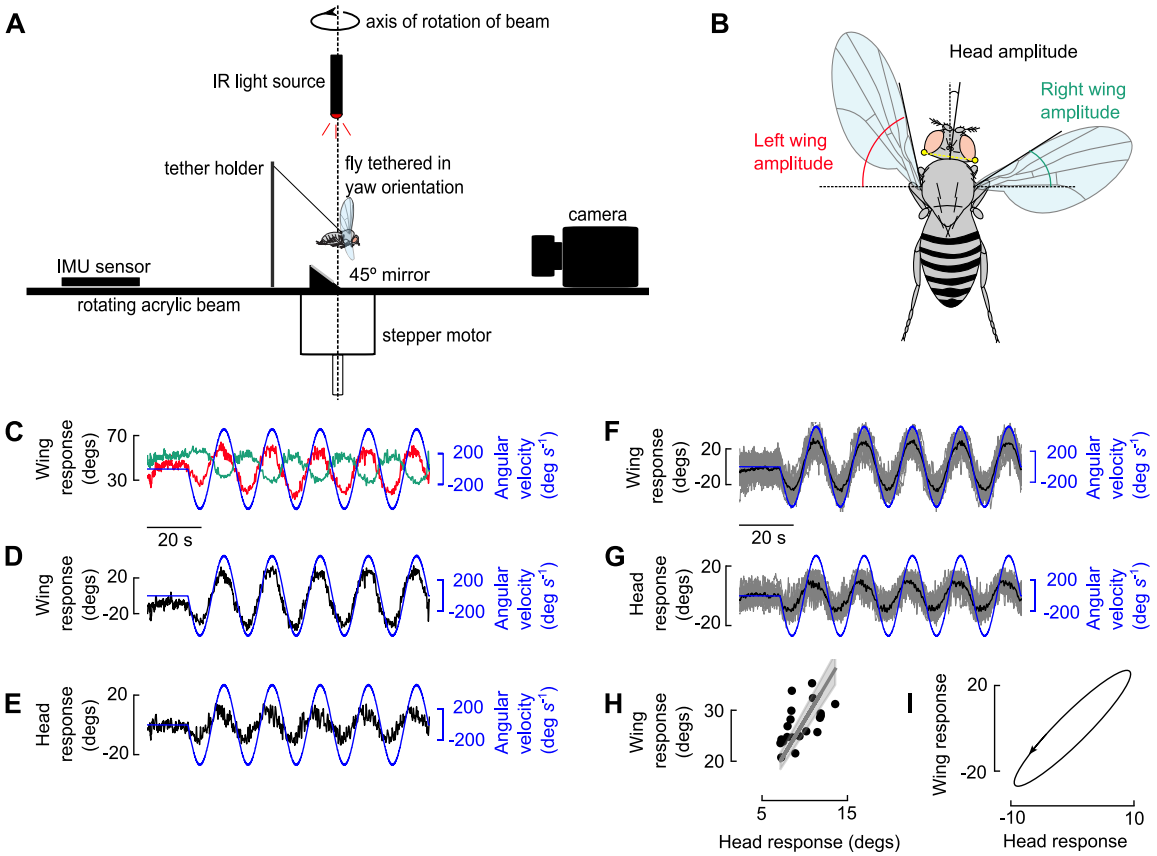

Figure 1. Control flies display wing and head equilibrium responses when subjected to mechanical rotation. (A) Experimental apparatus. The beam is rotated using a servo motor and a tethered fly is positioned such that the axis of rotation passes through its anatomical yaw body axis. (B) Measures of left and right wing beat amplitude and head yaw amplitude. Points tracked using DeepLabCut are shown in yellow. (C) Left (red) and right (green) wing amplitudes for an example fly plotted against angular velocity (blue) of the rotating acrylic beam over three trials of 5 sinusoidal rotations each. (D) Left minus right wing beat amplitude for data shown in C. (E) Head yaw response for the fly in C. (F) Wing response for all control flies (n=20, empty-Gal4 crossed with Kir2.1) with grand mean in black. (G) Head yaw amplitude for the control flies. (H) Mean wing response plotted against mean head response for all control flies (n=20). For the regression line, wing response = 1.13 * (head response) + 16.54. (I) Lissajous figure showing phase difference between the wing and head response averaged across all control flies.

2.2 Methods

Animals

For each genotype, we collected data from 3-to-5-day-old female flies raised on cornmeal medium at 25^{o}C on a 12:12 light dark cycle. For tethering, we anaesthetized flies on a 4^{o}C cold plate before removing their pro- and meso-thoracic legs near the trochanter so they would not interfere with wing tracking by our machine vision system. Flies were tethered to a fine tungsten pin using a drop of UV curing glue (Bondic) and allowed to rest at least 30 min prior to an experiment. If flies stopped flying during an experimental session, we gave them a brief puff of air to reinitiate flight.

We identified 72 candidate Gal4 driver lines in the FlyLight database (Jenett et al., 2012) that showed expression in the haltere nerve. After acquiring the stocks, each line was crossed to UAS-GFP to confirm expression in haltere neurons. Based on our own confocal imaging, we judged 62 of the lines to be too faint or not specific enough for use. Unfortunately, one line (R94C04) was lost from our lab stock and was no longer available from either Janelia or the Bloomington Stock Center. Thus, our analysis was based on 9 lines that predominantly target haltere afferents and minimally target wing afferents. To determine the number and peripheral positions of the campaniform sensilla targeted, we crossed in each line with UAS-mCD8-GFP; UAS-RedStinger and imaged the halteres on a confocal using a combination of fluorescent and bright field imaging (Fig. 2C-E). Mounting halteres so that the anteroposterior axis was parallel to the image plane enabled us to view longitudinal sections of the sensory dendrites (Fig. 2C), whereas mounting them so that the dorsoventral axis was parallel to the image plane provided a

view of the dendritic cross-sections near the campaniform domes (Fig. 2D). In the dorsoventral view, we counted neurons only if the GFP-labelled dendrite was clearly connected to a dome (visible in bright field) and DsRed-labelled cell body. In the anteroposterior preparations, the regions of the cuticle where horizontal projections were originating from was used to determine the field targeted. Using these guidelines, two independent observers (Tarun Sharma, Anne Sustar) counted the number of sensilla labeled in each image stack and marked their location within the haltere fields in three preparations for each line (Table 1), thus generating the anatomical maps shown in Fig 2E.

We performed a loss-of-function analysis of the haltere campaniforms by crossing the 9 driver lines with either Kir2.1.eGFP to drive expression of an inward rectifying potassium channel (Baines et al., 2001) or reaper-hid to drive expression of the pre-apoptotic genes (Goyal et al., 2000). Unfortunately, four of the crosses of did not yield viable adults: GMR74B09 x UAS-Kir2.1, GMR17G01 x UAS-rpr,hid, GMR58F02 x UAS-rpr,hid, and GMR14B04 x UAS-rpr,hid. For controls, we crossed either UAS-Kir2.1 or UAS-rpr,hid with a so-called ‘empty Gal4’ line (Bloomington 68384) that contains the same vector and insertion site as the campaniform driver lines but lacks a necessary regulatory fragment (Pfeiffer et al., 2008).

Experimental Apparatus

Figure 1A shows our experimental setup for subjecting flies to mechanical rotation, consisting of a spinning acrylic beam equipped with an inertial measurement unit

(Adafruit BNO055), a holder for placing the tethered fly, a 0.13 mm mirror placed at a 45 deg angle (Thor Labs, H45a), a camera and lens for tracking wing and head motion (PointGrey BFLY-U3-05S2C-CS; InfiniStix 94mm 0.5x lens), and a custom-made infrared backlight (https://github.com/willdickson/ring_light_17mm_id_1_row_18_led). The beam was mounted to a servo motor (Teknic Clearpath CPM-SDSK-3432S-ELN) and controlled using custom Python code interfacing with a microcontroller running the GRBL library (https://github.com/gnea/grbl). The cables of all electronic components passed through a set of slip rings (Senring SNU11-0210) so that the rotating beam could spin continuously. The entire setup was enclosed in a large black box and covered with a thick black cloth to exclude rotational cues based on optic flow. We programmed the beam to follow a sinusoidal angular trajectory that reached a programmed maximum velocity in one direction, slowed to a rest, and then rotated in the opposite direction. Each fly was tethered and placed such that it was subjected to rotation perpendicular to its longitudinal body axis, i.e. through the anatomical yaw axis of the fly. Although fruit flies do not typically orient their body axis horizontally when they fly (David, 1978), we chose a yaw vector that was normal to the animal's longitudinal axis as this orientation has been shown to generate strong behavioral responses (Dickinson, 1999). A trial began with a 15-s baseline period with no rotation followed by 5 cycles of the sinusoidal motion reaching a maximum angular velocity of 350

deg s^{-1}, followed by a 15-s rest interval and then another 5 cycles of sinusoidal motion reaching a maximum angular velocity of 500 deg s^{-1}. This entire sequence was repeated

three times for each fly. The inertial measurement unit captured the angular velocity of the rotating beam. Between flies, we alternated the starting direction of rotation.

Data analysis

We used a previously described IR machine vision system called *Kinefly* (Suver et al., 2016) to track wing motion from a backlit camera image of the fly sampled at 30 frames s^{-1}. Left and right wingbeat amplitude, angular velocity, and the raw image frames were recorded using the bagfile format in ROS (Robot operating system, https://www.ros.org/), and then subsequently converted into hdf5 and avi files for efficient data accessibility. To quantify head yaw, we used DeepLabCut (Mathis et al., 2018) to track the two edge points on the back of the head capsule as shown in Fig. 1B. We calculated head yaw on a per frame basis by determining the slope of a line joining two points on the posterior edge of the head capsule. Left wingbeat amplitude, right wingbeat amplitude, head yaw angle, and the angular velocity of the apparatus were resampled to a common rate of 72 Hz. Data were averaged over the three trials of each fly and conditioned with an off-line, zero phase, 5^{th}-order lowpass Butterworth filter. The sign of data from experiments in which the initial direction of rotation was in the anticlockwise direction was flipped by multiplying head yaw, angular velocity and wingbeat amplitude traces by –1. For each fly, we determined mean response waveforms for the wings and head by averaging across the 5 stimulus cycles and 3 trials. The amplitude of the left minus right wingbeat amplitude and the head yaw responses were then determined by using a Fourier transform. To quantify the change in amplitude for individual wings, we subtracted the

pre-stimulus baseline from the mean response of each wing and measured the average wing amplitude in 1-s windows at the peaks of angular velocity. To estimate the variation within the results from a given genotype, we used bootstrapping (10000 iterations with replacement) to calculate the mean and 95% confidence intervals. For brevity, we only show data from the fastest of our two rotational speeds (maximum velocity 500 deg s^{-1}), because the behavioral responses were larger under this condition.

Statistics

We used a Mann-Whitney U rank test to test for differences among genotypes because the relevant data were not normally distributed. A Bonferroni correction was used to correct for multiple comparisons. We used an ordinary least squares method to perform linear regression on the amplitude of the wing and head responses and the number of campaniform sensilla perturbed.

Data and code

Code along with documentation can be found here – https://github.com/tarunsharma1/haltere_campaniform_data_analysis. Per fly behavioral data can be found at https://drive.google.com/file/d/1d4FBP9NVpkOE-AwK88oRjoqHghT36-bw/view?usp=sharing

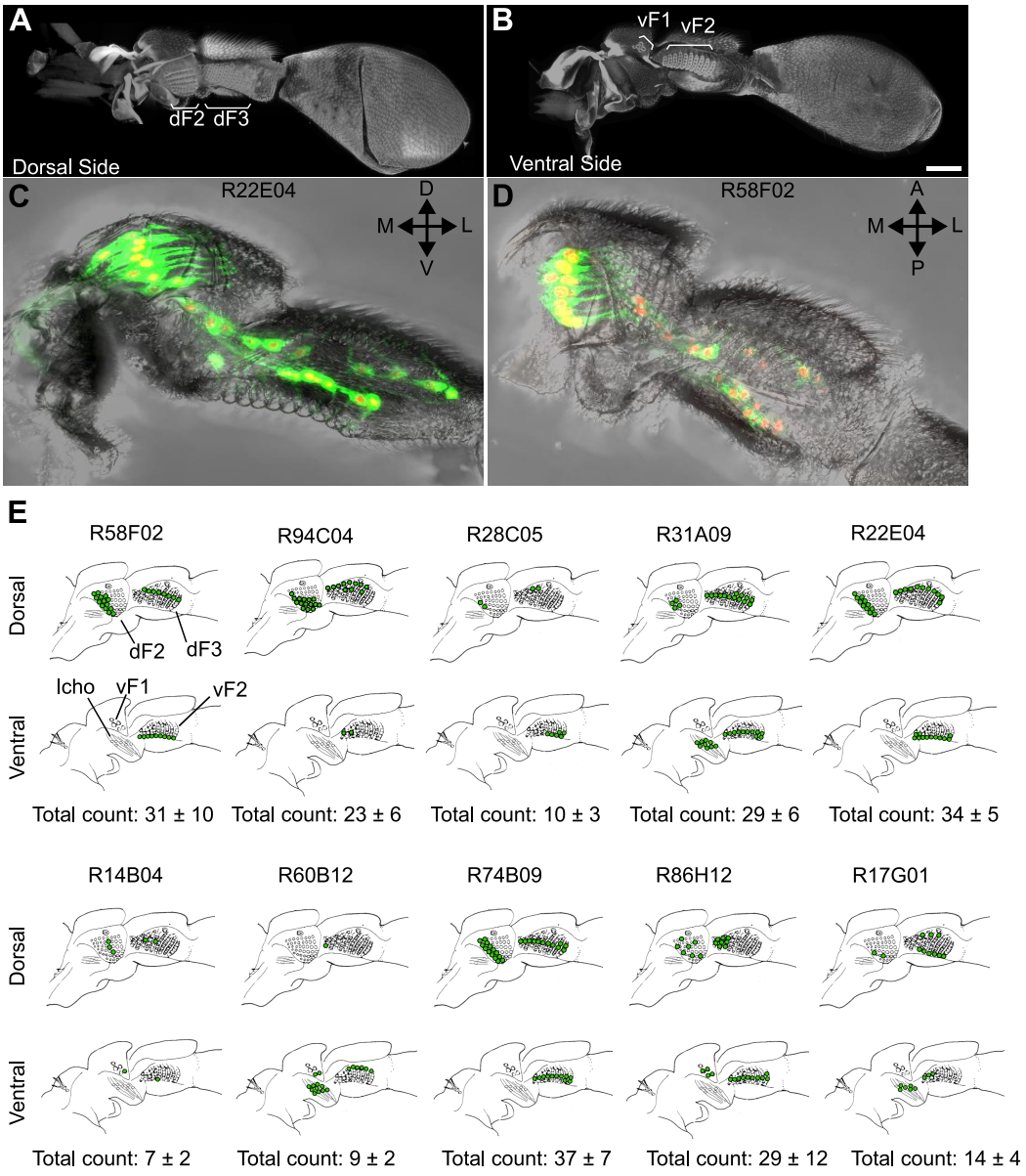

Figure 2. Expression patterns of Gal4 driver lines in campaniform fields. (A, B) Confocal images of a fly haltere using cuticular autofluorescence with dorsal (A) and ventral (B) campaniform fields labeled. (C) R22E04 mounted with anterior side toward the reader. (D) R58F02 mounted with dorsal side toward the reader. Z-projections of membrane-targeted GFP and nuclear-targeted DsRed expression in campaniform neurons are superimposed with a brightfield image showing the domes. Areas of yellow are overlapping regions of membrane GFP and DsRed. Such images were used to map the spatial expression patterns of each line (Table 1). (E) Schematized summary of expression data from all lines tested. Large chordotonal organ is marked as lcho.

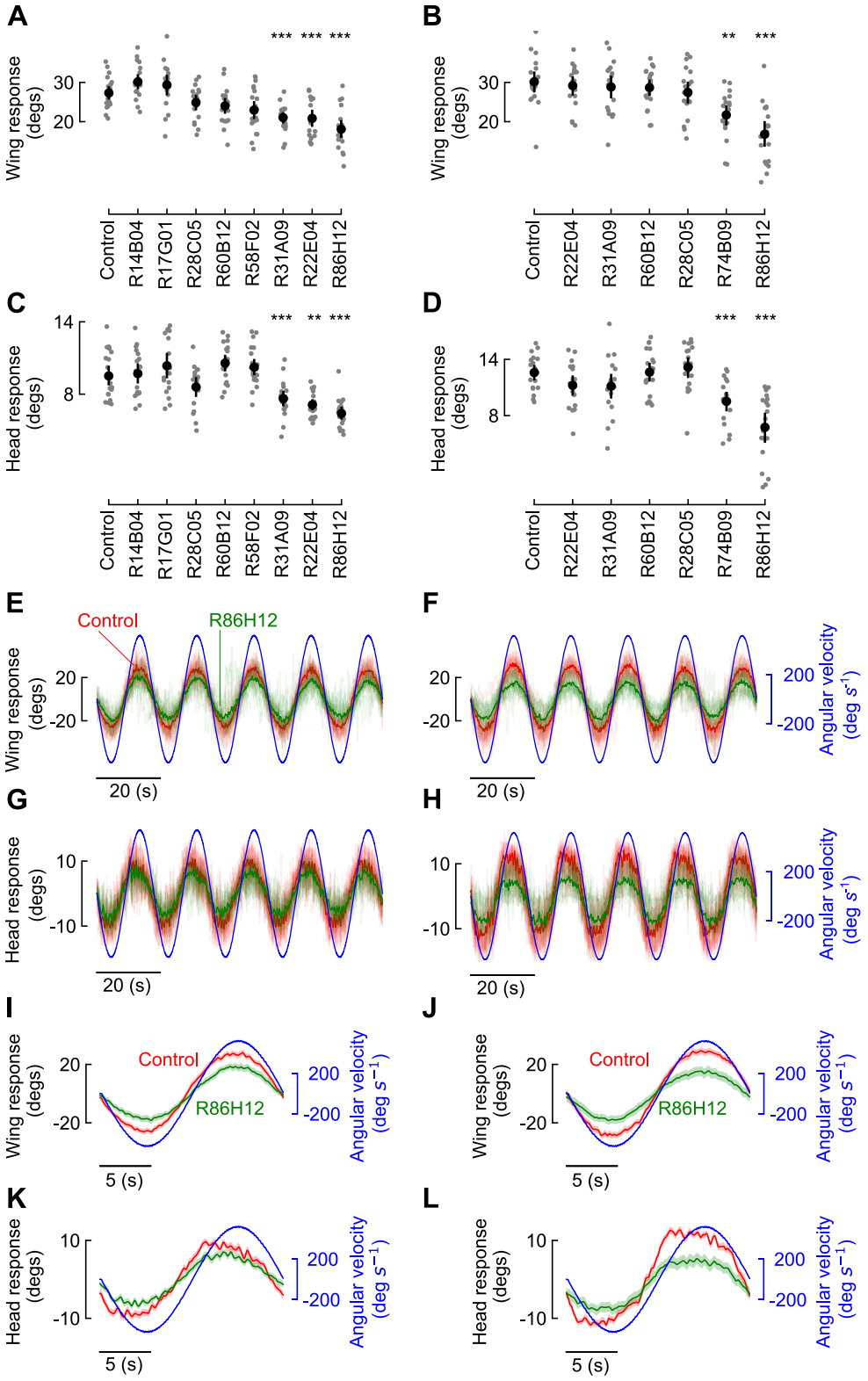
A
B
C
D
E
F
G
H
I
J
K
L
Wing response (degs)
Head response (degs)
Angular velocity (deg s^{-1})
Control
R14B04
R17G01
R28C05
R60B12
R58F02
R31A09
R22E04
R86H12
R74B09
20 (s)
5 (s)
***
**

Figure 3. Genetic silencing and ablation of haltere campaniforms reduces the magnitude of wing and neck motor responses to body rotation. (A, B) Wing responses (n=20, 18, 21, 19, 19, 19, 18, 19, 19 flies respectively) using UAS-Kir2.1 (A) or (n=20, 19, 20, 19, 19, 18, 19 flies respectively) UAS-rpr,hid (B); driver lines sorted by descending wing response magnitude and controls to the left. (C, D) Head yaw responses for individuals in (A) and (B) respectively, sorted by their wing response magnitudes. All plots start at 0. Asterisk indicates level of significance- *: $p<0.05$, **: $p<0.01$, ***: $p<0.001$. (E,F) Raw data for n=19 flies of driver line R86H12 (green) crossed with UAS-Kir2.1 and UAS-rpr,hid respectively, plotted with their respective empty vector controls (n=20 flies for each in red), along with mean traces across flies, and angular velocity of the rotating beam. (G,H) As in E and F, but showing data for head response. (I, J) Mean left minus right wing response over 5 cycles along with 95% confidence interval for n=19 flies of the driver line R86H12 crossed with UAS-Kir2.1 and with UAS-rpr,hid, respectively, plotted with their respective empty vector controls (n=20 flies for each) and angular velocity of the rotating beam. (K, L) As in I and J, but showing data for head response.

2.3 Results

Compensatory equilibrium reflexes of wing and head motor systems

In response to imposed sinusoidal rotation about their anatomical yaw axis, control flies (empty-Gal4 x UAS-Kir2.1) modulated their left and right wingbeat amplitudes in a compensatory fashion (Fig. 1C), consistent with prior studies (Dickinson, 1999; Sherman and Dickinson, 2003).

As expected, the time course of the difference in left and right wingbeat amplitudes was roughly sinusoidal in response to a sinusoidal modulation of angular velocity (Fig. 1D). We quantified the behavior by determining the amplitude of a sine wave fit to the animal's response at the frequency of the stimulus (Fig. 1D). The behavioral responses were robust and consistent across flies (n=20).

As has been shown previously in blowflies (Hengstenberg, 1984; Hengstenberg et al., 1986; Nalbach and Hengstenberg, 1994), *Drosophila* exhibited compensatory head movements in response to body rotation about the yaw axis (Fig. 1E, G; n=20). We

quantified these angular changes in head motion in the same manner as the wings, by fitting sine functions to the data from each fly averaged over 15 stimulus presentations (3 trials of 5 rotation cycles). Figure 1H shows the wing responses plotted against corresponding head responses for the population of control flies (n=20). We observed a linear relationship (slope = 1.13, $p<0.05$, 95% CI = [0.27, 1.98]; Pearson r = 0.55, $p<0.05$) between responses of the two motor systems. The measured behavioral responses led the angular velocity stimulus by average phases of -6.3°, (95% CI =3.8° to 8.8°) and -27.1° (95% CI = 25.2° to 28.8°) for the wing and head responses, respectively. Thus, the wing responses led the head responses by 20.8° (95% CI =19° to 22.3°).

The fact that the responses of the wing and head motor systems both led the sinusoidally varying stimulus is consistent with the known physiological characteristics of campaniform sensilla. Recordings from individual campaniform sensilla on cockroach legs (Chapman and Duckrow, 1975) and fly wings (Dickinson, 1990) exhibit phase leads in response to a sinusoidal stimuli. As first shown by Chapman and Smith, insect mechanoreceptors that exhibit a slowly or rapidly adapting response to a step deformation also exhibit a phase advance to sinusoidal stimuli, and both phenomena are accurately predicted by a single transfer function (Chapman and Smith, 1963). Given that the compensatory responses driven by the halteres are mediated by campaniform neurons, the phase leads in behaviors that we observed were expected. Hengstenberg also noted that this phase lead in his study of haltere input to the head motion responses of blowflies (Hengstenberg, 1988).

Expression screen of haltere campaniform sensilla driver lines

Indicative of the complex genetic regulatory networks that underly neuronal identity, the different driver lines we used labeled an assortment of campaniform neurons across fields. However, the expression patterns were consistent within each line, with sensilla labeled at the same location within campaniform fields (Fig. 2E). Unfortunately, we did not identify driver lines that labeled all the campaniform sensilla within any of the 5 previously defined fields, which limited our ability to assess the contribution of individual fields to equilibrium responses. However, the lines did vary significantly with respect to the number of campaniform neurons targeted (Table 1), which allowed us to test the influence on the gross number of sensilla contributing to the wing and head equilibrium responses.

Genetic silencing or ablation of haltere campaniform sensilla diminishes the amplitude of wing and head equilibrium reflexes

To investigate the role of haltere campaniform sensilla in the compensatory reflexes, we drove expression of two genetic loss-of-function reagents, the inwardly rectifying potassium channel, Kir2.1 (Baines et al., 2001), and two pre-apoptotic genes, reaper and hid (Goyal et al., 2000). We tested all successful crosses using the same experimental paradigm as described for control flies (Fig. 3A-D; n=18-20 flies per genotype, exact numbers in figure legend). The amplitude of wing and head responses for the genetic controls and each of the driver lines expressing Kir2.1 are shown in Fig. 3A and Fig. 3C, with the driver lines sorted according to wing response magnitude and controls to the left.

The corresponding wing and head behavioral responses with reaper and hid expression are shown in Fig. 3B and Fig. 3D, also sorted according to response magnitude. We observed no differences in the baseline wingbeat amplitudes across different genotypes prior to the onset of the rotational stimulus. The change in the amplitude of the equilibrium responses did, however, vary across the different driver lines. We observed a strong correlation between the wing and head responses across all the genotypes tested; every loss of function manipulation that led to a statistically significant reduction in the wing response also yielded a statistically significant reduction in the head response. For the lines crossed to UAS-Kir2.1, R22E04 (wings, $p < 0.001$; head, $P < 0.001$), R31A09 (wings, $p < 0.001$; head $p < 0.01$) and R86H12 (wings, $p < 0.001$; head, $p < 0.001$) showed statistically significant differences in both wing and head responses compared to controls. For the lines crossed to UAS-rpr,hid, R74B09 (wings $p < 0.01$; head, $p < 0.001$) and R86H12 (wings, $p < 0.001$; head, $p < 0.001$) showed statistically significant differences in both wing and head responses. Crossing either loss-of-function reagent with R86H12 generated the strongest reduction in both the wing and head equilibrium responses (Fig. 3A-D; Green in 3E-L).

Across genotypes screened, we observed a linear relationship between the total number of campaniform sensilla silenced using Kir2.1 and the amplitude of both the wing and head responses, suggesting a causal role for campaniform sensilla in the compensatory reflexes (Fig. 4A: slope = -0.24, $p< 0.001$, 95% CI = [-0.30, -0.18], Pearson r = -0.49, $p<0.001$; Fig. 4C: slope = -0.07, $p<0.001$, 95% CI = [-0.09, -0.04], Pearson r = -0.38, $p<0.001$). We found a weaker linear trend in case of reaper, hid for both the wing (Fig.

4B: slope = -0.17, $p<0.001$, 95% CI = [-0.25, -0.09], Pearson r = -0.31, $p<0.001$) and head response (Fig. 4D: slope = -0.10, $p<0.001$, 95% CI = [-0.14, -0.07], Pearson r = -0.43, $p<0.001$). We did not see an effect of number of campaniforms silenced on wing or head phase values when using hid-reaper or Kir2.1 (t test for slope of a line fitted to phase against number of campaniform silenced, $p>0.05$ for head, wing for hid-reaper and head for Kir2.1; $p=0.02$; $R^2=0.03$ for wing phase in the case of Kir2.1 implying a very weak effect size). The responses of both the outside wing (which increased in amplitude), and the inside wing (which decreased in amplitude) exhibited linear changes with increasing numbers of campaniform neurons ablated or silenced: Kir2.1 (outside wing), slope = -0.097, 95% CI = [-0.141, -0.052], $p<0.001$; Kir2.1 (inside wing): slope = -0.127, 95% CI = [-0.176, -0.078], $p<0.001$; reaper-hid (outside wing): slope = -0.0763, 95% CI = [-0.132, -0.020], $p<0.01$; reaper-hid (inside wing): slope = -0.0743, 95% CI = [-0.124, -0.025], $p<0.01$). These results indicate that reducing haltere feedback affects both increases and decreases of wingbeat amplitude.

When data from flies of all driver lines were pooled, we observed a strong correlation between the wing and head responses (Fig. 4E, Kir2.1: slope = 1.62, $p<0.001$, 95% CI = [1.26, 1.98], Pearson r = 0.59, $p<0.01$ for; Fig. 4F, reaper,hid: slope = 1.56, $p<0.001$, 95% CI = [1.27, 1.86], Pearson r = 0.7, $p< 0.001$). These correlations within the loss-of-function experiments did not differ from those measured in control flies (Fig. 4E, Kir2.1: slope = 1.13, $p<0.05$, 95% CI = [0.27, 1.98], Pearson r = 0.55, $p<0.05$: Fig. 4F, reaper,hid: slope = 2.08, $p<0.01$, 95% CI = [0.89, 3.27]; Pearson r = 0.65, $p<0.01$).

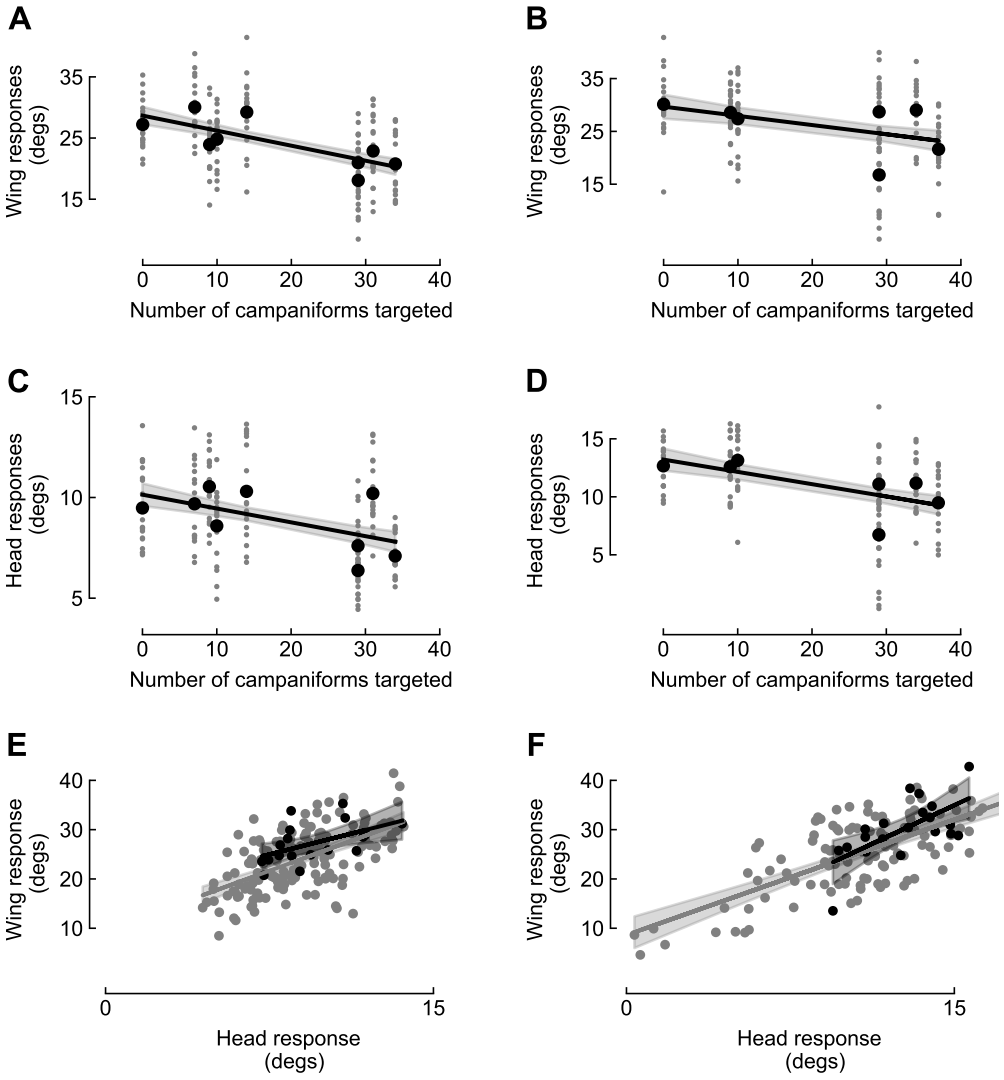

Figure 4. Linear relationship between number of campaniforms targeted and wing response. (A, B) Wing response of individual flies per driver line (small gray dots) and bootstrapped means (black dots) plotted against number of campaniform sensilla targeted in each driver line using UAS-Kir2.1 (n = 172 flies) (A) or UAS-rpr,hid (n = 134 flies) (B) as the effector line. For the regression in A, wing response = -0.24 * (number of campaniform silenced) + 28.66. For the regression in B, wing response = -0.17 * (number of campaniform ablated) + 29.68. (C, D) Head responses of flies in (A, B). For the regression in C, head response = -0.07 * (number of campaniform silenced) + 10.14. For the regression in D, head response = -0.10 * (number of campaniform ablated) + 13.21 (E, F) Wing response plotted against head response for control flies (black dots) and of all other genotypes pooled together (gray dots) along with lines of best fit for UAS-Kir2.1 (E) and UAS-rpr,hid (F) data. For regressions in E, wing response = 1.13 * (head response) + 16.54 for controls (black), wing response = 1.62 * (head response) + 9.5 for all other genotypes (gray). For regressions in F, wing response = 2.08 * (head response) + 3.73 for controls (black), wing response = 1.56 * (head response) + 8.62 for all other genotypes (gray).

2.4 Discussion

In this study, we investigated the role of campaniform sensilla at the base of the halteres in the equilibrium responses elicited by rotation about the yaw axis. Using a new experimental setup, we confirmed the results of prior studies that flies execute robust wing and head equilibrium reflexes in response to body rotation (Fig. 1F, G). By using a genetic approach, we were able to silence or ablate sensory neurons on the haltere without physically damaging the structure or its ability to oscillate during flight. We observed that the magnitude of the wing and neck motor responses decreased with the total number of campaniform afferents silenced via expression of the inward rectifying potassium channel, Kir2.1 (Fig. 4A). We also found a linear correlation between the magnitude of the compensatory reflexes of the wing and head motor systems, suggesting that the two motor reflexes are mediated by the same distributed population of haltere campaniforms. We observed similar results when we attempted to genetically ablate the cells using the pro-apoptotic genes hid and reaper, although the effect was weaker (Fig. 4B) and two of the crosses did not yield viable adults. Although it is difficult to ascertain the reason for the observed differences between the two loss-of-function reagents, the mechanism of action and/or possible differences in efficacy due to the genomic location of the relevant constructs may have been factors (Pfeiffer et al., 2010). Further, the success rate of the two reagents likely depends on the specific driver line and the specific cells that are targeted. Nevertheless, the data demonstrate that campaniform loss-of-function leads to a diminishment of head and wing equilibrium responses.

Role of individual campaniform fields

Based on its lattice-like morphology, Pringle argued that only one particular campaniform field, dF2, was well suited for discriminating the tiny lateral force components generated by the Coriolis effect from the much larger tangential and radial force components present during oscillation (Nalbach, 1993; Pringle, 1948). He further argued that dF3 and vF2 are well positioned to detect the large primary forces caused by oscillation of the haltere. However, a recent study shows that the dF2 field is continuously active during tethered flight when the Coriolis forces on the halteres should be absent (Verbe et al., 2024), which is inconsistent with Pringles' hypothesis. To elucidate the contributions of individual fields to the equilibrium responses, a regression analysis could be conducted with wing or head response as the dependent variable and the number of cells targeted per field as the independent variables. However, to ensure sufficient statistical power, this would require additional driver lines targeting distinct campaniform distributions beyond those currently available in our collection, as well as a more detailed quantification of the precise number and identity of the campaniforms targeted in each individual.

It would also be helpful, but laborious, to map the campaniforms targeted in each individual fly tested. It is possible that the encoding properties and function of individual campaniform sensilla may vary within a particular field. According to results from the blowfly, *Calliphora vicina*, the central projections of campaniform neurons vary with respect to the position of their domes within the sensilla arrays (Chan and Dickinson,

1996). A recent connectomic analysis revealed that campaniform neurons form five morphologically and synaptically distinct clusters (Dhawan et al., 2025), a number roughly equivalent to the number of sensilla fields at the base of the haltere. However, the neurons within each of the clusters defined by the connectome do not originate from individual campaniform fields, but rather exhibit a distributed pattern. Thus, the logic by which the peripheral location of the haltere campaniform neurons relates to their function in equilibrium reflexes remains enigmatic. Despite the parsimonious nature of Fraenkel and Pringle's original hypothesis (Fraenkel and Pringle, 1938), more recent evidence supports an alternative scenario in which the campaniform neurons sensitive to Coriolis forces are distributed across multiple fields (Dhawan et al., 2025; Verbe et al., 2024). Future behavioral analyses guided by morphological subtypes within and across fields may be necessary to identify the spatial encoding logic underlying flies' equilibrium responses. Another challenge is disentangling the phenotypic consequences of campaniform perturbation attributable to the putative role of the haltere as a clock and gyroscope. Given the dual role of the haltere in both encoding angular velocity via Coriolis forces and providing precise timing signals for tuning motor neuron activity, we are currently unable to determine the relative effect of our manipulations of campaniform activity on these two functions (i.e. gyroscope vs. clock). The availability of large, densely reconstructed connectomic datasets that preserve topological information from the campaniform fields to the central nervous system will likely inform how afferent projections distribute to downstream networks.

Relationship between wing and head responses

The results of our study demonstrate a strong correlation between the amplitudes of wing and head equilibrium responses across flies (Fig. 4). The driver lines that, when silenced or ablated, have a significantly impact on wing responses also have a strong effect on head responses. In principle, if the driver lines we tested targeted campaniform sensilla that were specialized for either the head or wing equilibrium responses, then one might observe a deviation from the trend we observed in Fig. 4C, D. The fact that we did not observe such a deviation suggests that the two motor reflexes are mediated by the same distributed population of haltere campaniforms. In summary, we have provided the first evidence for the direct involvement of campaniform sensilla at the base of the haltere in the wing and head equilibrium response of *Drosophila melanogaster*. These experiments provide a proof of concept for a method to investigate the role of the campaniform sensilla on the haltere using a behavioral setup, whereby the haltere is oscillating under the action of its own endogenous motor drive, and genetic toolkit available in *Drosophila*. We expect that the future availability of specific driver lines targeting subclasses of sensilla, or downstream interneurons, will soon make it possible to test the role of these cells in the head and wing equilibrium response along different axes.

Driver line	dF2	dF3	vF1	vF2	Chordotonal
R28C05	2 ± 1	2 ± 1	0 ± 0	6 ± 1	0 ± 0
R60B12	0 ± 0	1 ± 1	2 ± 0	6 ± 1	10 ± 0
R31A09	4 ± 2	14 ± 1	0 ± 0	11 ± 3	9 ± 1
R74B09	14 ± 2	12 ± 1	0 ± 0	11 ± 4	0 ± 0
R58F02	14 ± 5	8 ± 2	0 ± 0	9 ± 3	0 ± 0

R22E04	11 ± 2	11 ± 1	0 ± 0	12 ± 2	0 ± 0
R14B04	3 ± 0	2 ± 1	1 ± 1	1 ± 0	0 ± 0
R86H12	7 ± 5	8 ± 3	4 ± 1	10 ± 3	0 ± 0
R17G01	2 ± 1	9 ± 2	0 ± 0	3 ± 1	6 ± 2

Table 1. Number of targeted neurons for multiple driver lines in each haltere campaniform field and the chordotonal organ. Counts are rounded averages of two independent observers averaged over 3 flies per driver line. Ranges in counts across 3 flies is also shown.

Chapter 3

MONITORING SOCIAL INSECT ACTIVITY WITH MINIMAL HUMAN SUPERVISION

The contents of this chapter are reproduced from

Tarun Sharma, Julian M Wagner, Sara Beery, William B Dickson, Michael H Dickinson, Joseph Parker. (September 2024). "Monitoring Social Insect Activity with Minimal Human Supervision." 2024 IEEE/CVF Conference on Computer Vision and Pattern Recognition Workshops (CVPRW). DOI: https://doi.org/10.1109/CVPRW63382.2024.00131.

Citation format has been modified for the sake of consistency across the thesis.

3.1 Introduction

Tracking the behavior of animals and their group dynamics in nature offers a crucial look into the delicate ecological networks that compose wildlife diversity. The velvety tree ant (*Liometopum occidentale*) is an ecologically dominant ant species found in South Western North America; their extensive foraging activity shapes forest communities, and their nests are a biodiversity hot-spot for a multitude of symbiotic invertebrates (myrmecophiles). Despite their vital role in the ecosystem, their activity is largely unstudied. In this work, we develop a multi-sensor camera trap, named 'Ethocam,' to capture ant behavioral patterns in the field, and combine this technology with a computer vision approach to track colony activity in an undisturbed fashion. We demonstrate an

accurate system for counting ants built with minimal human labeling. We show that *L. occidentale* activity drops rapidly through the morning and study the effect of environmental conditions on ant count. We also report the occurrences of the ants' interactions with other invertebrates in our camera trap data. Together, these findings demonstrate the potential of our system to capture the behavior of *Liometopum occidentale* as well as its complex associations with various local species including symbionts, potentially at landscape scale. Our study provides proof of concept for the promise of low-cost remote monitoring of social insect populations.

Studying animal activity patterns in natural habitats is a crucial complement to studying behaviors in the lab, since it is usually impossible to recapitulate the complex web of interspecies associations under laboratory conditions (Markow, 1988; Pritchard et al., 2016; Tsutsui, 2018). Moreover, quantifying animal behavior in natural contexts is critical for understanding how a given species contributes to the dynamics of ecological communities and higher-level ecosystem processes. This is especially true for ecologically important social insects such as ants, bees and termites, where colonies are often large and exert major effects on the habitat at large by way of their associations with other species and impacts on nutrient distribution and habitat structure. In many terrestrial ecosystems, ants in particular are keystone organisms that control the populations of diverse other invertebrates, both via predation and by forging beneficial symbioses with mutualistic herbivores (Parker and Kronauer, 2021). The ramifications of these interactions can permeate whole communities, even re-configuring the predator-prey dynamics in large mammals (Kamaru et al., 2024). Ecosystems can thus be

especially sensitive to changes in the composition of the ant fauna. Human-mediated habitat loss and fragmentation, climate change, and the introduction of exotic species, including invasives, have all been shown to disrupt native ant communities, with often dramatic consequences for the native ecosystem (Parker and Kronauer, 2021). The ability to monitor the collective behavior and ecological interactions of ants in the field, long term, is hugely desirable (Underwood and Fisher, 2006). Such data would not only illuminate natural, colony-level behaviors that are impossible to reconstitute in the lab, but could also permit quantification of the ecosystem services that ants provide, as well as lead to predictive models for how ant species may respond to different types of disturbance. Potentially, such a monitoring system could be implemented at a large scale, across multiple colonies within a habitat. To our knowledge, no such automated approach has to date been developed.

The velvety tree ant (*Liometopum occidentale*) is an ecologically dominant ant species in Southern California, forming extensive colonies containing hundreds of thousands to millions of workers. Despite the high prevalence of this ant species in semi-intact ecosystems across its range, little is known about its biology and behavior in the wild (Hoey-Chamberlain et al., 2013). These ants are known to have large foraging areas, are speculated to form massive supercolonies spreading multiple kilometers, and may maintain nest locations in trees for several years (Wang et al., 2010). Species of the genus *Liometopum*, including *L. occidentale*, are also known to engage in a diversity of interspecies relationships, including trophic mutualisms with hemipteran bugs. Colonies of *L. occidentale* ant are also targeted by several species of socially parasitic

"myrmecophile" beetles of the family Staphylinidae (rove beetles) (Hoey-Chamberlain et al., 2013; Parker, 2016). Previous reports suggest that activity patterns of *Liometopum* are equally diurnal and nocturnal (Shapley, 1920a) with temperature determining activity level. Here, we leverage *L. occidentale's* stable nest locations, large colony size, rich inter-species associations and vital ecological role to pioneer a field-based ant tracking method. Our system detects and tracks the activity of *L. occidentale* ants at colony locations using modern computer vision techniques and is scalable to habitat-wide monitoring. In this proof-of-concept study, we use an in-house designed and built camera trap to record high-quality videos of an ant nest entrance for 2 minutes every hour throughout the day. Using a combination of traditional image processing techniques for weak supervision combined with a small set of human annotations, we train and evaluate a computer vision pipeline consisting of Faster R-CNN (Ren et al., 2015) for object detection and a modified version of SORT (Bewley et al., 2016a) for multi-object tracking. We successfully track ant trajectories over the day and obtain a measure of ant count. We evaluate the performance of our method both in and out of distribution and show that our method closely follows ground truth ant count trends. We also show that our method predicts ant counts as well as single-frame human annotations (that is annotations without using temporal information). Our methods are sufficient to extract novel scientific insight on the behavior of *L. occidentale* in their natural habitat. In particular, we demonstrate that our method generates robust estimates of ant counts in the field with small amounts of initial training data.

3.2 Related Work

Detection. Object detection seeks to localize objects of a certain category or set of categories in images, and is a highly-studied challenge in the computer vision community (Huang et al., 2017). In this work, we rely on the well-established Faster R-CNN (Ren et al., 2015) two-stage object detection architecture with a ResNet50 backbone (He et al., 2016). Our system is modular, allowing for drop-in replacement of newer architectures (Duan et al., 2019; Lin et al., 2017; Tan et al., 2020) as-needed.

Multi-Object Tracking. Multi-object tracking is a notoriously difficult problem, requiring robust detections in often crowded scenes, management of occlusions, and reidentification of individuals returning to view (Jr and Belangour, 2021; Luo et al., 2014). Canonical multi-object tracking challenges use pedestrian data (Dendorfer et al., 2020), and algorithmic approaches range from simple IOU overlap in subsequent frames to assign ID (Bewley et al., 2016a) to methods using object appearance through time (Wang et al., 2019) to learning whole graph structures to generate tracks (Brasó and Leal-Taixé, 2020). Methods using feature information require objects to have visually distinguishable appearance, which make their value tentative for groups of genetically similar sister ants which look nearly identical. Hence, we employed the simple and well performing SORT algorithm (Bewley et al., 2016a) for our ant tracking task.

Tracking Social Insects. Previous approaches to tracking social insects in a lab setting are predominantly marker based (Crall et al., 2015; Mersch et al., 2013), which is not feasible for natural colonies with tens of thousands of individuals. (Imirzian et al., 2019a)

developed an ant detector plus tracker using framewise detections with MaskRCNN, and subsequent tracking by minimizing an optimal transport cost function between consecutive frames. The tracker maintains identities by minimizing the cost, based on spatial distance and appearance, of each ant in frame K with all other ants in frame K+1. This work is designed for tracking foraging paths of carpenter ants (*Camponotus rufipes*) at night, under consistent IR light. These methods are insufficient to handle the fluctuation in ambient lighting and massive changes in ant density and trajectory direction seen at *L. occidentale* nests. (Cao et al., 2020) propose a method for tracking ants at nests. They use a ResNet to obtain appearance features and combine appearance and motion features to obtain the final trajectories. Instead of collecting their own data they use short stock videos and images obtained online from random ant nests, and their approach relies on a large number of hand-labeled training examples. In contrast, we show accurate ant counts even in out-of-distribution videos with fewer than a thousand hand labeled in-distribution training images using transfer learning for detection and using tracking to eliminate false positives. (Patel et al., 2021a) train a U-Net architecture to produce a density map given an image containing a cluster of monarch butterflies, and subsequently obtain a count by integrating over the density map. This approach is not suitable for our data as it is sometimes difficult to see individual ants in a single frame due to motion blur. Our separate detection + tracking approach allows us to use temporal information to resolve such cases.

3.3 Methods

Data Collection.

Data were recorded using an in-house camera trap dubbed 'Ethocam.' The Ethocam is a cheap (~$250) and open-sourced setup consisting of a 12.3 MP raspberry pi HQ camera, temperature, humidity and light level sensors, GPS, power management unit WittiPi with a 10000mAh rechargeable battery, solar charger, relays for external light control and an e-ink persistent display. The source code and design files are available at https://github.com/ willdickson/ethocam. The Ethocam schematic is shown in Figure 1A. To optimize video for ant detection, we tested a range of camera parameters and external lighting, first in the lab, capturing images of ants on bark in a plastic tub (we will refer to this data subset as DATA-LAB), then tuned for lighting variations by placing the tub and camera outside in natural light (we will refer to this data subset as DATA-NL for "natural light"), and made final adjustments at the ant nest field site (we will refer to this data subset as DATA-NEST). The final set of parameters used by the camera were a frame rate of 30 FPS, a bitrate of 20000000, auto white balance, a dynamic range compression set to high, auto exposure and ifx set to denoise. The camera was placed roughly 10cm from the ant nest entrance and was supported with a custom 80-20 aluminum rail. Ultimately, there was some motion blur when the ants were moving quickly, but the proximity of the camera to the ants allowed us to successfully detect and track the ants. The ant nest we used for our proof-of-concept study was in a hollowed-out bay tree, slightly off the path at Chaney trail in the Angeles National Forest. We collected 2 minute

long videos every hour for 41 hours from the ant nest (13 hours from May 13th, 2021, and 14 hours each day on July 17th and 19th, 2021). As we did not use any external lighting in this pilot study, only footage between 7am - 7pm from May, and 6:20am - 7:20pm from July, were usable. Collecting nighttime data remains an area of future work.

Detection

Generating Weak Supervision. To reduce the need for hand-labeling, we use traditional computer vision techniques to provide initial weak supervision. We use color channel information to locate the ants' distinctive orange brownish thorax. For each frame, we first perform a histogram equalization of the value channel in the HSV color space, then convert back to the RGB. We then create a mask by subtracting the red and blue channels and manually threshold to handle lighting variation using data collected at 3 different timepoints within the DATA-NL subset - 10:30am, 1pm and 7pm. We repeat the same for the red and green channels, and take the intersection of the two. We then use contour detection on this mask and OpenCV's (Bradski, 2000) boundingrect function to draw bounding boxes around the ants. This method fails when the thorax is not in view (e.g. when the ants are in a crevice in the bark). To address this, we add an adaptive background subtraction using OpenCV's MOG detector, and clean the results using morphological opening and closing. Bounding boxes are again obtained via boundingrect. We ensemble the two approaches to increase our recall and remove overlapping boxes ($IoU \geq 0.3$), giving preference to the boxes extracted using the RGB method as it qualitatively provided more precise localization. The detections from this simple method

work well for DATA-NL, where there is little background texture or lighting variation. We found qualitatively that the performance declines significantly when moving to DATA-NEST for a few reasons: 1. The ant nest entrance was more complex than the bark from the DATA-NL set (the ant nest tree was highly textured and also redder in color causing the RGB method to perform poorly), 2. there were moving rays of sunlight at different locations (because of leaves in the canopy above) and 3. wind led to some slight camera shake which interfered with background subtraction. To build a more robust, generalizable model to handle diverse data at the nest site, we use our traditional computer vision approach to extract approximate ant locations from DATA-NL for weak supervision of a Faster R-CNN ant detection model. We extract weakly-supervised bounding boxes from 10,500 frames across DATA-NL, and use a 75-25 random train-test split (note that here the test data is also weakly-labeled). We train a Faster R-CNN with a Resnet-50 (Ren et al., 2015) backbone, starting with Imagenet weights, on this data for 5 epochs using the Detectron2 library (Wu et al., 2019).

Fine-tuning on DATA-NEST. The DATA-NEST set contains 2 minutes of video collected every hour between 7am-7pm on May 13th and between 6:20am-7:20pm on July 17th and July 19th, 2021. We manually annotated 507 frames - 200 “dense frames” and 307 “sparse frames” where dense frames have a large number of ants (videos between 7am-10am) and sparse frames have few ants (1- 5 ants, videos between 11am-7pm). All hand annotations were generated with data from May 13th, hence we term the May subset of the data as DATA-NEST-ID (ID for in distribution), and the set of videos entirely unseen by our model as DATA-NEST-OOD (OOD for out-of-distribution). We

make this distinction in order to ensure we are evaluating our system as it is intended to be used, where the evaluation data will shift from the training distribution both visually and in ant density over time (real-world applications almost always encounter distribution shift in deployment, a known challenge for automated monitoring approaches (Beery et al., 2018; Koh et al., 2021)). DATA-NEST-ID annotations are shuffled and randomly divided into a train, val, and test set using a 60-20-20 split. This resulted in 119, 43, 38 dense frames and 185, 58, 64 sparse frames in the training, validation and test sets respectively. Starting from our weakly-supervised DATA-NL-trained Faster R-CNN model, we fine-tune on this small manually labeled dataset to transfer our model to DATA-NEST. We do not see training and validation loss diverge, indicating either little-to-no overfitting or, more likely, a large amount of similarity between the randomly subsampled training and validation data. Our operating point for use in downstream tracking is selected using precision-recall curves on the DATA-NEST-ID test set.

Tracking

To estimate ant counts across each video from frame-wise ant detections, we implement a tracking module - a modified version of the multi-object tracker SORT (Bewley et al., 2016a). SORT uses a Kalman filter based on linear velocity changes and Hungarian algorithm for ID assignment. We generate new detections by linearly interpolating bounding box coordinates over detection gaps in tracks generated by SORT. This SORT+interpolation adaptation allows us to use video information to reduce false negatives and improve detection, while the ID maintained across a track allows us to

capture trajectory information for each ant. In some lighting conditions, particularly in DATA-NEST-OOD, parts of the bark of tree roughly resemble the shape of an ant, resulting in repeated, stationary false positives. In order to address this, a track is considered a stationary false positive if it moves less than a threshold distance of 10 pixels (frames are 640 x 480) for more than 100 frames. To account for ants that stop moving temporarily, we check if the furthest distance moved by the entire track is less than 20 pixels.

Statistical Analysis

We perform a regression analysis in order to study the effects of the recorded environmental variables on ant count. We fit a linear regression model using the mean ant counts, calculated per video, as the dependent variable, and temperature, humidity, light level, time and day of collection (1, 2 or 3) as the independent variables. We could not use a mixed effects model to account for day of collection as a random effect as we only have 3 random effect levels (3 days) as opposed to the minimum of 5-6 required for statistically significant variance (Harrison et al., 2018), and hence use day of collection as another independent variable.

3.4 Results

Detection

To evaluate the performance of our preliminary, motion and color-based method we manually counted the number of successfully detected ants and misses across 100

randomly selected frames from the DATA-NL set. Out of 970 ant occurrences, this traditional approach missed 67 ants and only had 3 false positives resulting in a recall of 0.93. Our weakly-supervised model trained using manually thresholded motion- and color- supervision on DATA-NL is evaluated vs. the weak labels on a held-out test set. The precision-recall curve has a high AUC of 0.91 with a maximum precision and recall corresponding to a threshold of 0.65. Table 1 shows the AP (11 point interpolation method with 0.5 IoU) calculated using the weakly supervised model (trained on DATA-NL) and the model fine tuned on DATA-NEST-ID, on both the DATA-NL and DATA-NEST-ID datasets. While we see good results of the weakly supervised model on DATA-NL (AP=0.89) and the fine tuned model on DATA-NEST-ID (AP=0.79), we see poor generalizations of the models across the two datasets. We visually analyze results and failure modes in Figure 4C. We find that most false negatives are quite small and difficult to distinguish without a motion signal. The annotations were done on higher resolution 1920x1080 frames within a video (model input resolution is 640x480), providing both motion signal and higher resolution for human annotation. We also see failures related to challenging lighting conditions, particularly as it gets dark later in the evening.

Tracking

In order to robustly assess the performance of our tracker, we manually annotated the trajectories of all ants in the first 500 frames of one dense high-activity video (9am video from May 13th). The first 196 of these 500 frames overlap with the densely-annotated frames from the DATA-NEST-ID detection train/val/test splits. This represents 64325

hand-labeled detections corresponding to tracks for 315 individual ants. Linearly interpolating to fill in missing detections within a SORT track improves the tracking metrics across the board. With our SORT+interpolate we achieve 26% (82/315) mostly tracked (ID label maintained for 80% of a given individual's track), and only have 14% (43/315) mostly lost tracks (individual tracked for less than 20% of their ground truth track). We have 421 ID swaps across the evaluation set, which contains 315 ground truth IDs. We also use the HOTA metric to evaluate our methods, which correlates well with human perception of tracking success (Luiten et al., 2021). This metric provides a single number that summarizes how well the generated trajectory tracks align while also docking for failed detections. The HOTA score for our tracking approach + interpolation is 40.4, whereas SORT without interpolation scores 38.1. These metrics indicate that our tracker is able to maintain a large number of nearly full-length trajectories and performs well on the DATANEST-ID set. We find that the filtering approach we propose to reduce stationary false positives in DATA-NEST-OOD reduces the HOTA score on DATA-NEST-ID, mostly due to the loss of ants that remain still through large portions of the video (Table 2). However, the filtering significantly improves our ability to generalize to DATA-NEST-OOD, which had a larger number of false positives since it is not represented in the training data. The increase in counting performance in DATA-NEST-OOD seems to be worth the trade-off in tracking score (see next section). In Figure 2 we visualize ant trajectories for DATANEST-ID. We see a slight increase in activity from 7am to 8am followed by a slight decrease up to 10am and then a massive decrease from 10am - 11am. The activity remains very low for the rest of the day.

Counting

We use the number of unique framewise track IDs to obtain ant counts per-frame in DATA-NEST-ID. We compare the counts from our algorithm to the count from the manual track annotations, when available. In addition, to investigate counting performance at different time points with different ambient lighting, we manually counted the number of ants in one frame per video from DATA-NEST-ID and DATANEST-OOD. Figure 3 shows predicted mean ant count vs time of day for each of the 3 days of field data, which gives us an estimate of stability, along with corresponding temperature, humidity and light level. Figure 4B shows the evaluation of the counts obtained from our pipeline against the counts obtained by manually annotating the full trajectories from the first 500 frames from a single DATA-NEST-ID video (the 9am from May 13th). The first 196 of these 500 frames are in the dataset used for the train-val-test splits whereas the remaining frames were not seen by the network. We see that the ant count generated by detector + tracker system closely follows the trend in the ground truth, thus serving as a good measure of ant activity. Additionally, we note that, compared to raw detections which fluctuate by 10-20 ants over just a few frames (Figure 4B) in dense videos; our tracker outputs much more consistent counts. Though we lose detections with the raw SORT algorithm, the interpolation step recovers misses and gives consistent counts that outperform the plain detections. Visual analysis (Figure 4C) reveals that the missed detections are difficult cases - partial occlusions, ants freshly entering the frame, etc.

To verify the performance of the system at different time points and more varied conditions, we compared counts from our tracker with human counts on a single frame from every video in DATA-NEST-ID and DATA-NESTOOD (Figure 4D, Table 2). We see a strong correlation with the human count on DATA-NEST-ID, with a slope not significantly different than one, indicating human-level performance, and a high R2 value (In-distribution results Table 2). Our raw tracker approach struggles to generalize to the out-of-distribution DATA-NEST-OOD, where we had an uptick in false positive detections (Figure 4D, upper inset, purple points, Out-of-distribution results in Table 2) in frames with lighting not similar to our training data. Since it appears that false positives rather than false negatives hamper generalization, we apply a simple filter to remove detections that scarcely moved through the video. This drastically improves generalization, increasing the R2 for the DATA-NEST-OOD count regressions from 0.54 to 0.9 and tightening the confidence interval on the slopes (Table 2, Out-of-distribution results). This illustrates that incorporating a simple filter into our pipeline largely improves the generalization issue with our network and allows for robust counts on out-of-distribution data, though quality control will be undertaken on all future data to catch model/data drift. The discrepancy in performance on the ground truth tracking (where we under-count) compared to human counts (where we match human accuracy) may be due to the different annotation techniques. While annotating tracks we used temporal clues from previous and subsequent frames to find partially occluded or blurred ants whereas the counts were obtained looking at only one frame. Though our tracker includes temporal information, it is difficult for our system to pick out every ant in a dense cluster

and we lose the tail of tracks post-occlusion. Although there is room for improvement, our approach succeeds in obtaining near human measures of ant count with a very small amount of manually-annotated data (507 frames).

Data analysis

In order to assess the impacts of different environmental factors on ant count, we fit a linear regression model with temperature, humidity, light level, time and day as the independent variables. We obtain an adjusted R2 value of 0.42 (p4) multicollinearity (Fox, 2016) (VIF(temperature) = 6.48, VIF(humidity) = 9.22, VIF(day) = 5.5). This makes sense due to the small dataset size. In order to fully tease apart the effects of temperature and circadian rhythm (time), we need to collect more data over varying conditions. We will address this in future work and leave this manuscript as proof-of-concept of our methodology. Figures 3D, 3E and 3F show the log of mean ant counts from all three days of collection, plotted against humidity, temperature and time respectively.

3.5 Discussion

Monitoring the behavior of ecologically dominant ant species like *Liometopum occidentale* in the wild promises rich insights into biological communities. Using computer vision approaches, we develop a pipeline to capture data, detect, track and then analyse behavior at the ant nest. Automating these steps using computer vision and GPU accelerated computing, as opposed to manually observing activity, makes it possible to

not only analyze extensive data (weeks to years) but also allows robust, quantitative metrics like accurate ant count and ant trajectory maps. Such data is prohibitively laborious to obtain with human annotation. Our data acquisition strategy allows us to collect a wealth of useful environmental factors such as temperature, humidity and ambient light level at the collection site.

With our proof-of-concept dataset we report a number of interesting observations which underscore the potential of our system: i. We observe a massive change in overall ant activity over the course of the day and quantify ant counts between 7am-7pm in May and between 6:20am-7:20pm in July. For data collected on May 13th, we qualitatively see that ant activity starts to increase again at 7:30pm, suggesting imaging nighttime activity using infrared lighting may offer further insights which we will explore in future work. We see significantly lower ant counts in the data collected in July as compared to May. This may be due to seasonal and temperature changes, but further analysis and monitoring over longer time horizons is needed. ii. We also observe ants performing an excavation behavior, bringing pieces of debris from inside to the edge of the ant nest to discard. iii. In addition to the ants themselves, we observe other arthropods (Figure 1H): two instances of the symbiotic beetle *Sceptobius lativentris*, which steals ant pheromones via grooming to move around freely inside the ant nest; a pseudoscorpion, which may also be a symbiont of these ants; and a member of the non-symbiotic beetle genus *Silis*, which, in contrast to *Sceptobius* was attacked by worker ants and dragged into the nest (*Liometopum occidentale* are known to be omnivores). It is exciting that we see such diverse behaviors and interactions in our proof-of-concept dataset, a total video time of

82 minutes over the course of 3 days, demonstrating the value of imaging animals in the wild in an undisturbed manner. Further data collection with longer video times over larger time scales along with data collection at night will provide further, previously inaccessible information for this little-studied ant species and its associated arthropod community. We generated numerous ant annotations with a semi-automated approach to train a network that performed well for DATA-NL. We then leveraged this network to obtain initialization weights to train a model to detect ants in DATA-NEST. We achieve good performance on DATA-NEST with a small number of manually annotated frames (507). Since the detector relies only on information in a single frame, we were further able to improve the detection performance and collect video level counts using our modified SORT tracker. The tracker uses a Kalman filter constant velocity model along with interpolation to recover ant detections missed by the network. The ID assignment using the Hungarian algorithm enables us to produce trajectories for individual ants, giving activity maps. Although we see from Figure 4B that our ant count undershoots human counts given a full video as context, our counts so approach the accuracy of a human given only single frames for annotation (Figure 4D). Qualitatively, raw videos clearly demonstrates that ant activity drops rapidly over the course of the day, and our tracking shows the same trend (Figure 2, Figure 3). Using a tracker stabilizes the ant counts (4A) during the videos, as seen in Figure 4B, where the raw detections change in count by 10-20 ants within a few frames.

Although there is room to improve the accuracy of our models, our system nevertheless provides an indication on the key focal times for future Ethocam acquisition, i.e. times of

high activity. We captured multiple instances of various other species interacting with the ants in our small data set. In future, we will investigate species classification approaches to automatically recognize symbionts and other arthropods, although we recognize that the large imbalance between ant and symbiont sightings will prove a challenge. If non-ant arthropods occur in-frame frequently (as our pilot data imply), and can be accurately detected, further work could include automated investigation of inter-species interactions involving *L. occidentale.*

In summary, we have successfully developed a data collection paradigm and computer vision methodology to extract quantitative activity information from natural ant colonies. We successfully tuned camera parameters and positioning to capture high quality ant nest data; we then generated detections on a per-frame basis with semi-automated and manually generated annotations. Subsequently, we tracked ants to improve detection, obtained trajectories and counted ants, and validated these counts and tracker performance both in and out of distribution. We found that *L. occidentale* activity drops rapidly over the course of the day and picks up again at night. We observed interesting trends in ant activity potentially resulting from different environmental factors and we look forward to collecting more data over longer time horizons to explore these further. This pilot study illustrates the potential of our system for further applications. Our low-cost, open source hardware and software together show promise for quantitatively observing the networks of interactions in natural populations. Quantitative measures will help elucidate complex, environmentally influenced animal behaviors and provide insight on how invasive species and our changing climate affect the rich, native ant biodiversity.

3.6 Figures and tables

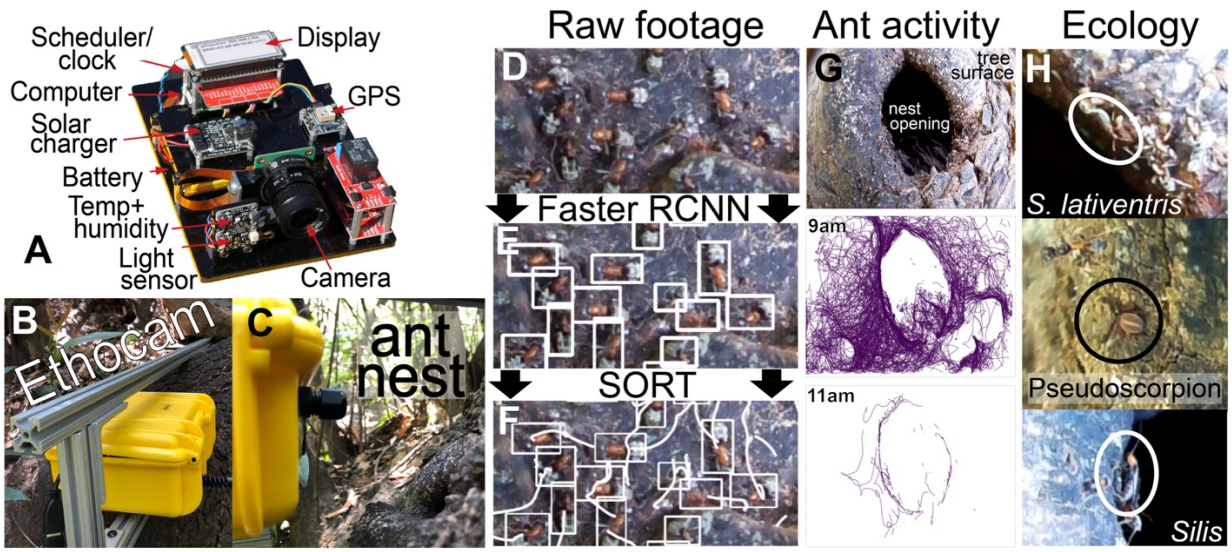

Figure 1. (A). Ethocam setup with various components annotated. (B). Ethocam inside waterproof enclosure attached to custom made 80-20 rail setup for imaging ant nest. (C). Ethocam positioned to be approximately 10 cm away from the surface of the nest. (D-F). Schematic of our machine vision pipeline. (D) Raw data collected from an ant nest was run through Faster R-CNN for detection. (E) The resulting detections were passed through a tracker (F) to generate ant trajectories. (G) Overlaid ant trajectories over the course of 2 minute videos at different time points obtained by our ant tracker (modified SORT) shows ant activity. (H) Examples of three other arthropods captured in raw camera trap footage illustrating ant nests as a biodiversity hub.

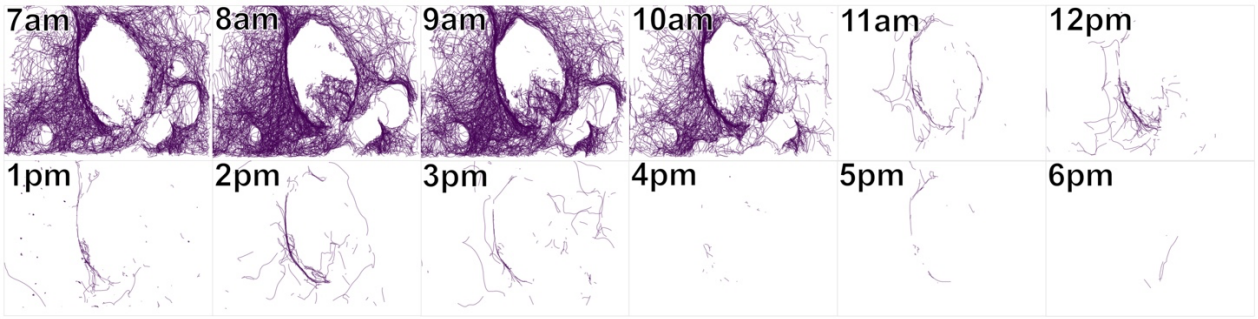

Figure 2. Activity maps produced at different times of day based on the output of the tracker

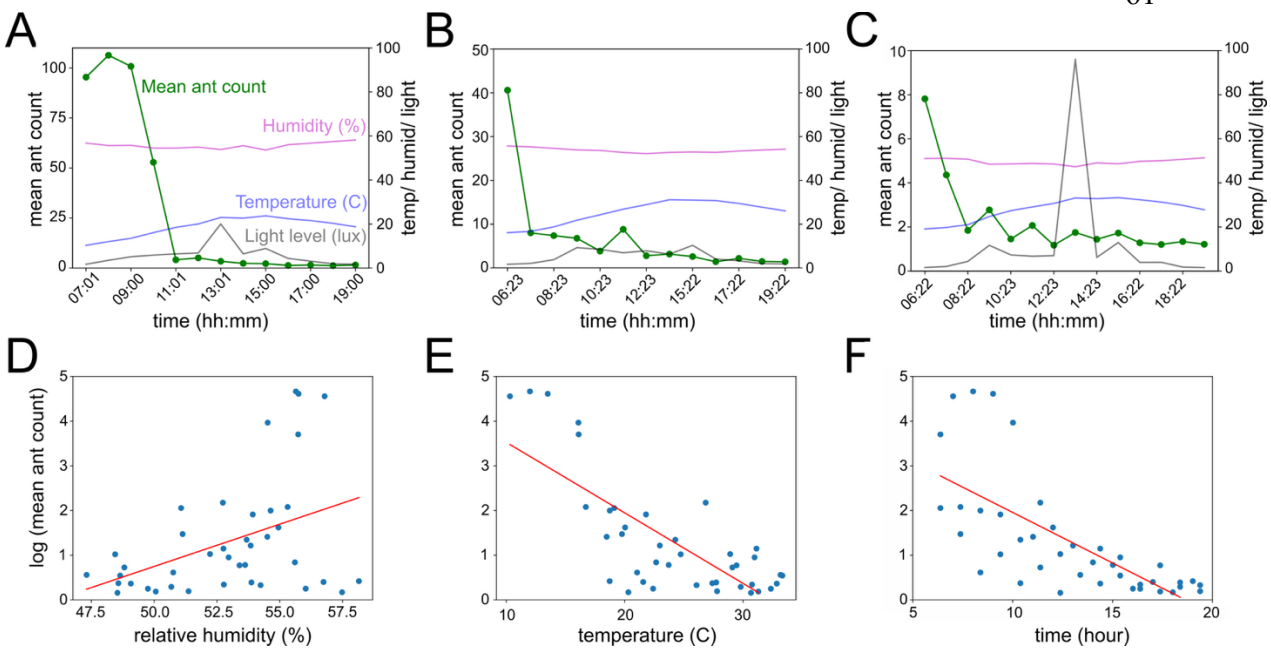

Figure 3. (A). Mean ant count along with recorded environmental factors for data collected on 13th May 2021. (B). Mean ant count along with recorded environmental factors for data collected on 17th July 2021. (C). Mean ant count along with recorded environmental factors for data collected on 19th July 2021. (D). Log of mean ant count plotted against humidity: log(mean ant count)=0.19 x (humidity) – 8.71 (R^2=0.17, p< 0.01). (E) Log of mean ant count plotted against temperature: log(mean ant count)=-0.16 x (temperature) + 5.10 (R^2=0.58, p<0.001). (F) Log of mean ant count plotted against time: log(mean ant count)=-0.23 x (time) + 4.22 (R^2=0.49, p<0.001).

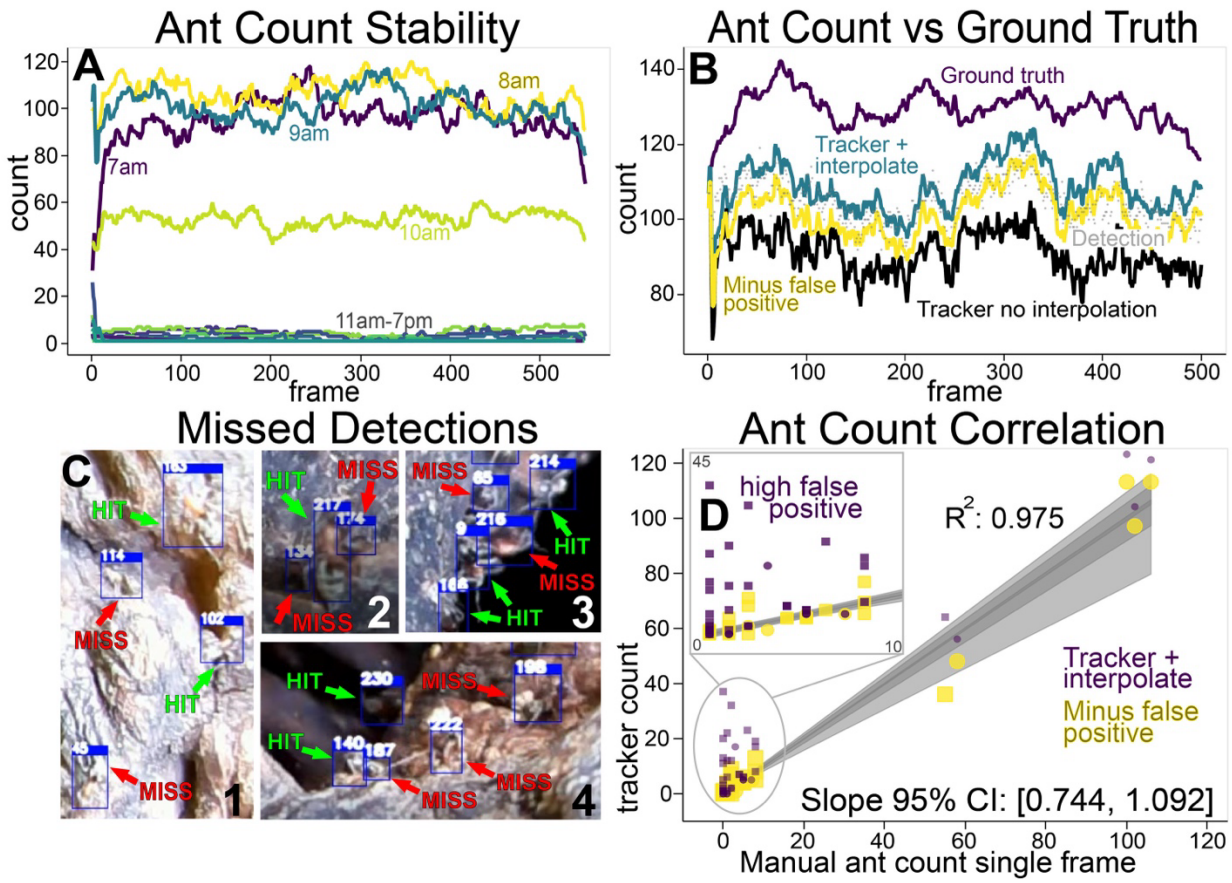

Figure 4. (A) Stability of ant count throughout two minute videos generated via our detector+tracker approach. (B) Comparison of ant counts in ground truth data (purple) versus raw detection counts from our fine tuned model (grey dots), plain SORT output (black), SORT+interpolation (green), or SORT+interpolation minus false positives (filtering)(yellow). Our approach consistently under-counts ants due to several difficult annotation types. (C) Examples of missed detections, likely due to 1) overexposure, 2) ant mostly occluded, 3) previously occluded ant freshly entering frame and 4) bark providing effective camouflage. (D) Human generated ant counts vs SORT+interpolation counts (one frame per video). Squares are from the DATA-NEST-OOD set, circles from DATA-NEST-ID. Yellow dots are after filtering out false positives, purple before filtering. Human ant count was lower than from the ground truth data in (B) since only a single frame without time series of ant movement was used for count. Our algorithm (which has temporal information) performs as well as a human without the timeseries, as indicated by a slope which is not significantly different than 1 (non-parametric bootstrapping on slope was used to generate a confidence interval). DATA-NEST-OOD had a large number of false positives from lighting conditions not similar to the training set (D upper left inset, purple squares), which we filtered out based on low movement to help generalization.

Model	Dataset	AP
Weakly supervised	DATA-NL	0.89
Weakly supervised	DATA-NEST-ID	0.05
Fine tuned	DATA-NL	0.28
Fine tuned	DATA-NEST-ID	0.76

Table 1. Detection results on different datasets.

Tracker	HOTA	Count R^2	Count slope 95% CI	Count R^2	Count slope 95% CI
SORT	38.1	0.99	0.71-0.95	0.58	0.11-1.0
SORT+Interp	40.4	0.98	0.96-1.2	0.54	-0.14-1.5
SORT+Interp+Postproc.	34.9	0.99	0.84-1.1	0.9	0.63-1.2

Table 2. HOTA and detector ant count correlation to hand labeled counts for our tracking approaches.

Chapter 4

COLONY LEVEL MONITORING OF ANT-MOVEMENT PATTERNS USING COMPUTER VISION

4.1 Abstract

Ant colonies are major drivers of ecosystem processes, yet their collective behavior unfolds over spatial and temporal scales that are difficult to capture with traditional field methods. Here we present a computer vision–based framework for long-term, automated monitoring of colony-scale movement and behavior in the ecologically dominant ant *Liometopum occidentale*. Using an extended, open-source camera trap capable of wide-field, day–night imaging, we recorded short hourly videos at nest entrances across multi-day sampling bouts from three colonies in a natural forest environment. By tracking thousands of ants, we quantified circadian activity patterns, directional traffic asymmetries, environmental drivers of ant abundance and speed, and spatiotemporal structure in movement along distinct trails. Colony activity exhibited a pronounced nocturnal rhythm, with a sharp, sunset-aligned surge in outbound traffic. Mixed-effects models revealed that ant abundance was governed primarily by circadian timing, whereas walking speed was driven mainly by temperature. Spatial analyses showed that outbound and inbound ants consistently used the same trail corridors, that major movement routes remained stable across weeks, and that individual trails exhibited distinct temporal and directional dynamics. Finally, we demonstrate that individual movement trajectories

alone can be used to identify task-specific behaviors such as excavation, highlighting the potential to infer aspects of division of labor from kinematics alone. Together, our results establish a scalable approach for linking individual movement, collective dynamics, and environmental context in large, free-living insect societies, enabling quantitative behavioral analyses that were previously infeasible outside the laboratory.

4.2 Introduction

There have numerous studies that document the critical roles ants play in maintaining ecosystem function, including but not limited to bioturbation of soil, seed dispersal, nutrient cycling, controlling bulk energy flow via predation, engaging in mutualistic relationships with hemipterans, serving as hosts to a range of myrmecophiles, and as indicators of ecosystem health (Del Toro et al., 2012; Folgarait, 1998; Perfecto and Philpott, 2023; Pętal, 1978; Underwood and Fisher, 2006; Wills and Landis, 2018). The scale of impact ants have on biota can be seen clearly in cases of introduction of invasive ant species to island ecosystems (O'Dowd et al., 2003) or by disruption of existing ant-plant mutualisms (Kamaru et al., 2024). Further the sheer abundance of ants, with recent estimates suggesting the total dry biomass of ants being greater than that of all wild birds plus mammals combined (Schultheiss et al., 2022), and their presence across all major land biomes (except polar regions), make them one of the most ecologically important animal taxa (Fayle and Klimes, 2022; Parker and Kronauer, 2021). There are more than known 14,000 species of ants, all of which form colonies ranging from small budding colonies to massive super-colonies of millions of individuals (Gordon, 2019; Holldobler

and Wilson, 2009; Wilson and Hölldobler, 2005). Colonies of this size, along with their myriads of complexities, cannot be recreated or housed in a lab setting. To fully understand the ecological roles and behavior of these eusocial insects at colony scale, long-term field-based automated monitoring strategies are much needed.

Existing field-based methods to monitor ant activity involve manual observations (Shapley, 1920b), mark and recapture experiments (Stradling, 1970), pitfall traps (Andersen, 1983), baiting assays (Fellers, 1989), and leaf litter samples (Olson, 1991). While these approaches have generated foundational insights, they are labor-intensive and typically limited in temporal resolution and sampling duration. Recent advances in artificial intelligence and computer vision have enabled new approaches to automated insect monitoring (Van Klink et al., 2022), including species identification using light sheets (Jain et al., 2024), tracking of flower visiting insects (Bjerge et al., 2022; Ratnayake et al., 2021; Sittinger et al., 2024), counting butterflies in clusters (Patel et al., 2021b), and automated tracking of bees at natural bee hives (Leocádio et al., 2023). These studies demonstrate the feasibility of applying computer vision to free-living insects under field conditions. Despite these advances, automated studies that extract sustained, colony-scale movement dynamics and behavioral organization in large, eusocial insect colonies over extended timescales and under natural field conditions remain comparatively rare. This limitation is particularly pronounced for ants, whose large colony sizes, high densities, and non-uniform movement patterns pose challenges for long-term automated monitoring. Automated tracking of ants in field conditions has

been demonstrated in localized contexts, such as along foraging trails (Imirzian et al., 2019b). However, comparable analyses focused on nest entrances, particularly across multi-day timescales, remain limited. Nest entrances offer a powerful vantage point for studying colony-scale movement and behavioral dynamics, allowing for the observation of ants entering and leaving the nest, transporting food and materials into and outside the nest, and engaging in entrance specific local behaviors such as patrolling and excavation.

Liometopum Occidentale is an ecologically dominant ant species endemic to the South-Western United States and parts of Mexico (Gulmahamad, 1995; Hoey-Chamberlain et al., 2013). They are a behavioral aggressive ant species, can be seen in large numbers in oak and pine forest, and form massive colonies of hundreds of thousands to millions of individuals. They are known to engage in mutualisms with aphids and to serve as hosts to a range of myrmecophiles including many species of rove beetles. As a result of their omnivorous diet, they can be seen carrying seeds and other insects as prey back into their nests. Their large nests, made inside trees such as California coast live oak, bay, and laurel trees, often have holes or crevices where ants can be observed entering and exiting in large numbers. The stability of their nests, pronounced yearlong activity, and large size of these ants make the nest entrances ideal vantage points for long-term monitoring of ant activity.

In this study, we build upon the work on Sharma et. al. (Sharma et al., 2024) extending the Ethocam, an open source field-based multi-sensor camera trap, to capture a wider

field of view around the nest entrance, and to extend video capture to night-time imaging. We collect a dataset comprising of 30 second videos at the start of every hour, along with environmental variables, at nest entrances from 3 separate ant nests along a canyon in the Angeles National Forest over several months, comprising a total of 24 hours and 24 seconds of video footage over 100 days. We compared multiple computer vision approaches for ant detection and optimized parameters for tracking. We demonstrate some key insights into *Liometopum* behavior at the individual and colony level. Ants from all three nest showed a strong circadian activity structure, with programmed onset of foraging behavior as seen by a large, stereotyped efflux of ants at sundown. We confirm that ant speed is modulated primarily by temperature and ant counts by time. We also looked at the spatio-temporal dynamics of ant movement along different trails emanating from nests and found that ants do not distribute themselves uniformly on trails. The movement dynamics varied between nests, possibly reflecting nutrition requirements, age, and local resource availability. We also demonstrate the ability to detect individuals engaging in behaviors such as excavation from movement data alone, illustrating the potential for future studies of task partitioning. Overall, we demonstrate a powerful approach of combining long-term field recordings with analyses methods derived from artificial intelligence and movement ecology. To our knowledge, this is the first long term automated behavioral monitoring of ant activity and we believe our results not only provide insight into the behavior and ecology of *Liometopum*, but our methods can be generally applied to gain insight into other species of ants as well.

4.3 Methods

Ethocam

Building upon the Ethocam design of Sharma et al. (Sharma et al., 2024), we implemented several modifications to accommodate wide-field, day-night monitoring of ant activity. First, we replaced the Raspberry Pi HQ camera with the Raspberry Pi Camera Module 3 (NoIR, wide-angle), which provides a substantially broader field of view (Fig. 1A). Second, to enable night-time imaging, we added an external IR illuminator (Tendelux 80ft AI-4). Third, to ensure sufficient power for extended field deployments, we added a second LiPo (3.7V 10 Ah Adafruit product ID: 5035) battery dedicated solely to the IR illuminator and rewired the system so that the Pi (camera and sensors) and the IR light each ran on their own independent battery and charger (Adafruit 1.5A USB/DC/Solar LiPo Charger). The Ethocam continues to use a Raspberry Pi Zero W, WittyPi board (Witty Pi 4 Mini) for scheduled recordings, a temperature-humidity sensor (Adafruit Si7021), light level sensor (Adafruit TSL2591), PiHat and E-ink display (Pimoroni Inky pHAT), and a relay for controlling the IR light. In the field, the system is powered by a 20W 6V solar panel (Voltaic systems SKU:P120). As shown in Fig. 1C, switching to the Camera Module 3 expanded the visual coverage from the narrow, close-up view of the HQ camera to a much wider view that captures the broader area surrounding the nest entrance. This expanded view enabled us to track ant movements along trails extending from the entrance while still preserving resolution of behaviors occurring near the nest entrance such as excavation.

Data collection

Modified Ethocam setups were placed in front of three separate ant nests (trees), henceforth referred to as nests 1,2,3, along a transect in Chaney Canyon, Angeles National Forest between the dates of August-Dec 2024 (Fig. 1B). Trees were identified as ant nests via manual observations of (1) significantly greater ant presence in comparison with surrounding trees, (2) presence of myrmecophiles such as rove beetles observed near entrances, and (3) significant efflux of ants along with the distinct Sulcatone smell (alarm pheromone) when one blows into the nest entrances. Each nest tree can have multiple nest entrances (in the form of holes or crevices on the bark) allowing ants to enter and exit. We tried to pick the most active nest entrances for monitoring with the constraint of feasible camera placement.

Nest 1 (coordinates: 34°13.0493, -118°.09.0888) is a large bay laurel tree slightly off the main trail at Chaney canyon. It is very close to the stream, and houses a large ant colony with a distinct hole in the front face of the bark where ants are often observed entering and leaving. This was the same nest site used in Sharma et. al. (Sharma et al., 2024). Nest 2 (coordinates: 34°13.0508, -118°09.1686) is a smaller bay laurel tree right along the main trail. Nest 2 has a distinct elongated hole small enough to be fully in the imaging view, where ants can be seen moving in and out of the tree. Nest 3 (coordinates: 34°13.0708, -118°09.0478) is on a coast live oak tree next to an abandoned house. Site 3 has a very long crevice along the length of its bark where ants can be seen entering and leaving all along its length. We chose a spot at the intersection of two major tree trunk branches for monitoring. For nests 2 and 3, we used an extendable tripod (Eicaus 74-inch

tripod) with the Ethocam placed a few inches away from the tree surface. For nest 1, we used a custom 80-20 built mount to hold the camera in front of the nest entrance. Data from each of these nests was collected in bouts (long periods of undisturbed imaging) between 10-25 days, where a 30 second video was captured at the start of every hour at 20 FPS. For consistency in lighting, the external IR light was turned on for the duration of video recording irrespective of the time of day. Videos were stored to a SD card in a h264 format. Videos were then individually converted to mp4 format for further processing. Temperature, humidity, light level and battery information were simultaneously logged to a text file at time of video recordings. Data from nest 1 comprises of two bouts of data: 10 days of video data between August 1st and August 10th, and 12 days of data between October 22nd and November 2nd. From nest 2, 3 bouts of data were collected: 12 days of data between August 22nd and September 2nd, 17 days of data between October 3rd and October 19th, and 22 days between November 15th and December 6th. Two bouts of data from nest 3 were collected: 26 days between August 1st and August 26th, and 24 days between August 26th and September 18th. This resulted in a total of 116 days of video data collected from 3 ant nests, equaling 24 hours and 24 minutes of video footage time analyzed (122 days x 24 hours a day x 30 seconds per video). As the mounted Ethocam remains still during a data collection bout, masks were created per data collection bout masking out the nest entrance (hole/crevice) and any areas in the frame that were outside the tree bark.

Background subtraction for motion detection

To enhance ant visibility for single-frame detection, we incorporated motion information using a background-difference approach inspired by (Kay et al., 2022). For each 30-s video, we computed an average frame, which effectively represents the static background (tree bark) since ants rarely remain completely motionless during the entire clip. For each frame, we then constructed a motion-encapsulated image: the original grayscale frame was retained as the blue channel, while the difference between the current frame and the average background frame was assigned to the green channel (Fig. 1C). This transformation highlights moving ants in green, substantially improving their visibility in single frames. Red channel was set to zero. These motion-encapsulated frames were used for annotation, and subsequently for ant detection and tracking.

Annotations and dataset

To train and evaluate object detection and multi-object tracking models, human annotations were generated using CVAT (Computer Vision Annotation Tool). For each selected video, 30 consecutive frames (1.5 s of footage) were annotated. Videos were chosen to span a wide range of lighting conditions, colonies, and ant densities. Annotating short temporal sequences, rather than isolated frames, allowed annotators to assign consistent track IDs across frames for evaluating tracking performance, and also enabled more reliable ant identification by leveraging motion cues when stepping forward and backward through the sequence. All annotations were performed on the motion encapsulated modified frames described above. A total of 15 videos, 5 from each of the three nests, were annotated, covering a range of daytime and nighttime recording

periods. Ant counts per video ranged from 13 to 209. Videos were divided among three annotators, and ants were marked using point annotations placed at the approximate center of each ant. Annotators were instructed to zoom as needed and to use frame-to-frame movement to verify ant positions. In total, this produced ~45,000 point annotations corresponding to ~1500 unique ants across 450 frames. Point annotations were converted into fixed-size bounding boxes (5×5 pixels) to serve as inputs for object detection models. We provide these videos and corresponding detection and multi-object tracking annotations as a dataset for further computer vision studies.

Training splits

Annotated videos were partitioned into training, validation, and test sets based on both colony identity and lighting conditions. For each of the three colonies, two videos—one recorded during daylight and one at night—were assigned to the training set. The validation set consisted of one video per colony either at day or night. The test set included two additional videos per colony, again one daytime and one nighttime recording. To ensure a realistic assessment of model generalization, entire annotated sequences (all 30 annotated frames per video) were kept intact when assigning videos to splits. Thus, all frames in the validation and test sets came from videos that were completely unseen during training, enabling evaluation on fully held-out hours and conditions rather than on partially overlapping footage.

Detection and tracking metrics

Object detection models for single-frame ant detections were compared on the validation set. For each trained model, the threshold was selected using a precision-recall score, and best F1 score on the validation set was reported. Tracking was performed using the SORT tracker. Tracking was evaluated on the validation set using the TrackEval library (Jonathon Luiten, 2020), which returns a set of metrics ranging from detection focused, to a balance of both, to tracking focused (DetA, MOTA, HOTA, IDF1, and AssA). HOTA score (Luiten et al., 2021) is a popular metric used to evalute multi-object tracking performance as it equally balances detection and association. Performance using various values of the three SORT parameters, max age, min hits, and IoU, were compared on the validation set and the best set of hyperparameters were chosen for tracking.

Ant counts and direction classification

Ant counts per frame were the number of unique IDs per frame after tracking. Ant counts per video were the average of ant counts across all frames of the video. For every data bout (10-25 consecutive days per colony), ant counts were plotted for every hour across all days. Bootstrapped mean and 95% confidence interval were also plotted. Each tracked ant was assigned a movement direction: toward the nest entrance, away from the entrance, or unknown, on a per-frame basis. Direction was determined by comparing two vectors: (1) the velocity vector, defined as the displacement from the ant's position in the previous frame to its position in the current frame, and (2) a radial vector, defined as the vector from the closest point on the manually drawn nest-entrance mask to the ant's current position. The angle between these two vectors provides a measure of whether the

ant is moving inward or outward relative to the entrance. In the idealized case, an angle of 180° indicates movement directly toward the entrance, whereas an angle of 0° indicates movement directly away from it. In practice, angles between 0° and 70° were classified as movement away from the nest, angles between 110° and 180° were classified as movement toward the nest, and intermediate angles (70°–110°) were labeled as unknown. Because this approach relies only on the nearest boundary point of a general entrance mask, it supports direction classification regardless of the entrance's geometry, whether a round hole, an irregular opening, or a narrow crevice (Fig. 3A).

Directional and speed difference metrics

Once ants are classified by direction of movement, for each hour and each day, we computed two hourly metrics for each day d and hour h: a net directional difference D(d,h) and a directional speed difference S(d,h). The net directional difference was defined as the difference between the average number of ants going away and the average number of ants going toward the nest entrance.

$D(d,h) = \text{count}(d,h)_{\text{away}} - \text{count}(d,h)_{\text{toward}}$

where positive values indicate a net outward movement of ants and negative values indicate a net inward movement. The directional speed difference was defined as the difference between the mean speed of ants moving away from the nest entrance and the mean speed of ants moving toward the nest entrance.

$S(d,h) = S(d,h)_{\text{away}} - S(d,h)_{\text{toward}}$

where positive values indicate that outbound ants moved faster on average than inbound ants.

For both D(d,h) and S(d,h), hourly values were aggregated across days within each bout and bootstrapped means and 95% confidence intervals were calculated (10,000 resamples) per hour. To summarize directional tendencies at the bout level, we computed the bout-averaged net directional difference, defined as the mean (bootstrapped) of all hourly values across the entire sampling period.

Coupling between directional traffic and directional movement speed

To test whether directional traffic imbalance in ant count was associated with corresponding differences in movement speed, we computed the Spearman rank correlation between the 24 hourly values of D(d,h) and S(d,h) for each day of each bout, yielding one correlation value per day. These values were bootstrapped (10,000 resamples) to obtain bout-level mean correlations and 95% confidence intervals. We also assessed directional agreement using a sign-alignment measure. For each day, we calculated the proportion of hours in which D(d,h) and S(d,h) had the same sign, yielding one alignment proportion per day. These proportions were bootstrapped to obtain bout-level mean alignment and confidence intervals. Because random sign matching is expected at 0.5, directional agreement was inferred when the confidence interval exceeded 0.5. Together, these analyses evaluate whether hours with greater traffic imbalance also show matching speed imbalance, both in pattern and direction.

Flux maps and test for overall bidirectionality

To quantify how outbound and inbound traffic was distributed across the field of view, we constructed flux maps for each video. Each frame was divided into fixed spatial bins

(20×20 px), and all detections were assigned to their corresponding bin. For every ant, the instantaneous velocity vector was decomposed into horizontal (u) and vertical (v) components. Within each bin, we computed (i) the average number of ants per frame across the video and (ii) the average velocity vector across all moving ants. Flux in each bin was defined as:

$Flux_{bin}$ = (average number of ants per frame in that bin) × (average velocity vector in that bin).

This formulation yields a vector field describing both the intensity and local direction of movement. It represents the density-weighted movement in a region. Importantly, computing flux using vector components preserves information about the coherence of movement: ants moving in a shared direction contribute to a strong net flux, whereas ants with high speeds but opposing headings cancel each other, producing little net flux. Using only speed would therefore lose essential information about whether ants travel cohesively along a shared path. Flux maps were computed separately for ants classified as moving away from or toward the nest entrance. For all downstream quantitative analyses including the cosine-similarity comparisons between directions and the cumulative flux maps used for trail segmentation, we used only the flux magnitude in each bin. Directionality was already encoded by the subset of ants included (away vs. toward). To assess whether overall colony traffic exhibited systematic bidirectionality, we computed flux maps for each hour of each bout and then constructed a 24×24 similarity matrix, where each entry corresponds to the cosine similarity between the "away" and "toward" flux-magnitude maps for a given pair of hours. In a colony with

consistent bidirectional trail use, the matrix should show a pronounced diagonal structure, indicating that movement away from and toward the nest occupy similar spatial paths within a given hour. To test whether the diagonal of this matrix was significantly higher than expected by chance, we performed a band-contrast permutation test. For the observed matrix, we computed the contrast between the main diagonal and the average of its ±1 and ±2 offset diagonals. Because daily activity patterns show strong circadian structure, resulting in higher similarity among daytime hours and among nighttime hours, we used a blocked permutation approach. Matrix entries were permuted within daytime and nighttime blocks separately, preserving circadian clustering while removing any hour-specific bidirectionality signal. For each of 1000 permutations, we recomputed the band-contrast statistic, generating a null distribution. The observed diagonal-contrast value was then compared with this null distribution to assess whether diagonal structure (i.e., consistent bidirectionality across hours) exceeded that expected by chance.

Persistence of spatial routing across days

To quantify the stability of spatial routing across days within a bout, we first constructed daily cumulative flux maps separately for ants moving away from and toward the nest entrance by summing the corresponding hourly flux maps across all 24 hours of a given day. The away and toward cumulative maps were then summed to obtain a total daily cumulative flux-magnitude map, capturing overall spatial routing independent of direction. Each daily cumulative flux-magnitude map was vectorized, and pairwise cosine similarity was computed between all pairs of days within the bout, yielding a day-by-day similarity matrix. Cosine similarity was chosen because it captures similarity in the

spatial distribution of movement while being insensitive to differences in overall activity magnitude across days. To establish a null expectation, we generated a shuffled control by randomly permuting the spatial bins of each daily cumulative flux map before computing cosine similarity, thereby preserving the distribution of flux values while destroying spatial structure. Similarity statistics were computed for both the observed and shuffled matrices, excluding diagonal entries.

Individual trail segmentation

To identify and segment individual trails for each data collection bout, we first constructed cumulative flux maps separately for ants moving away from and toward the nest entrance by summing hourly flux maps for each direction across all days of the bout. These two direction-specific cumulative flux maps were then summed to obtain a direction-agnostic cumulative flux map used solely for trail segmentation. The cumulative flux map was thresholded at the 70th percentile of pixel intensities to generate a binary trail mask. This mask was thinned to single-pixel centerlines using the skeletonize function from scikit-image. The resulting skeleton was converted into an undirected graph in which each skeleton pixel corresponded to a node, and edges were added between adjacent (8-connected) pixels. This graph representation enabled identification of endpoints (nodes with degree = 1), branch points, and overall trail connectivity using the NetworkX library (Hagberg et al., 2007). Starting points were defined as skeleton pixels located closest to the manually delineated nest entrance mask (created per data bout). Individual trails were then extracted as the shortest paths between

each start point and its nearest endpoint, yielding a set of distinct trail segments for further geometric and topological analyses. This procedure establishes a one-to-many mapping from start points (along the nest entrance) to endpoints, where each endpoint is linked to its nearest start point via the shortest path on the skeleton graph. Trails shorter than 10 pixels or greater than 90% overlap with others were excluded, keeping the longer trails (Fig 4D).

Length-normalized ant density and directional density differences per trail

For each trail identified within a bout, we quantified ant usage by computing a length-normalized density at each hour of each day. For a given trail t, hour h, and day d, density was defined as:

$\rho(t,d,h)$ = (average number of ants on trail t at hour h)/(number of spatial bins composing trail t)

As spatial bins have uniform size (20px), the denominator provides a length-normalization that allows direct comparison across trails of different lengths. Hourly densities were then aggregated across all days within a bout to obtain a distribution of density values for each trail and hour. Bootstrapped means and 95% confidence intervals (10,000 resamples) were computed to characterize temporal activity patterns along each trail. To assess whether directional movement differed across trails directional density for outbound and inbound ants were computed separately. We then defined the directional density difference as

$\rho(t,d,h)_{away} - \rho(t,d,h)_{toward}$

As with overall densities, directional density differences were aggregated across days within each bout, and bootstrapped means and 95% confidence intervals (10,000 resamples) were computed for each trail and hour. This approach allowed us to resolve spatiotemporal patterns of directional flow, identifying which trails contributed most strongly to outbound or inbound movement during specific time windows.

Trajectory clustering and classification

Individual ant trajectories were extracted from tracking data by grouping detections by unique ant ID across consecutive video frames. Short trajectories with fewer than 20 detections were excluded. For each trajectory, four features were computed: (1) efficiency, defined as the straight-line distance from start to end divided by the total path length, quantifying path directness; (2) straight-line distance, the Euclidean distance between trajectory start and end points; (3) average absolute angle change, the mean change in movement direction between consecutive frames, and (4) total trajectory length, the cumulative distance traveled along the path. Features were standardized using z-score normalization to ensure equal weighting across different scales. Trajectories were grouped using K-means clustering. To select the appropriate number of clusters without imposing prior assumptions about behavioral categories, we used an automated elbow-detection procedure. K-means was evaluated for K values ranging from 2 to min(10, n/2), where n is the number of trajectories. For each K, we computed the within-cluster sum of squares (inertia). The elbow point was defined as the value of K that maximized the second derivative of the inertia curve, corresponding to the onset of diminishing returns

in cluster compactness. This procedure balances model complexity with cluster quality, avoiding over-segmentation. The resulting clusters were then interpreted as putative behavioral modes based on their characteristic feature profiles (e.g., highly direct outbound paths, tortuous local search, short displacement movements near the nest entrance). To evaluate whether a specific behavior, namely excavation, could be automatically detected from trajectory geometry alone, we trained a binary classifier using a manually annotated dataset. Excavating ants were identified directly from the videos: individuals could be seen exiting the nest entrance while carrying a small piece of material, flicking or dropping it outside, and then returning back inside. The characteristic flicking motion was especially visible and served as the primary cue for annotation. Using this criterion, we annotated 30 excavating ants across 5 videos. An equal number of non-excavating ants, trajectories in which no carrying or flicking behavior was observed, were also annotated. All annotations were performed on a single data-collection bout from one nest (1–10 August 2024, nest 1), where excavation was most clearly visible. This analysis is therefore intended as a feasibility demonstration, rather than a fully general behavioral model. For each annotated trajectory, we extracted the same four movement features used for clustering. We additionally computed nest proximity, defined as the Euclidean distance between the trajectory's starting point and the closest pixel of a binary nest mask, to test whether spatial information improved classification performance. All features were standardized using z-score normalization prior to model training. Classification was performed using logistic regression with L2 regularization trained using leave-one-video-out cross-validation. Performance was

quantified using accuracy, precision, recall, F1 score, and AUC-ROC, and we compared models trained with vs. without the nest proximity feature to assess its contribution.

4.4 Results

Ant detection and tracking

Sharma et. al (Sharma et al., 2024) demonstrated reliable single-frame detection of individual ants using Faster R-CNN (Ren et al., 2015), enabled by close-range, high-resolution color imaging. In contrast, ants in our recordings occupy fewer pixels and were imaged using grayscale infrared illumination, substantially reducing visual contrast and making single-frame detection challenging (Fig. 1C). In preliminary experiments on a subset of the data, training YOLO-v8 (Jocher et al., 2022) directly on raw frames resulted in substantially lower detection performance than when motion-based preprocessing was applied, motivating the use of background subtraction as described in the methods. Motion-encapsulated frames highlight moving ants, substantially improving visibility in single frames (Fig. 1D). Using these motion-encapsulated frames, we compared several ant detection approaches, including simple blob detection, a general-purpose object detector (YOLO-v8), and a detector designed for dense collections of small objects (HerdNet) (Table 1). For YOLO-v8, we additionally evaluated sliced inference using SAHI (Akyon et al., 2022) to improve small-object detection, but this did not yield performance gains in our setting. HerdNet (Delplanque et al., 2023), originally developed to count dense herds of animals in aerial imagery and optimized for detecting small,

visually similar objects with non-uniform densities, achieved the highest F1 score on the validation set and was therefore used for all subsequent analyses. The overall F1 score on the held-out test set was 0.759. Detections using HerdNet on a single frame are shown in Fig. 1E. Performance on the test set, reported separately by nest and video (two videos per nest, one day and one night), is summarized in Table 3. For tracking, we performed a grid search over SORT (Bewley et al., 2016b) parameters using the validation set (Table 2). The best performance was obtained with a maximum track age of 7 frames, IoU threshold of 0.1, and a minimum of 1 hit. Our best configuration achieved a HOTA score (53.17) on our test set. Using this tracker, 47.69% (227/476) of annotated ants were mostly tracked (≥80% of their ground-truth trajectory), 43.7% (208/476) were partially tracked (20–80%), and 8.61% (41/476) were mostly lost (<20%). Results on the test set (Table 4) show no significant differences in tracking performance between day and night conditions per nest (Fig. 1F).

Hourly ant counts reveals sharp increase in count at sundown

The number of unique track IDs per-frame are used as ant count. Plots showing average counts per hour across all days of collection per data bout, along with their bootstrapped means and 95% confidence intervals per hour are shown in Fig. 2. No day light savings change was implemented. Except for data collected between mid-November – early December (Fig. 2E), we see that ant count rises sharply between the hours of 19:00 – 20:00 in August (Fig. 2A, C, F, G), and 18:00 to 20:00 in late October to November (Fig. 2B, D) across all nests. Ant count rises sharply, stays relatively high, and then starts to gradually taper off during early daylight hours. The sharp rise in ant count seems to align

well with sunset time, as days get shorter later in the year, the sharp increase in ant activity is advanced. Ant count is lowest during 15:00 to 18:00 in August, and 9:00 to 17:00 in October. Data from mid-November – early December follows a different trend. As we go from August to December, overall ant count decreases.

Ant direction classification reveals large efflux of ants at sundown

To quantify directional traffic around each nest entrance, moving ants were classified as traveling away from the entrance, toward the entrance, or tangentially (unknown) (see Methods). For each hour h of day d, we computed the net directional difference ($D(d,h)=Counts(d,h)_{away} - Counts(d,h)_{toward}$), across all days within a bout and calculated bootstrapped means and 95% confidence intervals. Positive values indicate net outward movement. Across the seven recording bouts from three nests, five bouts exhibited clear outward pulse at sundown, coinciding with the sharp increase in overall ant activity and aligned with local sunset times. Outside this sunset window, directional patterns varied considerably among nests and sampling periods, highlighting colony-level and temporal variation in movement dynamics. Nest 1: Both bouts (Aug 1-10; Oct 22-Nov 2) showed a pronounced outward pulse at sunset (Fig. 3B, C). and an outward tendency through much of the night, with a brief, weak inward shift near 06:00-07:00. Nest 2: Two bouts (Aug 22-Sept 2; Oct 3-19) showed strong outward movement restricted to the sunset period, followed by nighttime values that trended inward (Fig. 3D, E). The third bout (Nov 15–Dec 6) showed a different structure, with outward movement in the early afternoon and evening and a reduced sunset pulse (Fig. 3F). Nest 3: One bout (Aug 1–26) exhibited a modest outward sunset pulse and near-zero net directional difference overnight, with a

slight inward bias at 06:00. The second bout (Aug 26–Sept 18) showed no consistent directional bias (Fig. 3G, H).

Taken together, these results indicate that the sunset increase in ant activity is typically associated with a coordinated net outward movement, but the magnitude, duration, and direction of movement after sunset vary substantially both among nests and between bouts at the same nest. This variation likely reflects differences in colony-level foraging schedules, nest architecture, and local ecological conditions.

Bout-averaged net directional difference reveals consistent outward bias across most bouts

To assess overall directional tendencies across each multi-day sampling period, we aggregated all hourly net directional difference values for each bout and computed bootstrapped mean and 95% confidence interval (Fig. 3I, Table 5). This measure reflects the average hourly imbalance between ants leaving and returning to the nest across the entire bout. Five of the seven bouts had bout-averaged net directional differences that were significantly greater than zero, indicating consistent hourly outward bias. Both bouts from Nest 1 showed strong outward asymmetry (means 5.6 and 2.0; CIs not overlapping zero). At Nest 2, two bouts exhibited moderate outward hourly bias (means 0.85 and 2.09; CIs excluding zero), whereas the third bout produced a slightly negative point estimate with a CI spanning zero, consistent with balanced or weakly inward-leaning movement. At Nest 3, one bout showed a small but statistically supported outward bias (mean 0.60; CI > 0), and the other showed no detectable directional

difference (CI spanning zero). Thus, although hourly directional differences varied among nests and across bouts, most sampling periods exhibited a consistent outward hourly bias when averaged across the full duration of observation.

Directional speed differences and their relationship to traffic imbalance

We next examined whether directional traffic differences computed above were accompanied by differences in movement speed. For each day d and hour h, we computed the directional speed difference

$$S(d,h) = S(d,h)_{away} - S(d,h)_{toward}$$

where positive values indicate faster outbound movement. Although speed differences were modest in magnitude (typically 1–3 px s^{-1}), their temporal structure frequently paralleled that of the directional count differences within the same bout. Across all bouts, both analyses showed strong coupling between directional traffic and directional speed. First, directional speed and directional traffic exhibited robust monotonic co-variation: daily Spearman correlations ranged from 0.60 to 0.73, with bootstrapped 95% confidence intervals excluding zero for every bout. Second, the sign-alignment analysis showed that the direction of the speed difference consistently matched the direction of the traffic difference. Mean sign-alignment proportions ranged from 0.56 to 0.79, with all confidence intervals exceeding the 0.5 expected under random alignment (Table 6). Together, these results indicate that hours with greater outward (or inward) traffic also

tended to show correspondingly faster movement in the same direction. In practical terms, when more ants were leaving the nest than returning, outbound ants moved slightly faster; likewise, during periods dominated by returning traffic, inbound ants tended to move faster. This reveals a consistent coupling between the magnitude and direction of traffic imbalance and the relative speeds of outbound and inbound ants.

Circadian rhythm dictates ant count while temperature dictates speed

To examine how environmental variables influence ant activity, we fit separate mixed-effects models predicting either total ant count or mean walking speed from temperature, humidity, light level, and time of day. Data from all three nests and all bouts were aggregated for analysis, with a random intercept included to account for differences in baseline activity across nests. Time-of-day was decomposed into cyclic sine and cosine components, all predictors were standardized, and both ant counts and ant speeds were log-transformed, which improved model fit as indicated by lower AIC. We focused on main-effects models to identify the dominant circadian and environmental drivers of activity and speed; interaction terms were not included as they were not central to the biological questions addressed. In the mixed-effects model for ant counts (Table 7), time-of-day emerged as the dominant predictor, with the cosine term showing the largest standardized effect ($\beta = 0.636$, $p < 0.001$). This indicates that circadian dynamics are the primary driver of colony-level activity patterns. Temperature ($\beta = 0.214$, $p < 0.001$) and humidity ($\beta = 0.185$, $p < 0.001$) also positively influenced counts, whereas light level had a negative association ($\beta = –0.193$, $p < 0.001$). Nests differed in their overall mean

activity levels (random intercept variance = 0.347), but the shape of the daily rhythm and the influence of environmental variables were consistent across nests. Seasonal changes in baseline activity and sunset timing were largely captured by temperature, humidity, and light, suggesting that environmental conditions modulate activity around a robust circadian rhythm. In contrast, variation in walking speed was driven primarily by environmental conditions, particularly temperature. In the corresponding mixed-effects model for log-transformed speeds (Table 8), temperature showed the largest standardized effect ($\beta = 0.376$, $p < 0.001$), indicating that warmer conditions substantially increased movement velocity. Time-of-day also contributed to speed modulation through both the sine ($\beta = 0.051$, $p < 0.001$) and cosine ($\beta = 0.113$, $p < 0.001$) terms, while humidity had a smaller positive influence ($\beta = 0.061$, $p < 0.001$) and light level again negatively predicted behavior ($\beta = –0.182$, $p < 0.001$). Nest-level variation in baseline walking speeds was minimal (random intercept variance = 0.012), suggesting that environmental factors played a stronger role than nest identity in shaping velocity patterns.

Flux maps revealed strong, spatially structured bidirectional traffic in every colony

For every hourly video, we generated separate flux maps for ants moving away from and toward the nest entrance. In each bin of a map, the direction of each arrow reflects the average velocity vector within that spatial bin, and arrow length scales with the flux magnitude (the product of average ant density and average velocity). Example flux maps from a representative hour (Fig. 4A) show that outbound and inbound traffic generally occupy the same trail corridor but flow in opposite directions. To quantify similarity between the spatial patterns of outbound and inbound movement, we computed a 24×24

cosine-similarity matrix for each day, comparing the flux-magnitude maps of ants moving away from versus toward the nest entrance for every pair of hours. A representative similarity matrix for one day (08-02-2024) from nest 1 (Fig. 4B) exhibits a clear block structure: daytime hours are more similar to other daytime hours, and nighttime hours to other nighttime hours, reflecting strong circadian modulation of total movement. Critically, all matrices also showed a pronounced diagonal, indicating that for each hour, the spatial distribution of outbound flux closely matched the spatial distribution of inbound flux. This pattern reflects bidirectionality at the colony scale: ants leaving and returning to the nest tend to use the same spatial routes within each hour. To evaluate whether the diagonal structure exceeded chance expectations, we applied the blocked band-contrast permutation test described in the methods. For every day across all data-collection bouts, the observed diagonal contrast was significantly greater than values from the circadian-preserving null distribution ($p < 0.05$) (Fig. 4C). Thus, bidirectional trail use is a robust and consistent feature of colony-level traffic organization.

Daily spatial routing patterns are stable across multi-day bouts

To test whether colony-level spatial routing patterns were preserved across days, we compared cumulative flux maps computed separately for each day within a bout. For each day, we constructed a daily cumulative flux map by summing hourly flux maps for ants moving both away from and toward the nest entrance. We then computed pairwise cosine similarity between all pairs of daily maps within a bout. Across all nests and bouts, daily cumulative flux maps showed high similarity to one another, indicating strong day-to-day consistency in the spatial distribution of traffic (Table 9). In the longest

sampling bout (26 days), cosine similarity values between daily maps were consistently high (median = 0.726; mean = 0.765; minimum = 0.522; maximum = 0.969) (Fig. S1). In contrast, cosine similarities computed from spatially shuffled versions of the same maps were substantially lower across all bouts (median range = 0.075–0.296; mean range = 0.079–0.299), confirming that the observed similarity reflects preserved spatial organization rather than shared overall activity levels. Day-to-day cosine similarity matrices exhibited a clear block structure (Fig. S1), with higher similarity among temporally adjacent days than among days farther apart. This pattern indicates that while the spatial layout of trails is highly stable across the bout, the relative distribution of traffic across trails changes gradually over time. Such slow shifts likely reflect changes in environmental conditions or colony state rather than reorganization of the trail network itself. These results demonstrate that the colony's major movement corridors near the nest entrance remain stable over extended periods, motivating a finer-grained, trail-resolved analysis of traffic dynamics.

Trail analysis reveals certain trails are used only at night, and others throughout the day

As described in the methods, for each sampling bout we identify trails using the cumulative flux map across the bout (Fig. 4D). This gives us around 5-12 trails per bout. As trails differ in length, we compare length normalized counts along trails at every hour over all days in a bout. Length-normalized ant densities on each trail matched the respective bout-level activity pattern: sharp sunset-driven nocturnal peaks in most bouts, and the distinct midday–evening structure in the late-season nest 2 bout (Nov 15-Dec 6).

This synchronization held across all trails and colonies. Despite this shared temporal structure, trails differed in overall usage and daytime inactivity. In each bout, a subset trails carried consistently higher nighttime densities than others, forming a set of prominent routes used heavily during peak activity periods. In contrast, several trails that were active at night showed pronounced daytime suppression, with densities dropping to zero or near zero for extended midday intervals (e.g., Nest 1 trails 3, 7, 9, 11 Fig. 4E; Nest 2 trails 2,3,5,6 Fig. 4F) while other trails maintained low but nonzero daytime traffic. Together, these results show that although the colony's daily movement cycle is synchronized across all trails, individual trails exhibit distinct temporal activity profiles, from routes that maintain steady low-level daytime traffic to routes that are essentially unused during the day and reactivated at night.

Directional differences reveal trail-specific spatiotemporal structure

To examine whether the bout-level directional imbalance was distributed uniformly across trails or structured spatially, we computed the directional density difference ($\rho(t,d,h)_{away} - \rho(t,d,h)_{toward}$) for each trail t, hour h of day d. These differences, though small in magnitude, consistently identified when and where directional flow occurred within the trail network. Nest 1 bout 1 illustrates these patterns clearly (Fig. 5). At the bout level, ants exhibited a strong outward movement surge at sunset, followed by a moderate inward return in the early morning. Trail-resolved directional differences showed that this outward surge was not uniformly expressed across the network. Instead, outbound movement at sunset was concentrated on trails 1, 6, and 7, which showed

significant positive density differences. Inbound return around 06:00–08:00 was highly localized, occurring almost exclusively on trails 3 and 9, while most trails remained weakly outbound or near zero. Trails 2, 4, and 5 exhibited a delayed outward increase, ramping up later during the night rather than exactly at sunset. Thus, the colony-level outward and inward biases emerged from coordinated but nonuniform contributions of specific trails, with different spatial routes preferentially used for outbound or inbound movement at different times. Across all seven bouts, we observed 1) outbound biases at sunset were typically expressed on several but not necessarily all trails; 2) inbound biases, when present, were usually restricted to a subset of trails; and 3) certain trails showed repeatable directional biases within specific time windows (e.g., at sunset or during morning return), whereas others exhibited weaker or more variable biases. In summary, our trail-resolved analyses reveal distinct spatiotemporal patterns: some trails exhibit strong outbound biases at sunset, others carry disproportionate inbound movement in early morning, and several remain weakly biased or directionally balanced throughout the day.

Unsupervised clustering reveals four recurring movement motifs

To characterize the natural structure of movement patterns in the tracking data, we applied K-means clustering to all trajectories from the nest 1 bout 1. Four robust clusters emerged (Fig. 6), representing distinct geometric movement motifs. Visual inspection of representative trajectories showed that these clusters corresponded approximately to long–loopy (Fig. 6B), long–straight (Fig. 6A), short–loopy (Fig. 6D), and short–straight paths (Fig. 6C). These motifs capture major axes of variation in both displacement and

tortuosity and provide a low-dimensional summary of the typical movement patterns observed around the nest. Because excavation behavior involves a characteristic outbound–deposit–return sequence, we examined whether annotated excavation trajectories tended to occupy specific regions of this feature space. Of the 30 annotated excavating ants, 19 fell into the long–loopy cluster, indicating that excavation movements exhibit a recognizable geometric signature even before applying supervised methods. This cluster-level organization motivated the use of a classification approach to test whether excavation could be detected automatically from trajectory features alone.

Excavation behavior is moderately predictable from geometric trajectory features

We trained a logistic regression classifier to distinguish excavating from non-excavating trajectories using the four geometric features (efficiency, displacement, total length, turning angle) and optionally a spatial feature (nest proximity). Classification performance was evaluated using leave-one-video-out cross-validation. A model trained on geometric features alone achieved an average accuracy of 0.76 (precision: 0.83, recall: 0.74, F1: 0.76, AUC-ROC: 0.82). Including nest proximity improved performance to 0.87 accuracy (precision: 0.89, recall: 0.88, F1: 0.88, AUC-ROC: 0.94), indicating that while excavation is primarily expressed through movement geometry, spatial context provides a modest but measurable benefit. Overall, cross-validated accuracies of 87% show that the behavioral state of excavating can be inferred from simple trajectory-level summaries with substantially better-than-chance performance. Because excavation was very clearly visible in this single data-collection bout, classifier training and evaluation were restricted

to this dataset. We therefore treat this analysis as a proof-of-concept demonstration rather than a general behavioral model.

4.5 DISCUSSION

In this study, we demonstrate a computer vision–based approach for long-term, automated monitoring of colony-scale movement and behavior in the ecologically dominant ant species, *Liometopum occidentale*. By tracking thousands of ants in short hourly videos collected over multi-day sampling bouts from 3 ant nests in the Angeles National Forest, we quantified circadian activity patterns, directional imbalances in traffic flow, environmental drivers of ant abundance and walking speed, and spatiotemporal structure in movement along distinct trails. We further show that individual movement trajectories alone are sufficient to identify task-specific behaviors such as excavation, highlighting the potential for recovering aspects of division of labor from tracking data. Together, our analyses reveal a pronounced circadian organization of colony activity, with ant numbers peaking sharply at sunset, a consistent outward surge during evening hours, and nest- and bout-specific patterns of return. Ant abundance was governed primarily by time of day, whereas walking speed was driven mainly by temperature. Directional differences in traffic and movement speed were tightly coupled, and trail-level analyses uncovered substantial heterogeneity in both overall usage and directional dynamics.

Previous field studies, based on manual observations, have suggested that *Liometopum* activity is broadly similar during day and night (Shapley, 1920b). By contrast, our long-term, hourly recordings across multiple nests reveal a more structured pattern: while some activity occurs throughout the day, ant traffic increases sharply at sunset and remains elevated throughout the night, indicating that colony activity is predominantly nocturnal. By simultaneously monitoring environmental variables, our results corroborate early manual observations by Shapley (Shapley, 1920b), confirming a strong positive relationship between temperature and walking speed under natural field conditions. Intraspecific temporal niche differentiation has been reported in some ant species (Houadria and Menzel, 2020) and can be a strategy to avoid competition between conspecifics. In contrast, our data show no evidence of temporal segregation among neighboring *Liometopum* nests. Instead, all monitored nests exhibited closely aligned circadian activity patterns, with synchronized nocturnal foraging and a shared sunset-driven outbound surge. Wang et al. (Wang et al., 2010) reported little to no aggression between workers collected several kilometers apart and proposed that this species may form polydomous or supercolony-like systems. However, aggression assays are highly context-dependent and can vary with group size, environmental conditions, and resource context, making colony boundaries difficult to infer from behavioral assays alone. While our results do not rule out spatial niche partitioning among nests, they indicate that neighboring nests do not differ in the timing of their collective activity. Definitive resolution of colony structure in *Liometopum* will require genetic analyses across nests

and spatial scales, which would complement the behavioral evidence provided by long-term automated monitoring.

While neighboring nests exhibited closely synchronized circadian activity, movement within each nest was structured across space as well as time. Although the colony's overall movement cycle is synchronized across all trails, individual trails express distinct temporal activity profiles, ranging from routes that maintain steady use across the day to pathways that are effectively inactive during daylight hours and reactivated at night. This heterogeneity suggests functional differentiation among trails rather than uniform routing. In *Liometopum*, such differentiation may reflect differences in destination type or task context, for example, trails ascending into the canopy may preferentially support aphid tending or arboreal resource use, whereas ground-oriented trails may serve terrestrial foraging routes. Although we cannot directly assign trail function from movement data alone, future experiments combining entrance monitoring with spatially distributed colored baits or labeled resources could link trail-specific traffic to resource type and destination, enabling functional annotation of trail networks and task routing in natural settings. Independent of trail function, however, spatial routing patterns near the nest entrance were stable across days within a bout, even though activity along some trails dropped to near zero during daylight hours. Daily cumulative flux maps remained highly similar over periods of weeks, indicating that major movement corridors persist beyond short-term fluctuations in traffic intensity. This persistence is consistent with prior manual observations of long-lived *Liometopum* trails (Wang et al., 2010).

Across most sampling bouts, we observed a pronounced outward movement of ants at sunset, resulting in a net efflux from the nest that likely reflects circadian initiation of nocturnal foraging. Following this initial outbound surge, the balance of directional movement varied among nests and bouts: some showed sustained outbound bias, others exhibited more balanced traffic, and some showed increased inbound movement later in the night or during the early morning hours. These nest- and bout-specific differences indicate that while the onset of outbound movement is conserved, return dynamics are flexible and context-dependent rather than governed by a fixed schedule. Several non-mutually exclusive mechanisms could underlie this variation, including differences in colony size, nutritional state, or the spatial distribution of foraging sites. For example, colonies exploiting a limited number of distant food sources might exhibit more synchronized early-morning returns, whereas colonies foraging across multiple locations or distances could show more temporally distributed inbound traffic. Seasonal changes in resource availability may further modulate these patterns, as suggested by shifts in net efflux observed in late-season bouts. We also observed a consistent coupling between directional traffic imbalance and directional movement speed: hours with stronger outbound or inbound traffic tended to show higher speeds in the same direction. This pattern is non-intuitive, as increased traffic might be expected to reduce walking speed through congestion or interference. Instead, the positive coupling between traffic and speed suggests that both reflect shared behavioral states associated with task engagement, such as rapid, goal-directed outbound movement during foraging initiation or coordinated

inbound return. Consistent with this interpretation, periods of high traffic were accompanied by recruitment across multiple trails, which may mitigate local congestion and allow higher speeds to be maintained even during peak flow. Together, these findings indicate that traffic flow and movement speed are co-regulated components of collective behavior rather than opposing effects of crowding. Beyond colony- and trail-level dynamics, our analyses demonstrate that individual movement trajectories alone contain sufficient information to distinguish specific behavioral states. Unsupervised clustering revealed distinct movement patterns, with annotated excavating ants overwhelmingly concentrated within a single cluster, and a supervised classifier trained solely on trajectory-derived features was able to identify excavation with high accuracy. These results show that task-specific behaviors can be inferred from kinematic signatures alone, without explicit visual cues of substrate manipulation or contextual annotation. This provides a scalable framework for studying division of labor in large, unmarked populations under natural field conditions and opens the door to linking individual task allocation to colony-level organization over extended timescales.

Several limitations frame the scope of our conclusions. First, monitoring was restricted to a single nest entrance per colony. Although entrances were selected based on high activity at the start of each sampling bout, *Liometopum* nests can have multiple openings, and patterns of entrance use may shift over time or across seasons. As a result, the observed traffic may not capture all colony-level movement. Second, monitoring was limited to nest entrances and proximal trail segments, and therefore does not capture full

foraging paths or interactions at distant resources. Third, although we observed inter-nest variation in directional dynamics, genetic relatedness among nests was not assessed, precluding inference about colony boundaries or super colony structure. Finally, while trajectory-based classification successfully identified excavation behavior, extending this approach to a broader behavioral repertoire will require additional annotation and training data. Addressing these limitations will require integrating entrance-based monitoring with larger spatial coverage and complementary genetic or experimental approaches. Despite these limitations, our study demonstrates the power of long-term, automated field monitoring for uncovering multiscale organization in social systems under natural conditions. By combining computer vision with sustained environmental sampling, we capture how circadian timing, environmental conditions, movement kinematics, and spatial routing interact to shape colony behavior. For ecologically dominant species such as *Liometopum occidentale*, whose activities influence nutrient flow, species interactions, and ecosystem structure, such approaches provide a critical bridge between individual behavior and landscape-level processes. More broadly, our framework offers a generalizable strategy for studying collective behavior in natural settings, enabling quantitative analyses that were previously infeasible outside the laboratory.

4.6 Figures and tables

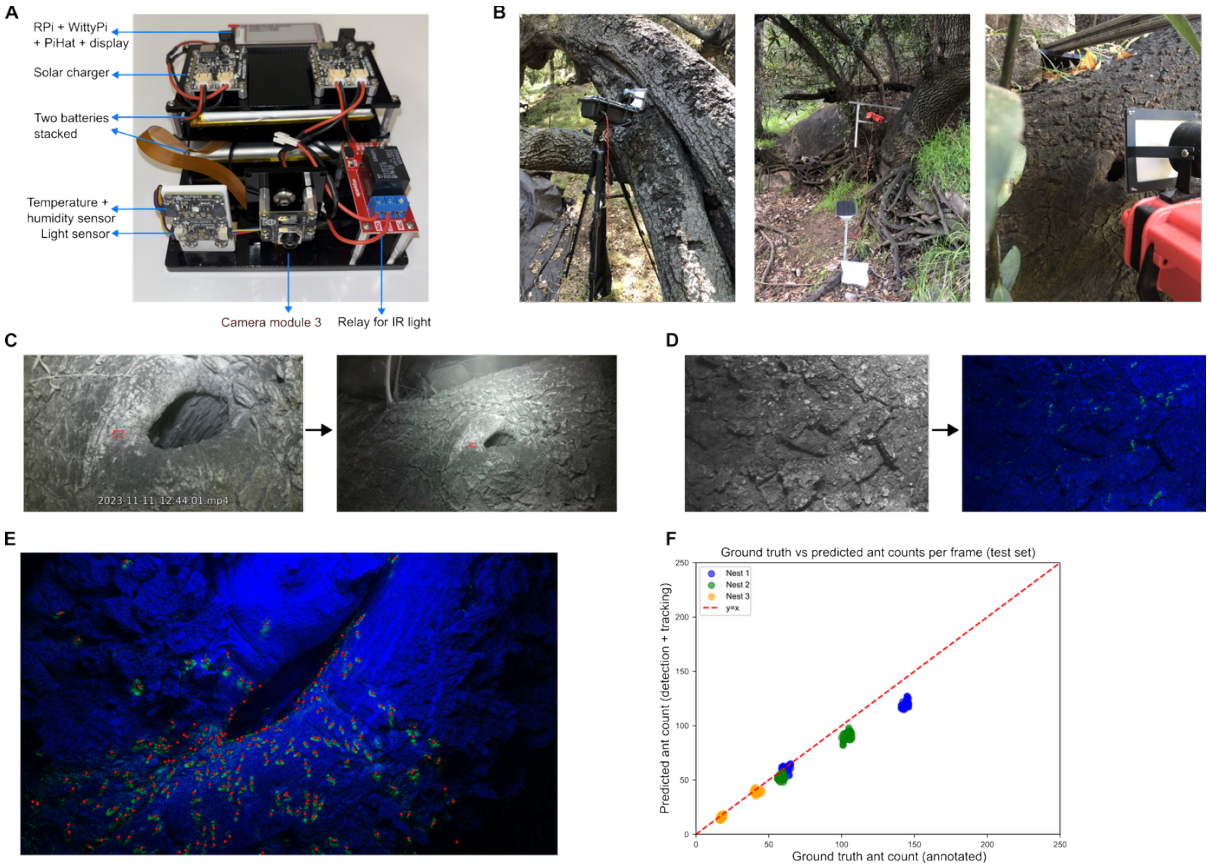

Figure 1: Overview of imaging setup, data, and computer vision. (A) Ethocam modified from Sharma et. al. Modifications include switching cameras to Raspberry Pi Camera module 3 wide no-IR, the addition of a second battery exclusively for the external IR light, and its corresponding second solar charger. (B) Ethocam in the field, mounted using a tripod and imaging the intersection of two barks for nest 3 (left), and mounted using a custom mount positioned in front of a hole on nest 1 (middle and right). (C) Same nest imaged in Sharma et. al. Going from the raspberry pi HQ camera (left) to the camera module 3 (right) greatly increases the area in the imaging plane, allowing for analysis of movement and behavior around nest entrance. Single ant shown in red box for scale. (D) Motion encapsulation via addition of the difference between current frame and background in the green channel, greatly increases visibility of moving ants. Original frame is retained as blue channel and red channel is set to zero. These transformed frames were used for annotation and subsequent analysis using computer vision. (E) Example transformed frame from nest 2 showing detections using our best model (HerdNet) as red dots. Nest entrance hole was masked for downstream analysis. (F) Ground truth vs predicted ant counts (after detection + tracking) for the test set containing two videos each from 3 nests, one at day and one at night. Each dot represents values for a single frame (annotated test set sequences were 30 frames each). Predicted counts closely follow ground truth counts.

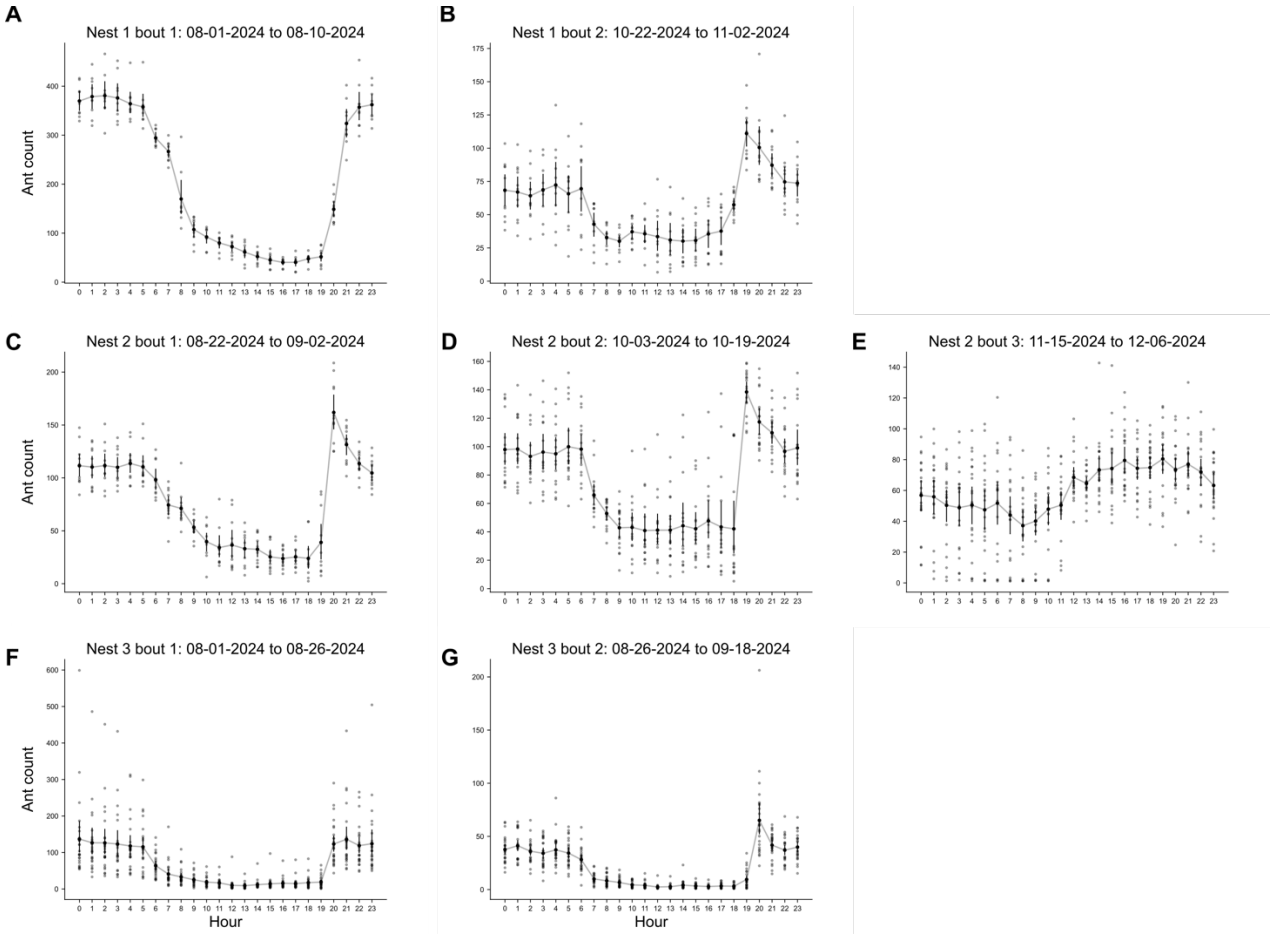

Figure 2: Increase in ant count at sundown across all nests. Gray dots depict average ant count per hour (average number of tracked ants across a 30 second video collected at the start of every hour) across multi-day sampling bouts for 3 ant nests ((A,B) nest 1; (C,D,E) nest 2; (F,G) nest 3). Bootstrapped means and 95% confidence interval are plotted in black for each hour. We see a sharp increase in mean ant count around sundown (20:00-21:00 in the months of August and September; 18:00-19:00 for mid-late October). Patterns for late November-December (E) show a different trend. Ant count remains elevated at night and drops down in the morning.

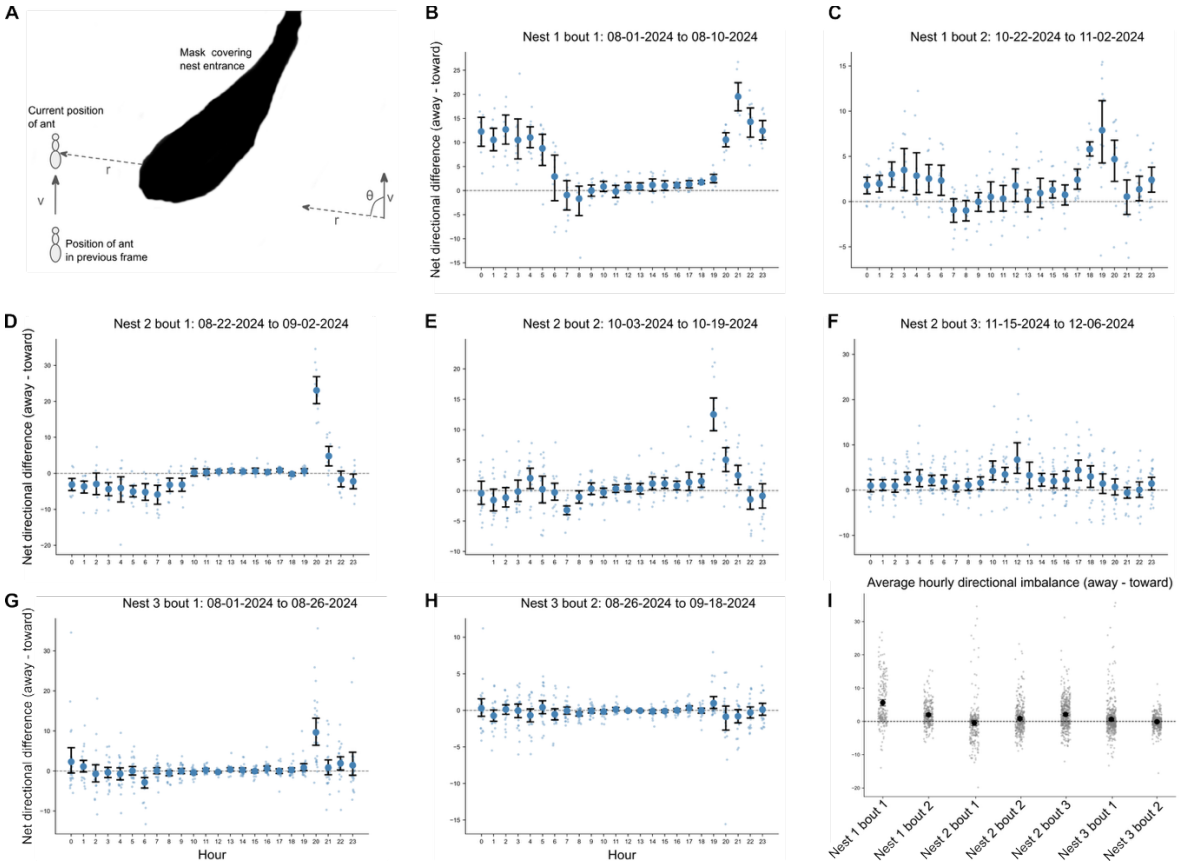

Figure 3: Net directional difference in ant count at every hour and aggregated across all hours. (A) Cartoon illustrating the procedure for classification of direction per ant. The angle between the velocity vector v (based on the ant's position in the previous frame), and radial vector r (vector drawn from the closest point on the mask covering the nest entrance to the ant's position) is used to determine direction. Ants with an angle between 0 and 70 are classified as moving away from nest entrance, between 70 and 110 as unknown (tangentially), and between 110 and 180 as toward the nest entrance. (B-H) For every video, the difference between the number of ants going away from nest entrance and number of ants going toward the nest entrance is plotted for each sampling bout. Bootstrapped means and 95% CI are plotted per hour. In 5 out of 7 bouts, we see a strong outbound directional bias at sundown. Subsequently patterns of movement differ between bouts and nests. (I) Hourly directional differences aggregated across all hours and days for each bout along with bootstrapped mean and 95% CI. Bouts show either balanced or net efflux of ants to varying extents potentially due to varying nutritional needs, nest sizes, resource quality etc.

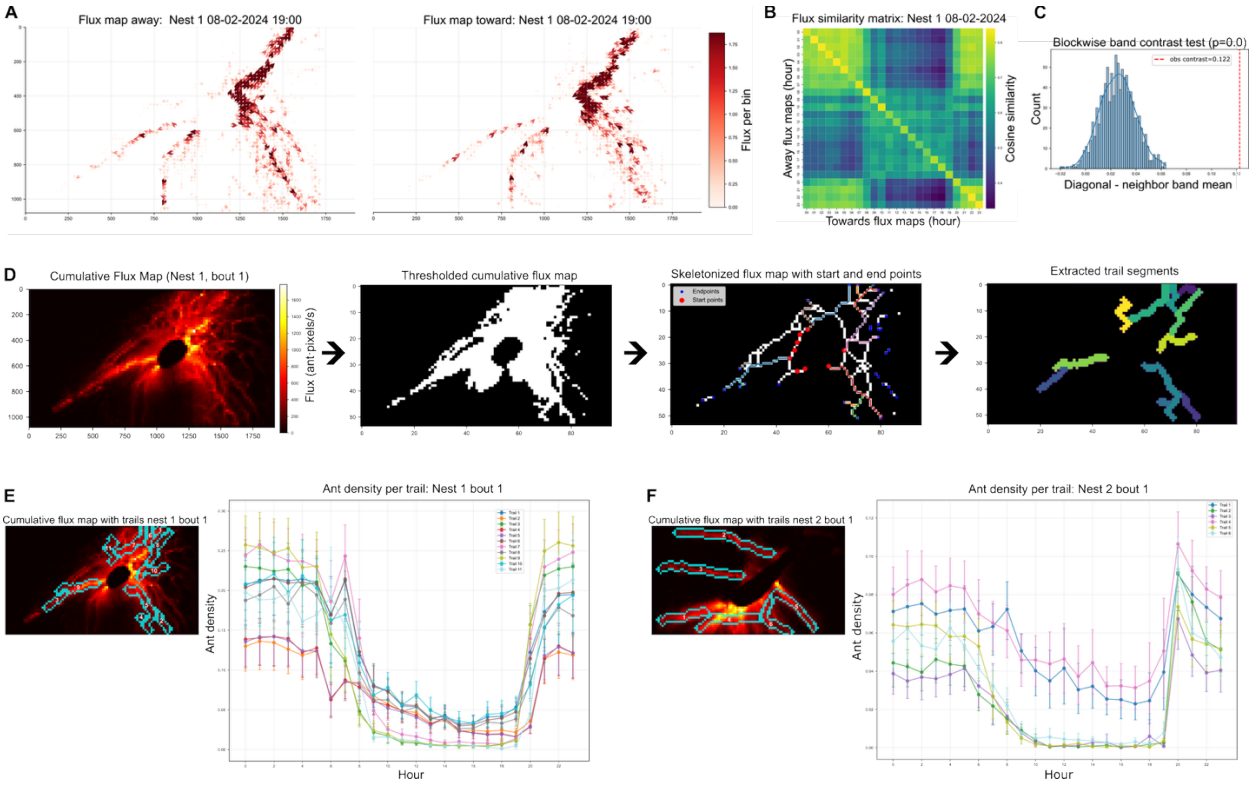

Figure 4: (A) Directional flux maps for one video (one hour of one day) for both away and toward directions. Values of flux are computed for every 20 x 20 pixel bin. Direction of arrow represents the vector average whereas color and size of the arrow represents magnitude of flux (ant count x velocity). (B) Similarity matrix constructed for one day (08-02-2024 nest 1 bout 1) where cosine similarity is calculated between flux maps in the away vs toward directions at every hour. (C) Corresponding histogram to test if the diagonal in (B) is significant. The difference between the diagonal and the 1 and 2 offset diagonals was compared before (red dashed line) and after block-wise shuffling. (D) Procedure for automatic trail segmentation per bout. Cumulative flux map for all ants (irrespective of movement direction) across all hours and days for a given sampling bout is computed. Binary thresholding is then performed using a threshold value at 70th percentile of cumulative flux map. This is followed by skeletonization using the skeletonize function from sklearn to reduce the mask to a one pixel wide skeleton. The skeleton is then converted to a graph with skeleton points treated as nodes. Endpoints (blue) are those with only one neighboring node (degree=1), and start points (red) are points on the skeleton that are within a set distance from the nest entrance mask. The shortest paths between every end point and start point are determined such that each end point is only associated with one start point. These shortest paths are the individual trail segments shown in color. (E) Cumulative flux map with trail segments (numbered) plotted on top. Length normalized ant counts (number of ants along a trail segment divided by the number of bins that the trail occupies), or density for each trail is plotted on the right. Bootstrapped means and 95% CI are plotted for all hours across all days of the sampling bout. Trails differ in density with some trails dropping to zero during the day. (F) Same as in (E) but for bout 1 (08-22-2024 to 09-02-2024) from nest 2.

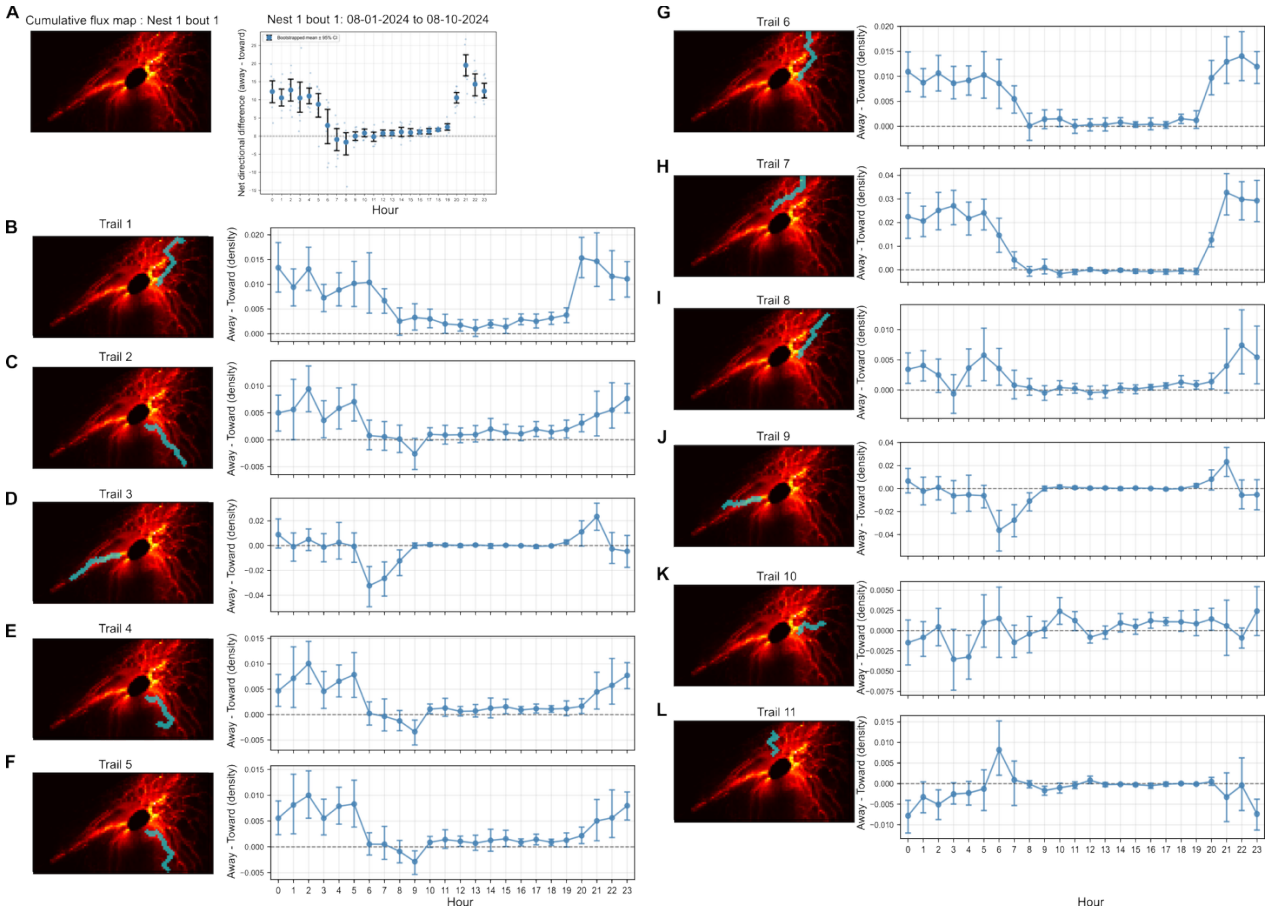

Figure 5: Non-uniform distribution of directional traffic across trails for nest 1 bout 1. (A) Cumulative flux map obtained by summing flux maps over all hours and days (irrespective of direction) along with overall net directional difference in ant counts. Same data as Fig. 4 replotted here for ease of reference of overall trend. (B-L) Individual trail segments plotted over cumulative flux map, along with the difference in length normalized ant counts per trail (average number of ants along a trail divided by the number of bins occupied by that trail mask), or density. Difference in densities (away – toward) were plotted as opposed to difference in counts to compare across trails. Bootstrapped mean and 95% CI are plotted per hour across all days from the entire bout.

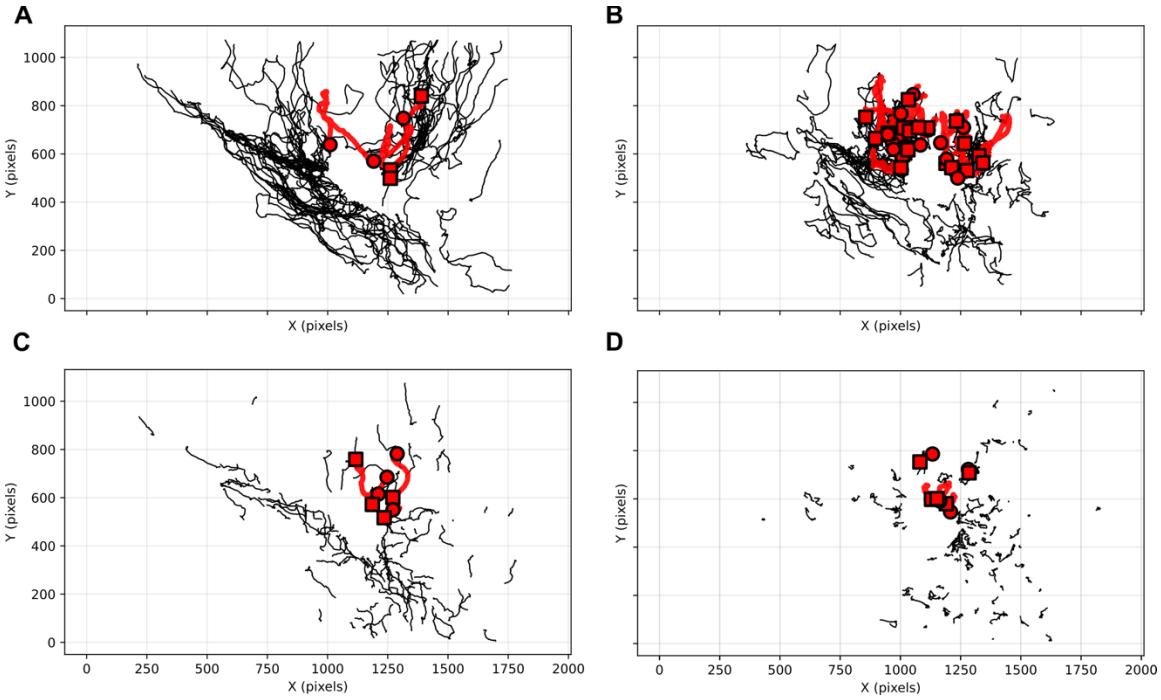

Figure 6: Clustering of individual ant trajectories. Clustering of trajectories from nest 1 bout 1 was performed after converting individual trajectories to feature vectors as described in the methods. 100 diverse examples from each cluster are shown along with 31 annotated excavating ants in red (circle: start point; square: end point). (A) Long straight trajectories. 3 out of 31 annotated excavators fell into this category. (B) Long loopy trajectories, containing 19 out of 31 annotated excavators. (C) Short straight trajectories, containing 4 out of 31 excavators. (D) Short loopy trajectories, containing 5 out of 31 excavators.

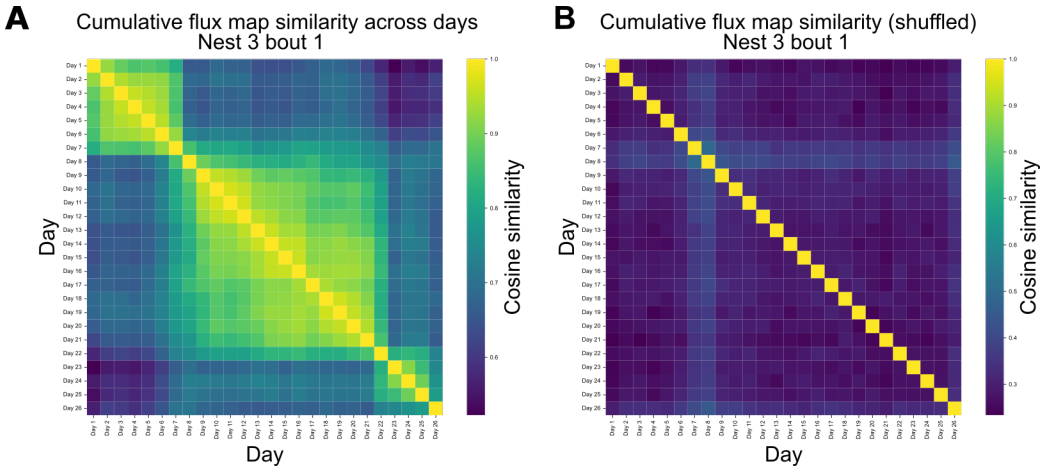

Supplemental figure 1: Persistence of spatial routing across multiple days. (A) Cosine similarity matrix between cumulative flux maps per day across 26 days from nest 3. Cumulative flux map for each direction (away, toward) was calculated separately and then maps summed to obtain cumulative flux map per day. Cosine similarity decreases between pairs of days further away but the minimum value (0.52) is still higher than the maximum similarity between pairs of the shuffled maps. Blocked structure shows gradual drift in spatial routing. (B) Same as (A) but values in cumulative flux maps per day were shuffled.

Method	F1 score on validation set
Blob detection	0.425
YOLOv8 trained on 4 videos	0.745
YOLOv8 trained on 6 videos	0.749
YOLOv8 trained on 6 videos + SAHI inference	0.750
HerdNet trained on 6 videos	**0.782**

Table 1: Comparison of various computer vision approaches for single frame ant detection on the validation set. In all cases raw frames were modified to contain motion information in their color channels (as described in methods).

Tracker parameters			Tracking metrics on validation set				
Max age	Min hits	IoU	DetA	MOTA	HOTA	IDF1	AssA
5	2	0.1	46.474	53.484	52.332	69.637	59.288
10	2	0.1	46.804	53.579	52.346	69.504	58.912
15	2	0.1	46.613	53.159	52.252	69.227	58.945
5	4	0.1	42.18	49.601	49.986	67.092	59.49
10	4	0.1	42.627	50.142	50.286	67.526	59.592
15	4	0.1	42.381	49.804	50.177	67.311	**59.687**
1	3	0.3	39.104	45.988	47.058	62.17	56.869
1	3	0.1	41.799	48.965	49.219	65.321	58.205
7	1	0.1	**49.286**	**55.419**	**53.663**	**70.557**	58.829
7	2	0.1	46.882	53.89	52.48	69.827	59.11
10	1	0.1	49.05	54.634	53.431	69.999	58.605

Table 2: Matrix of parameter values tested for SORT tracker. Common multi-object tracking metrics, ranging from detection focused to tracking focused metrics, on the validation set.

Colony	Date time	Precision	Recall	F1 score
Nest 1	2024-08-09 11am	0.860	0.878	0.869

	2024-10-22 10pm	0.856	0.748	0.798
Nest 2	2024-10-04 12pm	0.661	0.643	0.652
	2024-08-22 9pm	0.649	0.651	0.650
Nest 3	2024-08-05 4pm	0.919	0.876	0.897
	2024-08-22 3am	0.839	0.820	0.829
Combined		0.777	0.741	0.759

Table 3: Single frame ant detection metrics using HerdNet model on the test set - 2 videos per colony, one during daylight and one at night. IoU of 0.5 was used.

Colony	Date time	DetA	MOTA	HOTA	IDF1	AssA	MT	PT	ML
Nest 1	2024-08-09 11am	56.28	68.29	58.82	79.26	61.68	46	20	1
	2024-10-22 10pm	52.73	63.09	58.13	76.60	64.49	89	44	19
Nest 2	2024-10-04 12pm	41.23	31.08	45.08	56.45	49.92	21	35	7
	2024-08-22 9pm	43.11	33.50	43.07	54.95	43.48	29	80	10
Nest 3	2024-08-05 4pm	59.46	72.74	58.01	77.58	56.74	13	10	1
	2024-08-22 3am	56.42	67.15	59.39	80.25	63.01	29	19	3
Combined		49.67	53.05	53.17	69.40	57.41	227	208	41

Table 4: Multi-object tracking metrics using final detection + tracking model on the test set - 2 videos per colony, one during daylight and one at night. MT, PT, and ML stand for mostly tracked (successfully tracked for 80% of track span), partially tracked (tracked for 20-80% of track span), and mostly lost (tracked for less than 20% of track span).

Nest	Bout (2024)	Bootstrapped mean of aggregated net direction movement (away – toward)	95 % confidence interval
Nest 1	08-01 to 08-10	5.63	[4.70, 6.58]
	10-22 to 11-02	1.99	[1.57, 2.41]
Nest 2	08-22 to 09-02	–0.47	[–1.22, 0.33]
	10-03 to 10-19	0.85	[0.44, 1.28]
	11-15 to 12-06	2.09	[1.70, 2.49]
Nest 3	08-01 to 08-26	0.60	[0.26, 0.96]

	08-26 to 09-18	–0.11	[–0.26, 0.03]

Table 5: Aggregated net movement direction (away – toward) across all hours and days per bout. Bootstrapped means show that while some bouts exhibit a net efflux of ants, others remain balanced with no net ant loss.

Colony	Bout (2024)	Spearman correlation (bootstrapped mean ± 95% CI)	Sign alignment (bootstrapped mean ± 95% CI)
Nest 1	08-01 to 08-10	0.6294 [0.5203–0.7261]	0.7634 [0.6991–0.8241]
	10-22 to 11-02	0.6636 [0.5614–0.7599]	0.5568 [0.5076–0.6061]
Nest 2	08-22 to 09-02	0.6916 [0.6407–0.7410]	0.7423 [0.7045–0.7879]
	10-03 to 10-19	0.7319 [0.6860–0.7787]	0.7787 [0.7396–0.8203]
	11-15 to 12-06	0.6450 [0.5821–0.7032]	0.6040 [0.5604–0.6500]
Nest 3	08-01 to 08-26	0.6555 [0.6170–0.6912]	0.7850 [0.7550–0.8167]
	08-26 to 09-18	0.6043 [0.5531–0.6533]	0.7590 [0.7153–0.8003]

Table 6: Coupling between ant movement direction and velocity. Across all bouts we see a positive correlation between overall net directional difference (away – toward) and difference in velocities of outbound – inbound ants. Sign alignment test confirms that inbound ants have greater velocity when directional flow is inbound, and vice versa.

Predictor	Standardized β	Std. Error	z-value	p-value	95% CI
Intercept	3.769	0.341	11.06	<0.001	[3.10, 4.44]
Time (sine)	0.214	0.021	10.43	<0.001	[0.174, 0.254]
Time (cosine)	0.636	0.02	31.93	<0.001	[0.597, 0.675]
Temperature	0.214	0.03	7.16	<0.001	[0.156, 0.273]
Humidity	0.185	0.025	7.46	<0.001	[0.136, 0.233]
Light level	-0.193	0.019	-10.36	<0.001	[-0.230, -0.157]

Table 7: Mixed-effects model of environmental and circadian predictors of ant abundance. Fixed-effect coefficients (standardized β), standard errors, z-values, p-values, and 95% confidence intervals are shown for a linear mixed-effects model predicting log-transformed ant counts. Time of day was modeled using sine and cosine terms to capture circadian periodicity. Nest identity was included as a random intercept (variance = 0.347) to account for baseline differences in activity across colonies. Model fit statistics (AIC, BIC) are AIC: 7470.4, BIC: 7517.9.

Predictor	Standardized β	Std. Error	z-value	p-value	95% CI
Intercept	3.624	0.063	57.48	<0.001	[3.50, 3.75]
Time (sine)	0.051	0.008	6.74	<0.001	[0.036, 0.066]
Time (cosine)	0.113	0.007	15.49	<0.001	[0.099, 0.128]
Temperature	0.376	0.011	34.2	<0.001	[0.355, 0.398]
Humidity	0.061	0.009	6.69	<0.001	[0.043, 0.079]
Light level	-0.182	0.007	-26.59	<0.001	[-0.196, -0.169]

Table 8: Mixed-effects model of environmental and circadian predictors of ant speed. Fixed-effect coefficients (standardized β), standard errors, z-values, p-values, and 95% confidence intervals are shown for a linear mixed-effects model predicting log-transformed ant speed. Time of day was modeled using sine and cosine terms to capture circadian periodicity. Nest identity was included as a random intercept (variance = 0.012) to account for baseline differences in speed across colonies. Model fit statistics (AIC, BIC) are AIC: 1827.8, BIC: 1875.4.

Nest	Bout	Orig_ Min	Orig_M edian	Orig_ Max	Orig_M ean	Shuff_ Min	Shuff_ Median	Shuff_ Max	Shuff_ Mean
Nest 3	Bout 1	0.5220	0.7260	0.9694	0.7646	0.2330	0.2881	0.4889	0.2993
Nest 3	Bout 2	0.4314	0.5836	0.9372	0.6339	0.1616	0.2274	0.3477	0.2291
Nest 1	Bout 1	0.9005	0.9673	0.9845	0.9596	0.2689	0.2969	0.3316	0.2970
Nest 1	Bout 2	0.7219	0.8530	0.9858	0.8595	0.0378	0.0753	0.1321	0.0791
Nest 2	Bout 1	0.7431	0.9122	0.9744	0.8986	0.2151	0.2457	0.2793	0.2449
Nest 2	Bout 2	0.8293	0.9241	0.9814	0.9193	0.1578	0.2114	0.2895	0.2136

Table 9: Persistence of spatial routing (cumulative flux maps) across days for every bout. Cosine similarity statistics (excluding diagonal) for daily cumulative flux maps (away + toward) compared across days within each bout. Shuffled matrices were generated by spatially permuting flux values within each day to disrupt spatial structure while preserving magnitude distributions. Across all nests and bouts, unshuffled (orig) flux maps show substantially higher cosine similarity than shuffled controls, indicating persistent spatial organization of trail usage across days.

BIBLIOGRAPHY

Agrawal, S., Grimaldi, D. and Fox, J. L. (2017). Haltere morphology and campaniform sensilla arrangement across Diptera. *Arthropod structure & development* **46**, 215–229.

Akyon, F. C., Altinuc, S. O. and Temizel, A. (2022). Slicing aided hyper inference and fine-tuning for small object detection. In *2022 IEEE international conference on image processing (ICIP)*, pp. 966–970. IEEE.

Andersen, A. N. (1983). Species diversity and temporal distribution of ants in the semi-arid mallee region of northwestern Victoria. *Australian Journal of Ecology* **8**, 127–137.

Baines, R. A., Uhler, J. P., Thompson, A., Sweeney, S. T. and Bate, M. (2001). Altered electrical properties in drosophilaneurons developing without synaptic transmission. *Journal of Neuroscience* **21**, 1523–1531.

Beery, S., Van Horn, G. and Perona, P. (2018). Recognition in terra incognita. In *Proceedings of the European conference on computer vision (ECCV)*, pp. 456–473.

Bewley, A., Ge, Z., Ott, L., Ramos, F. and Upcroft, B. (2016a). Simple online and realtime tracking. In *2016 IEEE International Conference on Image Processing (ICIP)*, pp. 3464–3468.

Bewley, A., Ge, Z., Ott, L., Ramos, F. and Upcroft, B. (2016b). Simple online and realtime tracking. In *2016 IEEE international conference on image processing (ICIP)*, pp. 3464–3468. Ieee.

Bjerge, K., Mann, H. M. R. and Høye, T. T. (2022). Real-time insect tracking and monitoring with computer vision and deep learning. *Remote Sens Ecol Conserv* **8**, 315–327.

Bolles Lee, A. (1885). Les balanciers des diptères, leurs organes sensifères et leurs histologie. *Recueil Zool. suisse, Sér. I, 2* 363–392.

Bradski, G. (2000). The OpenCV Library. *Dr. Dobb's Journal of Software Tools*.

Brasó, G. and Leal-Taixé, L. (2020). Learning a neural solver for multiple object tracking. In *Proceedings of the IEEE/CVF Conference on Computer Vision and Pattern Recognition*, pp. 6247–6257.

Braun, A. (1939). *Zool. Jb. (Zool. Physiol.)* **59**,.

Buddenbrock, W. V. (1919). Die vermutliche Lösung der Halterenfrage. *Pflügers Arch.* **175**, 125–164.

Cao, X., Guo, S., Lin, J., Zhang, W. and Liao, M. (2020). Online tracking of ants based on deep association metrics: method, dataset and evaluation. *Pattern Recognition* **103**, 107233.

Chan, W. P. and Dickinson, M. H. (1996). Position-specific central projections of mechanosensory neurons on the haltere of the blow fly, Calliphora vicina. *Journal of Comparative Neurology* **369**, 405–418.

Chapman, K. M. and Duckrow, R. B. (1975). Compliance and sensitivity of a mechanoreceptor of the insect exoskeleton. *J. Comp. Physiol.* **100**, 251–268.

Chapman, K. M. and Smith, R. S. (1963). A linear transfer function underlying impulse frequency modulation in a cockroach mechanoreceptor. *Nature* **197**, 699–700.

Cole, E. S. and Palka, J. (1982). The pattern of campaniform sensilla on the wing and haltere of Drosophila melanogaster and several of its homeotic mutants. *Development* **71**, 41–61.

Computer Vision Annotation Tool.

Crall, J. D., Gravish, N., Mountcastle, A. M. and Combes, S. A. (2015). BEEtag: a low-cost, image-based tracking system for the study of animal behavior and locomotion. *PloS one* **10**, e0136487.

David, C. T. (1978). The relationship between body angle and flight speed in free-flying *Drosophila*. *Physiological Entomology* **3**, 191–195.

Del Toro, I., Ribbons, R. R. and Pelini, S. L. (2012). The little things that run the world revisited: a review of ant-mediated ecosystem services and disservices (Hymenoptera: Formicidae). *Myrmecological News* **17**, 133–146.

Delplanque, A., Foucher, S., Théau, J., Bussiere, E., Vermeulen, C. and Lejeune, P. (2023). From crowd to herd counting: How to precisely detect and count African mammals using aerial imagery and deep learning? *ISPRS Journal of Photogrammetry and Remote Sensing* **197**, 167–180.

Dendorfer, P., Rezatofighi, H., Milan, A., Shi, J., Cremers, D., Reid, I., Roth, S., Schindler, K. and Leal-Taixé, L. (2020). MOT20: A benchmark for multi object tracking in crowded scenes. *arXiv:2003.09003[cs]*.

Deora, T., Singh, A. K. and Sane, S. P. (2015). Biomechanical basis of wing and haltere coordination in flies. *Proceedings of the National Academy of Sciences* **112**, 1481–1486.

Derham, W. (1714). *Physico-theology: Or, A Demonstration of the Being and Attributes of God, from His Works of Creation...* W. Innys.

Dhawan, S., Huang, Z. and Dickerson, B. H. (2025). Neural connectivity of a computational map for fly flight control. *bioRxiv* 2025–05.

Dickerson, B. H., de Souza, A. M., Huda, A. and Dickinson, M. H. (2019). Flies regulate wing motion via active control of a dual-function gyroscope. *Current Biology* **29**, 3517–3524.

Dickinson, M. H. (1990). Linear and nonlinear encoding properties of an identified mechanoreceptor on the fly wing measured with mechanical noise stimuli. *Journal of experimental biology* **151**, 219–244.

Dickinson, M. H. (1999). Haltere–mediated equilibrium reflexes of the fruit fly, Drosophila melanogaster. *Philosophical Transactions of the Royal Society of London. Series B: Biological Sciences* **354**, 903–916.

Duan, K., Bai, S., Xie, L., Qi, H., Huang, Q. and Tian, Q. (2019). Centernet: Keypoint triplets for object detection. In *Proceedings of the IEEE/CVF International Conference on Computer Vision*, pp. 6569–6578.

Faust, R (1952). Untersuchungen zum Halterenproblem. *Zool. Jahrb. Allg. Zool. Physiol.* **63**, 325–366.

Fayle, T. M. and Klimes, P. (2022). Improving estimates of global ant biomass and abundance. *Proc. Natl. Acad. Sci. U.S.A.* **119**, e2214825119.

Fayyazuddin, A. and Dickinson, M. H. (1996). Haltere afferents provide direct, electrotonic input to a steering motor neuron in the blowfly, Calliphora. *Journal of Neuroscience* **16**, 5225–5232.

Fellers, J. H. (1989). Daily and seasonal activity in woodland ants. *Oecologia* **78**, 69–76.

Folgarait, P. J. (1998). Ant biodiversity and its relationship to ecosystem functioning: a review. *Biodiversity and Conservation* **7**, 1221–1244.

Fox, J. (2016). *Applied Regression Analysis and Generalized Linear Models: 3rd edition*. Los Angeles: Sage Publications.

Fox, J. L. and Daniel, T. L. (2008). A neural basis for gyroscopic force measurement in the halteres of Holorusia. *J Comp Physiol A* **194**, 887–897.

Fox, J. L., Fairhall, A. L. and Daniel, T. L. (2010). Encoding properties of haltere neurons enable motion feature detection in a biological gyroscope. *Proc. Natl. Acad. Sci. U.S.A.* **107**, 3840–3845.

Fraenkel, G. (1939). The Function of the Halteres of Flies (Diptera). *Proceedings of the Zoological Society of London* **A109**, 69–78.

Fraenkel, G. and Pringle, J. W. S. (1938). Biological sciences: halteres of flies as gyroscopic organs of equilibrium. *Nature* **141**, 919–920.

Gnatzy, W., Grünert, U. and Bender, M. (1987). Campaniform sensilla of Calliphora vicina (Insecta, Diptera): I. Topography. *Zoomorphology* **106**, 312–319.

Gordon, D. M. (2019). The Ecology of Collective Behavior in Ants. *Annu. Rev. Entomol.* **64**, 35–50.

Goyal, L., McCall, K., Agapite, J., Hartwieg, E. and Steller, H. (2000). Induction of apoptosis by Drosophila reaper, hid and grim through inhibition of IAP function. *EMBO J* **19**, 589–597.

Gulmahamad, H. (1995). The genus Liometopum Mayr (Hymenoptera: Formicidae) in California, with notes on nest architecture and structural importance.

Hagberg, A., Swart, P. J. and Schult, D. A. (2007). *Exploring network structure, dynamics, and function using NetworkX*. Los Alamos National Laboratory (LANL).

Hallmann, C. A., Sorg, M., Jongejans, E., Siepel, H., Hofland, N., Schwan, H., Stenmans, W., Müller, A., Sumser, H. and Hörren, T. (2017). More than 75 percent decline over 27 years in total flying insect biomass in protected areas. *PloS one* **12**, e0185809.

Harrison, X. A., Donaldson, L., Correa-Cano, M. E., Evans, J., Fisher, D. N., Goodwin, C. E., Robinson, B. S., Hodgson, D. J. and Inger, R. (2018). A brief introduction to mixed effects modelling and multi-model inference in ecology. *PeerJ* **6**, e4794.

He, K., Zhang, X., Ren, S. and Sun, J. (2016). Deep residual learning for image recognition. In *Proceedings of the IEEE conference on computer vision and pattern recognition*, pp. 770–778.

Hengstenberg, R. (1984). Roll-Stabilization During Flight of the Blowfly's Head and Body by Mechanical and Visual Cues. In *Localization and Orientation in Biology and Engineering* (ed. Varjú, D.) and Schnitzler, H.-U.), pp. 121–134. Berlin, Heidelberg: Springer Berlin Heidelberg.

Hengstenberg, R. (1988). Mechanosensory control of compensatory head roll during flight in the blowflyCalliphora erythrocephala Meig. *J. Comp. Physiol.* **163**, 151–165.

Hengstenberg, R., Sandeman, D. C. and Hengstenberg, B. (1986). Compensatory head roll in the blowfly Calliphora during flight. *Proceedings of the Royal Society of London. Series B. Biological Sciences* **227**, 455–482.

Hicks, J. B. (1856). On a New Organ in Insects. *Zoological Journal of the Linnean Society* **1**, 136–140.

Hoey-Chamberlain, R., Rust, M. K. and Klotz, J. H. (2013). A review of the biology, ecology and behavior of velvety tree ants of North America. *Sociobiology* **60**, 1–10.

Holldobler, B. and Wilson, E. O. (2009). *The superorganism: the beauty elegance and strangeness of insect societies*. WW Norton & Company.

Houadria, M. and Menzel, F. (2020). Temporal and dietary niche is context-dependent in tropical ants. *Ecological Entomology* **45**, 761–770.

Huang, J., Rathod, V., Sun, C., Zhu, M., Korattikara, A., Fathi, A., Fischer, I., Wojna, Z., Song, Y., Guadarrama, S., et al. (2017). Speed/accuracy trade-offs for modern convolutional object detectors. In *Proceedings of the IEEE conference on computer vision and pattern recognition*, pp. 7310–7311.

Huston, S. J. and Krapp, H. G. (2009). Nonlinear integration of visual and haltere inputs in fly neck motor neurons. *Journal of Neuroscience* **29**, 13097–13105.

Imirzian, N., Zhang, Y., Kurze, C., Loreto, R. G., Chen, D. Z. and Hughes, D. P. (2019a). Automated tracking and analysis of ant trajectories shows variation in forager exploration. *Scientific reports* **9**, 1–10.

Imirzian, N., Zhang, Y., Kurze, C., Loreto, R. G., Chen, D. Z. and Hughes, D. P. (2019b). Automated tracking and analysis of ant trajectories shows variation in forager exploration. *Scientific reports* **9**, 13246.

Jain, A., Cunha, F., Bunsen, M., Pasi, L., Viklund, A., Larrivée, M. and Rolnick, D. (2024). A machine learning pipeline for automated insect monitoring.

Jenett, A., Rubin, G. M., Ngo, T.-T., Shepherd, D., Murphy, C., Dionne, H., Pfeiffer, B. D., Cavallaro, A., Hall, D. and Jeter, J. (2012). A GAL4-driver line resource for Drosophila neurobiology. *Cell reports* **2**, 991–1001.

Jocher, G., Chaurasia, A., Stoken, A., Borovec, J., NanoCode012, Kwon, Y., Michael, K., TaoXie, Fang, J., Imyhxy, et al. (2022). ultralytics/yolov5: v7.0 - YOLOv5 SOTA Realtime Instance Segmentation. *Zenodo*.

Jonathon Luiten, A. H. (2020). TrackEval.

Jr, S. B. and Belangour, A. (2021). Multi object tracking: a survey. In *Thirteenth International Conference on Digital Image Processing (ICDIP 2021)* (ed. Jiang, X.) and Fujita, H.), pp. 142–152. SPIE.

Kamaru, D. N., Palmer, T. M., Riginos, C., Ford, A. T., Belnap, J., Chira, R. M., Githaiga, J. M., Gituku, B. C., Hays, B. R., Kavwele, C. M., et al. (2024). Disruption of an ant-plant mutualism shapes interactions between lions and their primary prey. *Science* **383**, 433–438.

Kay, J., Kulits, P., Stathatos, S., Deng, S., Young, E., Beery, S., Van Horn, G. and Perona, P. (2022). The Caltech Fish Counting Dataset: A Benchmark for Multiple-Object Tracking and Counting. In *Computer Vision – ECCV 2022* (ed. Avidan, S.), Brostow, G.), Cissé, M.), Farinella, G. M.), and Hassner, T.), pp. 290–311. Cham: Springer Nature Switzerland.

Koh, P. W., Sagawa, S., Xie, S. M., Zhang, M., Balsubramani, A., Hu, W., Yasunaga, M., Phillips, R. L., Gao, I., Lee, T., et al. (2021). Wilds: A benchmark of in-the-wild distribution shifts. In *International Conference on Machine Learning*, pp. 5637–5664. PMLR.

Land, M. F. (1973). Head Movement of Flies during Visually Guided Flight. *Nature* **243**, 299–300.

Leocádio, R. R. V., Segundo, A. K. R. and Pessin, G. (2023). Multiple Object Tracking in Native Bee Hives: A Case Study with Jataí in the Field. In *Intelligent Systems* (ed. Naldi, M. C.) and Bianchi, R. A. C.), pp. 176–191. Cham: Springer Nature Switzerland.

Leydig, Franz (1860). uber Geruchs- und Gehororgane der Krebs und Insecten. Arch. f. Anat. u. Phys. 265–314.

Lin, T.-Y., Goyal, P., Girshick, R., He, K. and Dollár, P. (2017). Focal loss for dense object detection. In *Proceedings of the IEEE international conference on computer vision*, pp. 2980–2988.

Luiten, J., Osep, A., Dendorfer, P., Torr, P., Geiger, A., Leal-Taixé, L. and Leibe, B. (2021). Hota: A higher order metric for evaluating multi-object tracking. *International journal of computer vision* **129**, 548–578.

Luo, W., Xing, J., Milan, A., Zhang, X., Liu, W., Zhao, X. and Kim, T.-K. (2014). Multiple object tracking: A literature review. *arXiv preprint arXiv:1409.7618*.

Markow, T. A. (1988). Reproductive behavior of Drosophila melanogaster and D. nigrospiracula in the field and in the laboratory. *Journal of Comparative psychology* **102**, 169.

Mathis, A., Mamidanna, P., Cury, K. M., Abe, T., Murthy, V. N., Mathis, M. W. and Bethge, M. (2018). DeepLabCut: markerless pose estimation of user-defined body parts with deep learning. *Nat Neurosci* **21**, 1281–1289.

Mersch, D. P., Crespi, A. and Keller, L. (2013). Tracking individuals shows spatial fidelity is a key regulator of ant social organization. *Science* **340**, 1090–1093.

Muijres, F. T., Elzinga, M. J., Melis, J. M. and Dickinson, M. H. (2014). Flies Evade Looming Targets by Executing Rapid Visually Directed Banked Turns. *Science* **344**, 172–177.

Mureli, S. and Fox, J. L. (2015). Haltere mechanosensory influence on tethered flight behavior in Drosophila. *The Journal of Experimental Biology* **218**, 2528–2537.

Nalbach, G. (1993). The halteres of the blowfly Calliphora. *J Comp Physiol A* **173**, 293–300.

Nalbach, G. (1994). Extremely non-orthogonal axes in a sense organ for rotation: behavioural analysis of the dipteran haltere system. *Neuroscience* **61**, 149–163.

Nalbach, G. and Hengstenberg, R. (1994). The halteres of the blowfly Calliphora: II. Three-dimensional organization of compensatory reactions to real and simulated rotations. *J Comp Physiol A* **175**,.

O'Dowd, D. J., Green, P. T. and Lake, P. S. (2003). Invasional 'meltdown' on an oceanic island. *Ecology Letters* **6**, 812–817.

Olson, D. M. (1991). A comparison of the efficacy of litter sifting and pitfall traps for sampling leaf litter ants (Hymenoptera, Formicidae) in a tropical wet forest, Costa Rica. *Biotropica* 166–172.

Outhwaite, C. L., McCann, P. and Newbold, T. (2022). Agriculture and climate change are reshaping insect biodiversity worldwide. *Nature* **605**, 97–102.

Parker, J. (2016). Myrmecophily in beetles (Coleoptera): evolutionary patterns and biological mechanisms. *Myrmecological news* **22**, 65–108.

Parker, J. and Kronauer, D. J. (2021). How ants shape biodiversity. *Current Biology* **31**, R1208–R1214.

Patel, S., Kulkari, A., Mukhopadhyay, A., Gujar, K. and de Roode, J. (2021a). Using Deep Learning to Count Monarch Butterflies in Dense Clusters. *bioRxiv*.

Patel, S., Kulkarni, A., Mukhopadhyay, A., Gujar, K. and de Roode, J. (2021b). Using deep learning to count monarch butterflies in dense clusters. *bioRxiv* 2021–07.

Perfecto, I. and Philpott, S. M. (2023). Ants (Hymenoptera: Formicidae) and ecosystem functions and services in urban areas: a reflection on a diverse literature. *Myrmecological News* **33**,.

Pętal, J. (1978). The role of ants in ecosystems. *Production ecology of ants and termites* **13**, 293.

Pfeiffer, B. D., Jenett, A., Hammonds, A. S., Ngo, T.-T. B., Misra, S., Murphy, C., Scully, A., Carlson, J. W., Wan, K. H., Laverty, T. R., et al. (2008). Tools for neuroanatomy and neurogenetics in *Drosophila*. *Proc. Natl. Acad. Sci. U.S.A.* **105**, 9715–9720.

Pfeiffer, B. D., Ngo, T.-T. B., Hibbard, K. L., Murphy, C., Jenett, A., Truman, J. W. and Rubin, G. M. (2010). Refinement of tools for targeted gene expression in Drosophila. *Genetics* **186**, 735–755.

Pflugstaedt, H. (1912). Die Halteren der Dipteren...

Pringle, J. W. S. (1948). The gyroscopic mechanism of the halteres of Diptera. *Philosophical Transactions of the Royal Society of London. Series B, Biological Sciences* **233**, 347–384.

Pritchard, D. J., Hurly, T. A., Tello-Ramos, M. C. and Healy, S. D. (2016). Why study cognition in the wild (and how to test it)? *Journal of the Experimental Analysis of Behavior* **105**, 41–55.

Ratnayake, M. N., Dyer, A. G. and Dorin, A. (2021). Tracking individual honeybees among wildflower clusters with computer vision-facilitated pollinator monitoring. *Plos one* **16**, e0239504.

Rauscher, M. J. and Fox, J. L. (2021). Haltere and visual inputs sum linearly to predict wing (but not gaze) motor output in tethered flying *Drosophila*. *Proc. R. Soc. B.* **288**, 20202374.

Ren, S., He, K., Girshick, R. and Sun, J. (2015). Faster r-cnn: Towards real-time object detection with region proposal networks. *arXiv preprint arXiv:1506.01497*.

Schilstra, C. and van Hateren, J. H. (1998). Stabilizing gaze in flying blowflies. *Nature* **395**, 654–654.

Schilstra, C. and Van Hateren, J. H. (1999). Blowfly flight and optic flow: I. Thorax kinematics and flight dynamics. *Journal of experimental biology* **202**, 1481–1490.

Schneider, G (1953). Die Halteren der SchmeiÞ£iege (Calliphora) als Sinnesorgane und als mechanische Flugstabilisatoren. *Z. Vgl. Physiol.* **35**, 416–458.

Schultheiss, P., Nooten, S. S., Wang, R., Wong, M. K. L., Brassard, F. and Guénard, B. (2022). The abundance, biomass, and distribution of ants on Earth. *Proc. Natl. Acad. Sci. U.S.A.* **119**, e2201550119.

Shapley, H. (1920a). Thermokinetics of Liometopum apiculatum Mayr. *Proceedings of the National Academy of Sciences of the United States of America* **6**, 204.

Shapley, H. (1920b). Thermokinetics of Liometopum Apiculatum Mayr. *Proc. Natl. Acad. Sci. U.S.A.* **6**, 204–211.

Sharma, T., Wagner, J. M., Beery, S., Dickson, W. B., Dickinson, M. H. and Parker, J. (2024). Monitoring Social Insect Activity with Minimal Human Supervision. In *Proceedings of the IEEE/CVF Conference on Computer Vision and Pattern Recognition*, pp. 1244–1253.

Sherman, A. and Dickinson, M. H. (2003). A comparison of visual and haltere-mediated equilibrium reflexes in the fruit fly Drosophila melanogaster. *Journal of experimental biology* **206**, 295–302.

Simpson, J. H. (2009). Mapping and manipulating neural circuits in the fly brain. *Advances in genetics* **65**, 79–143.

Sittinger, M., Uhler, J., Pink, M. and Herz, A. (2024). Insect detect: An open-source DIY camera trap for automated insect monitoring. *Plos one* **19**, e0295474.

Stradling, D. J. (1970). The estimation of worker ant populations by the mark-release-recapture method: an improved marking technique. *The Journal of Animal Ecology* 575–591.

Suver, M. P., Huda, A., Iwasaki, N., Safarik, S. and Dickinson, M. H. (2016). An Array of Descending Visual Interneurons Encoding Self-Motion in *Drosophila*. *J. Neurosci.* **36**, 11768–11780.

Tammero, L. F. and Dickinson, M. H. (2002). The influence of visual landscape on the free flight behavior of the fruit fly Drosophila melanogaster. *Journal of Experimental Biology* **205**, 327–343.

Tan, M., Pang, R. and Le, Q. V. (2020). EfficientDet: Scalable and Efficient Object Detection. *CVPR*.

Tracey, D. (1975). Head movements mediated by halteres in the fly, Musca domestica. *Experientia* **31**,.

Trimarchi, J. R. and Murphey, R. K. (1997). The shaking-B2 Mutation Disrupts Electrical Synapses in a Flight Circuit in Adult Drosophila. *Journal of Neuroscience* **17**, 4700–4710.

Tsutsui, N. D. (2018). Wild vs. Lab Box 1.2 Understanding the Nature of Ant Cognition by Studying Ant Cognition. *Field and Laboratory Methods in Animal Cognition: A Comparative Guide* 23.

Underwood, E. C. and Fisher, B. L. (2006). The role of ants in conservation monitoring: if, when, and how. *Biological conservation* **132**, 166–182.

Van Klink, R., August, T., Bas, Y., Bodesheim, P., Bonn, A., Fossøy, F., Høye, T. T., Jongejans, E., Menz, M. H. M., Miraldo, A., et al. (2022). Emerging technologies revolutionise insect ecology and monitoring. *Trends in Ecology & Evolution* **37**, 872–885.

Verbe, A., Lea, K. M., Fox, J. L. and Dickerson, B. H. (2024). Flies tune the activity of their multifunctional gyroscope. *Current Biology* **34**, 3644-3653.e3.

Wagner, D. L., Grames, E. M., Forister, M. L., Berenbaum, M. R. and Stopak, D. (2021). Insect decline in the Anthropocene: Death by a thousand cuts. *Proc. Natl. Acad. Sci. U.S.A.* **118**, e2023989118.

Wang, T. B., Patel, A., Vu, F., Nonacs, P., and others (2010). Natural history observations on the velvety tree ant (Liometopum occidentale): unicoloniality and mating flights. *Sociobiology* **55**, 787–794.

Wang, G., Wang, Y., Zhang, H., Gu, R. and Hwang, J.-N. (2019). Exploit the Connectivity: Multi-Object Tracking with TrackletNet. In *Proceedings of the 27th ACM International Conference on Multimedia*, pp. 482–490. New York, NY, USA: Association for Computing Machinery.

Weinland, E. (1891). Über die Schwinger (Halteren) der Dipteren. *Z Wiss Zool* **51:55–166**,.

Wills, B. D. and Landis, D. A. (2018). The role of ants in north temperate grasslands: a review. *Oecologia* **186**, 323–338.

Wilson, E. O. and Hölldobler, B. (2005). Eusociality: Origin and consequences. *Proc. Natl. Acad. Sci. U.S.A.* **102**, 13367–13371.

Wu, Y., Kirillov, A., Massa, F., Lo, W.-Y. and Girshick, R. (2019). Detectron2.

Yarger, A. M. and Fox, J. L. (2018). Single mechanosensory neurons encode lateral displacements using precise spike timing and thresholds. *Proceedings of the Royal Society B: Biological Sciences* **285**, 20181759.